A NOVEL METHOD FOR THE EVALUATION OF MECHANICAL PROPERTIES OF CANCELLOUS BONE IN THE RAT DISTAL FEMUR

A Thesis

by

MATTHEW WALTON LUCAS

Submitted to the Office of Graduate Studies of
Texas A&M University
in partial fulfillment of the requirements for the degree of

MASTER OF SCIENCE

August 2009

Major Subject: Mechanical Engineering

A NOVEL METHOD FOR THE EVALUATION OF MECHANICAL PROPERTIES OF CANCELLOUS BONE IN THE RAT DISTAL FEMUR

A Thesis

by

MATTHEW WALTON LUCAS

Submitted to the Office of Graduate Studies of
Texas A&M University
in partial fulfillment of the requirements for the degree of

MASTER OF SCIENCE

Approved by:

Co-Chairs of Committee, Harry Hogan
                        Susan Bloomfield
Committee Members,   Cris Schwartz
Head of Department,   Dennis O'Neal

August 2009

Major Subject: Mechanical Engineering

ABSTRACT

A Novel Method for the Evaluation of Mechanical Properties of Cancellous Bone in the

Rat Distal Femur. (August 2009)

Matthew Walton Lucas, B.S., Lipscomb University

Co-Chairs of Advisory Committee: Dr. Harry Hogan
                                  Dr. Susan Bloomfield

The mechanical properties of the cancellous bone in the laboratory rat animal model are of great interest to the research community for the evaluation of treatments for osteoporosis. Cancellous bone responds rapidly and dramatically to disuse, various pathologies, nutritional deficiencies, and hormonal deficiencies and hence is often a primary focus in animal studies. Previous methods for evaluating the mechanical properties of cancellous bone in rat test specimens included both cortical and cancellous bone. This thesis introduces a new method to core cancellous specimens using a diamond wire saw in concert with specially designed fixtures. This method has been termed Isolated Cancellous Coring (ICC). The location and the geometry of the cored specimens were determined based on μCT analysis. The isolated cancellous specimens were subjected to uni-axial compression testing to evaluate the mechanical properties. Furthermore, the new method is evaluated by directly applying it to a study investigating the effects of estrogen replacement therapy in post-menopausal osteoporosis as simulated by the ovariectomized rat model.

The results show that the ICC method can be applied to bone specimens with a large range in density and micro-architecture parameters. The compression testing of the isolated cancellous specimens provides a sensitive indicator of the effects of osteoporosis and treatment on the mechanical properties of the cancellous bone in the distal rat femur. Also, the results indicate a possible discordant relationship between bone mineral density and bone strength with respect to estrogen treatment. Power law

regressions show that approximately 50% of the variation in ultimate strength can be accounted for with bone mineral density and the percent of bone volume per total volume.

DEDICATION

This thesis is dedicated to:

My wife, Amy, for her never ending love and support.

My family, for providing encouragement throughout my education.

ACKNOWLEDGEMENTS

NOMENCLATURE

BMD	Bone Mineral Density
BMC	Bone Mineral Content
BV/TV	Bone Volume per Total Volume
BS	Bone Surface
Tb.Th	Trabecular Thickness
Tb.Sp	Trabecular Separation
Tn.N	Trabecular Number
Tb.Pf	Trabecular Bone Pattern Factor
DA	Degree of Anisotropy
SMI	Structure Model Index
Po	Porosity
pQCT	Peripheral Quantitative Computed Tomography
μCT	Micro Computed Tomography
PBS	Phosphate Buffered Saline
ROI	Region of Interest
ICC	Isolated Cancellous Coring

TABLE OF CONTENTS

LIST OF FIGURES

LIST OF TABLES

1. INTRODUCTION

1.1 Problem

The laboratory rat animal model is used frequently in evaluating treatments for osteoporosis, various types of bone disease and cancer, and the osteopenic effects of spaceflight on bone. In many animal studies the type of bone of interest is spongy, or cancellous bone, because often it reacts more potently to treatment or disease. Additionally, cancellous bone forms near the ends of long bones near joints, and therefore prosthetic joints can interface directly with cancellous bone. For these reasons it is very important to have the ability to evaluate the mechanical properties of this tissue.

An extensive amount of research has focused on the mechanical properties of cancellous bone in human cadavers and large animals. This research utilizes the testing of isolated cancellous cylinders or cubes by compression. Some of the advantages of the rat animal model to study bone are cost, time, and, most pertinent to this study, the ability to readily evaluate the mechanical properties. Currently, the majority of research that utilizes the laboratory rat model focuses on the mechanical properties of the cortical bone or mixed bone sites because there has not been a successful method developed and presented in the literature for the mechanical testing of samples of isolated cancellous bone. The ability to core and test isolated cancellous bone in the rat model will permit direct assessment of the mechanical properties, the most functionally relevant of all bone outcome measures, for this highly significant skeletal tissue type. In addition, the results can then be compared with values found in other animal and most importantly human studies. Therefore, the primary objective of this thesis is to develop a method to core and test cancellous specimens from the distal femur metaphysis in the rat. A complete listing of the objectives is presented in the next section.

_____

This thesis follows the style of the *Journal of Bone and Mineral Research*.

1.2 Objectives

The detailed objectives of the thesis are:

1. To develop a new method to core isolated cancellous cylindrical bone specimens from the distal femur metaphysis in rats.

2. To develop the methods and procedures to test the mechanical properties of these isolated cancellous bone specimens in axial compression.

3. To evaluate the range of applicability and corresponding limitations by testing a large number of animals with wide variations in bone density and structure. In order to obtain a result that can be used in a larger number of laboratories, these bone parameters will be assessed by two different scanning methods, namely micro-computed tomography (μCT) and peripheral quantitative computed tomography (pQCT).

4. To investigate the effects of estrogen replacement as an effective treatment to mitigate detrimental effects on cancellous bone mechanical properties due to postmenopausal osteoporosis as simulated by the ovariectomized rat model.

5. To investigate correlations between mechanical testing results such as ultimate strength as the dependent variable with single or multiple independent variables such as bone volume per total volume (BV/TV), anisotropy (AN), or volumetric bone mineral density (vBMD) that will be measured by micro-computed tomography.

1.3 Overview

This remainder of this thesis is divided into five sections. First, background on cancellous bone and testing methods is presented. Next, the methods for the experiment will be presented including specimen preparation, testing procedure, statistics, and analysis. Then, the results from the coring and mechanical testing will be presented, followed by the discussion. The last section describes possible future work.

2. BACKGROUND

2.1 Bone Function and Structure

Bone can be categorized into two different types: cancellous and cortical as can be seen in Figure 1. Cancellous bone, also called trabecular or spongy, is the porous bone found in the cuboidal bones (e.g. vertebrae), flat bones, and in ends long bones. Its porosity generally ranges from 75-90%.[1] Trabeculae are the plates or struts that make up the cancellous bone and are about 200 μm thick.[1] As a note of interest, the word trabeculae comes from the Latin for "little beams". In long bones like the femur or tibia the trabecular bone is found in the ends of the bones near joints. Cortical bone, also referred to as compact bone, is the dense bone found in shafts of long bones and forming a cortex or shell around vertebral bodies and other spongy bone and is characterized by a porosity of 5-10%.[1]
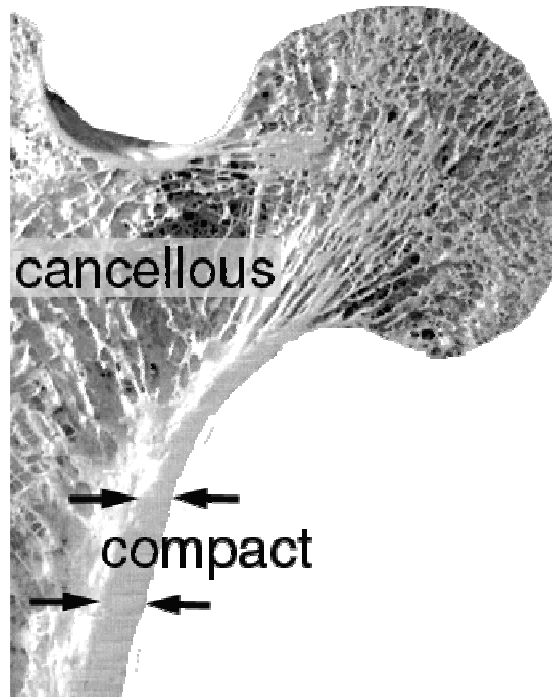
Figure 1: Compact (Cortical) & Cancellous (Trabecular) Bone[2]

Bone tissue serves three primary functions:[3]

    1. Mechanical - support and muscle attachment points for movement.

    2. Protective - Vital organs and Bone Marrow (i.e. rib cage).

    3. Metabolic - a reserve for ions, especially calcium and phosphate, and the maintenance of serum homeostasis the essential to life.

In 1892, Julius Wolff postulated that bones are able to sense the mechanical loads which they bear and modify their structures to accomodate changes in these loads.[1] Today this concept is known as Wolff's Law or functional adaptation. This concept is shown nicely in Ward's analogy between the trabecular structure in the femoral neck and a classic street lamp (See Figure 2). The trabecular structure in the femoral neck is oriented in such a way so that it can best support the loads applied to the femoral head.
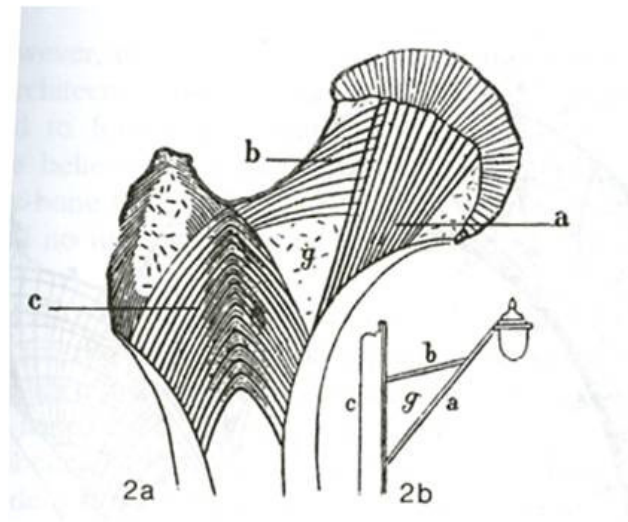
Figure 2: Ward's Analogy between the Femoral Neck and a Streetlamp[1]

2.2 Osteoporosis and the Ovariectomized Rat Model

As mentioned previously, the laboratory rat animal model is used frequently in evaluating treatments for a wide range of bone diseases. One of the most well known medical conditions affecting bone is osteoporosis. Osteoporosis presents itself as reduced bone mass and structural defects that lead to increased fracture risk.[4] While there are many types of osteoporosis, post menopausal osteoporosis is the most common.[5] One out of every two women over 50 will have an osteoporosis-related fracture in their lifetime.[6] The ovariectomized (OVX) rat model has been proven to be an acceptable model for post menopausal osteoporosis.[5] Furthermore, the OVX rat model is used more than any other animal model in osteoporosis studies.[4] The OVX rat model has been called "a gold standard model for evaluating drugs for prevention and reversal of osteoporosis."[7] Osteoporosis caused by estrogen deficiency is characterized by high bone turnover rates, where bone resorption outweighs bone formation causing a reduction in total bone content.

2.3 Mechanical Testing of Cancellous Bone in Rats

The ability to test cancellous bone in the laboratory rat model is important because it can give valuable insight into the effects of various treatments and conditions on the mechanical properties of bone. Directly testing an isolated specimen of cancellous bone from rats has remained difficult and elusive. The difficulty is primarily due to the size constraints and fragility of the specimens. There are testing methods that evaluate mixed bone sites, those containing cortical and cancellous bone. Also, various attempts to extract the mechanical properties from the cancellous bone in rats have been made through the evaluation of a specimen with the cortical portion of the bone remaining intact; these studies will be reviewed in the following sections.

2.3.1 Femoral Neck Testing

One testing method that interrogates a region of bone containing both cortical and cancellous bone is the femoral neck test. This method is illustrated in Figure 3. On the left, the standing testing configuration is shown and on the right the fall

configuration. In this test, force is applied to the femoral head as the bone is held by the testing apparatus. Inherent in these testing procedures is a three dimensional stress field which is difficult to model. Generally, only maximum force and stiffness are reported for these types of tests.
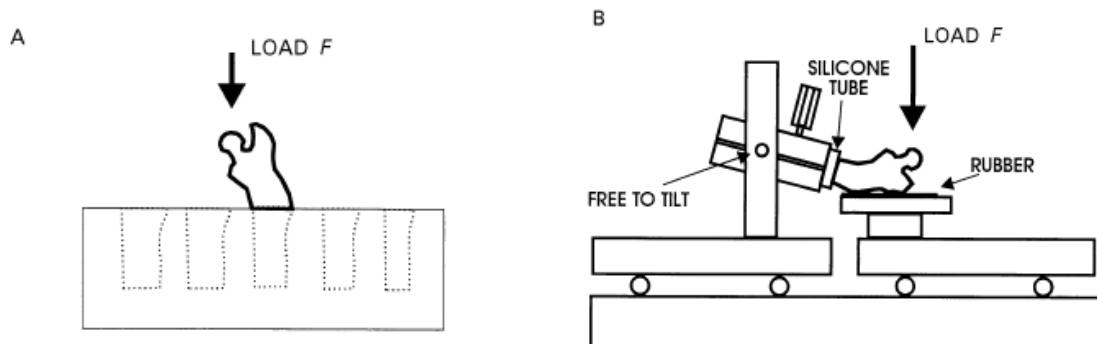
Figure 3: Femoral Neck Testing Configurations: (A) Standing (B) Fall[8]

2.3.2 Vertebral Body Compression

The spine is a clinically relevant location of interest. In studies using rats that investigate the spine vertebral compression is often used to ascertain the mechanical properties. The vertebral compression method is shown below in Figure 4. In this method, vertebrae from the lumbar section of the spine are excised from the rat corpse and the ends are made plano-parallel. The vertebrae are then compressed at a constant rate to failure to determine the mechanical properties. Since the vertebra contains cancellous bone, this method provides an indication of the effects of pathologies and treatment on the mechanical properties on cancellous bone, but also being tested is the cortical shell.
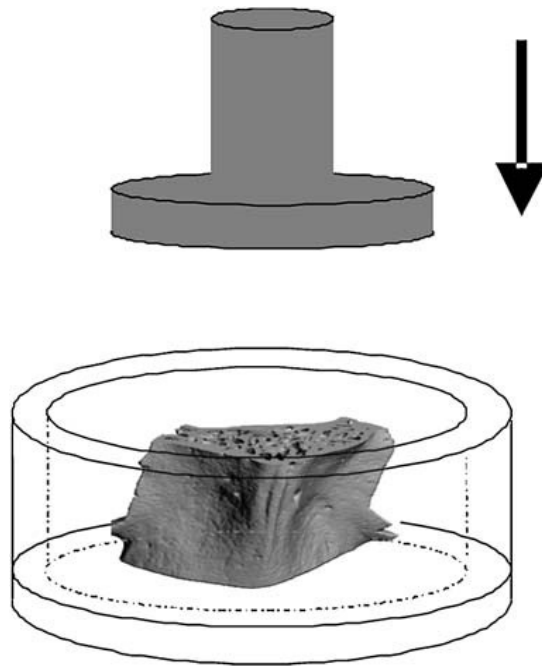
Figure 4: Vertebral Compression[9]

2.3.3 Indentation Testing

An et al. studied the mechanical properties of cancellous bone in the epiphysis of adult female Sprague-Dawley rats.[10] Mechanical testing was done on the femoral head, distal femur, tibial plateau and the humeral head by indentation with a 1.31 mm cylindrical platen. In each test, the outer cortical shell was removed by grinding to expose the cancellous bone for indentation testing. The ultimate strength of the cancellous bone ranged 38 to 71 MPa. This article is of special significance because it was the first to look at the properties of cancellous bone in rats.

Other studies have investigated the mechanical properties of the cancellous bone in the metaphysis of the distal femur using a similar indentation method as depicted in Figure 5. [11,12,13] The specimen is a 4 mm transverse section is cut just proximal of the condyles. The test consisted of a cylindrical platen of 1.6 mm that was applied to the center of the cancellous cavity of the distal face of the specimen and inserted 2mm at a constant velocity into the specimen. At 30 days and 60 days post-OVX in three-month-old rats there was a significant reduction in maximum load (75% and 82%, respectively)

and stiffness by (72% and 76%, respectively).[12] Another study using older rats (4 months) found that six weeks post OVX the load and stiffness were both diminished by 50% and 45%, respectively.[13]
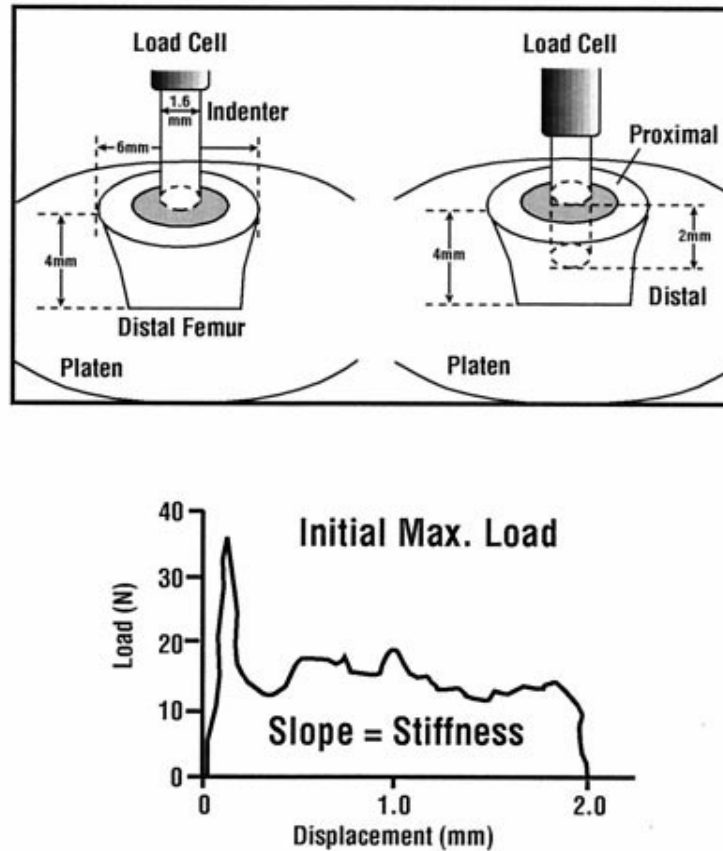
Figure 5: Indentation Test of Trabecular Bone on the Distal Femur[12]

2.3.4 Reduced Platen Compression Method

Previously, the Bone Biomechanics Lab at Texas A&M University developed the reduced platen compression method (RPC) to test cancellous bone in the metaphysis of rats.[14, 15] In this method a 2 mm transverse section is cut from the metaphysis region and then the slice is compressed between two platens of reduced size that contact only the cancellous portion of the bone (Figure 6). This is the most prominent method that has been presented in the research community, but the specimen contains both cortical and

cancellous bone. The study by Hogan et al. found a reduction in strength and elastic modulus of about 60% in the OVX animals (14 weeks old at OVX with duration of 5 weeks).[15] Oxlund et al. also used this method, but followed a recommendation proposed by Hogan et al.[14] to include the use of exchangeable platens with custom diameters sized to each individual specimen.[16] Many recent studies in our lab have used the custom diameter platen sizing.[17,19] Custom platen diameters are chosen as a percentage of the maximum endocortical circle (EC) diameter. The endocortical circle is found by drawing superimposing circles on an X-ray or photographic image of the RPC slice cross-section that fit just within the cortical shell (Figure 7). Using µCT images, H. Lemmon proposed the use of external landmarks for determining the first cut location for obtaining RPC specimens from the rat femur and tibia (Figure 8).[18] The primary limitation of this method is that while it is closer to simulating uni-axial compression than the indentation method, there remains tri-axial stress caused by the intact cortical shell.
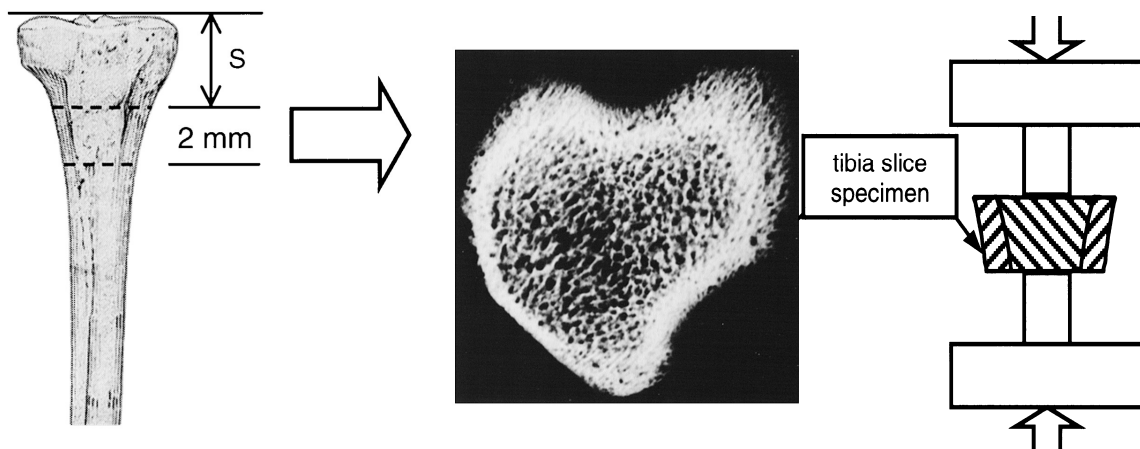
Figure 6: RPC Specimen Selection and Testing Method[14]
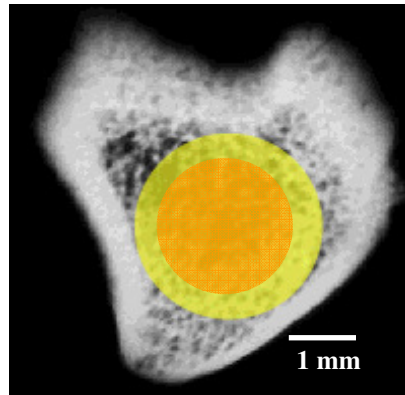
Figure 7: Endocortical Circle (Yellow), 70% EC (Orange), Adapted from Ref. 19

Figure 8: The External Landmarks Chosen as RPC Specimen First Cut Locations for the Tibia (left) and Femur (right)[18]

2.4 Mechanical Testing of Human & Large Animal Cancellous Bone

Due to the size of human cadaver and bovine bones, researchers are able to evaluate isolated cancellous bone specimens of many different bones from each. There are many lessons that have been learned from these studies that can be applied to the current study. Also, this provides further motivation to study the cancellous bone in the rat animal model. The ability to quantify mechanical strength of cancellous bone in a similar procedure to that of human studies will allow for further validation of the animal

model and additional correlation. The information presented here covers the basic information found in the literature, though it is not meant to be exhaustive.

2.4.1 Tomography

The ability to use noninvasive methods, such as computed tomography (CT) imaging, to determine fracture risk in a patient is an ongoing and important field of bone research. Generally CT imaging provides densitometric parameters that have given some insight to bone strength, but these parameters do not fully account for the strength found through biomechanical testing. Advances in CT imaging resolution have provided architectural measures that provide further insight and the ability to create high resolution three-dimensional models.

2.4.2 Anatomical Location and Anisotropy

As mentioned previously, Julius Wolff postulated the idea that bones are able to sense the mechanical loads which they bear and modify their structures to suit changes in these loads.[1] Today this concept is known as Wolff's Law. Each bone in the body has its own unique general loading conditions and function and each bone is designed and has adapted to work in concert meet the requirements of the body as a whole. Because of this it is easy to see why the mechanical properties would vary from one anatomical site to another.

The mechanical properties of human cancellous bone vary greatly even within the same compartment of cancellous bone. Compressive modulus can vary 100-fold from one location to another within a single human proximal tibia metaphysis.[20] Also, it has been shown that the strength can vary 5-fold in the human proximal femur.[21]

Isotropic materials are considered to be the same in all directions. In this context, that would imply that the material would react the same way no matter the loading direction. For bone, especially cancellous bone, this is not the case. Thus, cancellous bone is considered to be anisotropic. This characteristic is further demonstrated in Figure 9, where the specimen on the right is more anisotropic. Just from a visual inspection one can see that in the specimen on the right the trabeculae are

oriented and spaced in such a way to better support a top to bottom load versus a side to side loading. Some researchers have shown that when specimens are not taken along the same axis in the human femoral head that the stress and modulus values can vary 40%.[22] Also, others have investigated this anisotropy effect by taking specimens that are oriented perpendicular to each other from the human mandibular condyle.[23] It was found that the cancellous bone was 3.4 times stiffer and 2.8 times stronger at failure in the axial loading direction than the transverse.[23]
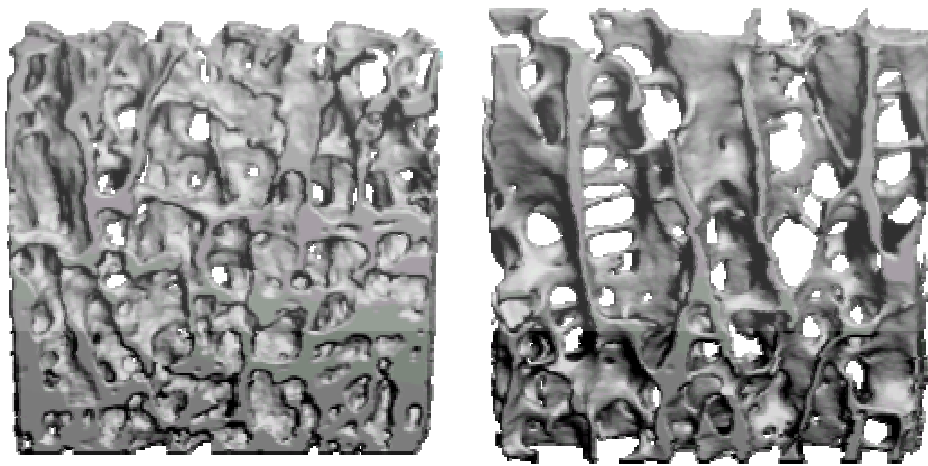
Figure 9: Illustration of Anisotropy, the Specimen on the Right is Considered More Anisotropic[24,25]

On a related note, the Structural Modeling Index (SMI) is a measure quantifying the prevalence of plate-like or rod-like structure in the cancellous structure, with lower values indicating more plate-like and higher values indicating a more rod-like structure (Figure 10).
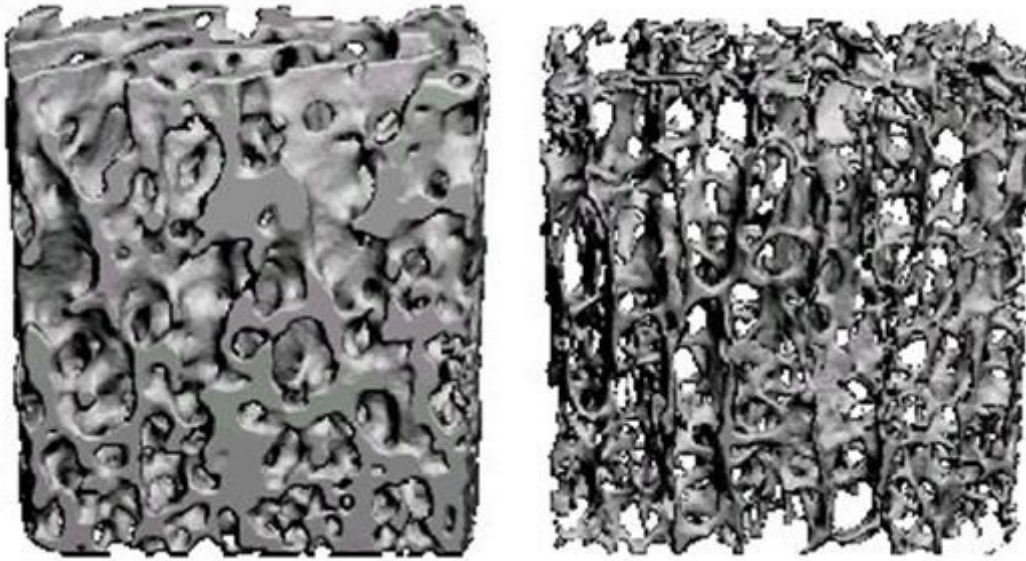
Figure 10: Plate-like (left) vs. Rod-like (right) Cancellous Structure[24,25]

2.4.3 Specimen Geometry

There are many factors that should be taken into consideration when selecting the optimal geometry for cylindrical cancellous specimens. The first and most obvious factor is the size of the cancellous compartment from which the bone is being cored. Secondly, to obtain the values most representative of pure axial compression one must minimize buckling and friction. Vrijhoef and Driessens used analytical tools to find that a length to diameter (L/D) ratio between one and five was acceptable with a L/D ratio of two being the optimal value for isotropic dental materials.[26] Linde et al. suggested a cylindrical specimen with a 7.5 mm diameter and at 6.5 mm length (L/D=.87) based on experimental studies with human cancellous bone.[27] One year later, Keaveny et al. studied the effects of geometry on bovine cancellous bone specimens and recommended a cylinder with L/D ratio of two.[28] Lastly, in order to satisfy the limitations of the continuum assumption the minimum dimension of the specimen should span at least three to five trabeculae.[29]

2.4.4 Testing Considerations

2.4.4.1 Physiological Conditions

Physiological loading rates are between 0.01/s and 0.08/s.[30]   While the physiological temperature for testing is 37 ℃, this is often not practical. At room temperature (23℃) the Young's modulus of bone has been shown to drop 2-4%.[30]

2.4.4.2 Structural End Phenomenon

The machining process to create the cancellous specimens causes disconnects in the trabecular matrix, weakening the specimen on the ends at the compression platen interface. The error derived from this has been termed end-artifact error and causes an underestimation of mechanical properties.[31]   This error is characterized by a low sloped portion on the front end of a load-deflection plot often referred to as the "toe". Different methods have been used to mitigate these effects including end-caps for the specimens[31], embedding the ends in PMMA[27], extensometers attached directly to the bone[31], optical systems[32], lubricants to reduce friction at the bone to platen interface, and preconditioning by cyclic loading[31,32]. Figure 11 illustrates the use of end-caps and extensometers directly attached to the cancellous specimen to mitigate the influence of end artifacts. The cyclic loading is performed to settle out the edge defects on the end surfaces of the cancellous specimens that come into contact with the compression platens.
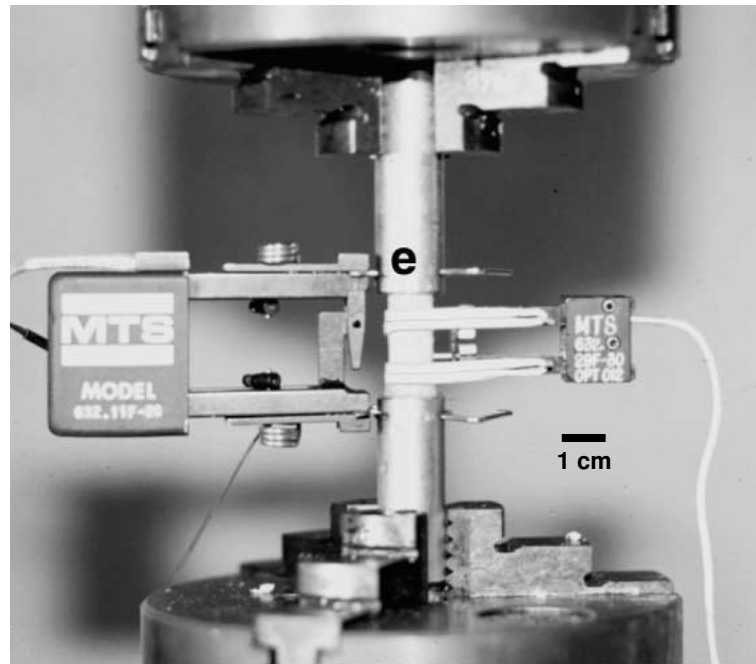
Figure 11: Human Cadaver Cancellous Bone Testing Set-up[41]

Odgaard and Linde tested human cadaver cancellous bone in an effort to quantify the combined effects of friction and this structural end phenomenon.[32] Orthogonal parallelepiped (7.0 x 6.0 x 6.0 mm) specimens were taken from proximal tibia and were compressed and displacement was recorded by both extensometer and an optical system. Comparing the optical strain and extensometer strain, they came to the conclusion that Young's modulus is underestimated by 20% with the conventional extensometer set-up. They also reported that, while it seems the underestimation does not seem dependent on bone density, it would be dependent on specimen size.[32]

2.4.4.3 Effect of Side-Artifacts

The interruptions in the trabecular matrix along the sides of the specimen are also a source of error in mechanical testing. The outer trabeculae in the machined specimens have a reduced ability to support axial compression because of the inherent disconnects that are caused by machining. These disconnects were coined "side-artifacts" by Űn et al.; they studied the effects of the side-artifacts on the elastic modulus in human

vertebral cancellous bone using a combined theoretical and micro-CT finite element analysis approach.[33]   They found that the edge effects are strongly correlated to trabecular spacing and presented an equation to calculate the following correction factor:

$$\alpha = \frac{E_{true}}{E_{measured}} = \left(\frac{1}{1-2\beta}\right)^2 \qquad (1)$$

where

$$\beta = \frac{t}{D} = \frac{a \times Tb.Sp + b}{D} \qquad (2)$$

where t is the thickness of the bone affected by side-artifacts, D is the diameter of the specimen, $Tb.Sp$ is trabecular spacing, and a and b are constants derived from the finite element analysis.[33]

Using similar methods Bevill et al. investigated the side-artifact on elastic modulus and yield strength at two different anatomical locations.[34] The study used micro-CT based finite element analysis that incorporated the stress-strain dependent nature of cancellous bone on virtual specimens from the human vertebral body and the femoral neck. They reported that while the correction factors (Eq.1) for both yield stress and elastic modulus did significantly depend on anatomical site, this dependency was accounted for by variations in BV/TV.[34] The correction factors were in the general range of 1 to 1.5; while the correction factors show a trend towards being higher for yield stress than elastic modulus.

2.4.4.4 Storage Considerations

Linde et al. looked at the effects of various storage methods of human cylindrical cancellous bone specimens. The study found no change in mechanical properties due to freeze–thaw cycles. Additionally, with specimens rehydrated in PBS before testing, they found no difference in mechanical properties due to storage in ethanol at 10°C when compared to the standard method of storing specimens in phosphate buffered saline (PBS) at -20°C.[35]

3. METHODS

3.1 Study Design

This study has been made possible by the donation of tissue from a study completed by M.D. Delp and J.M. Delp at West Virginia University (currently faculty at University of Florida, Gainesville, FL, USA) examining the effects of estrogen replacement in the ovariectomized (OVX) rat model. Additionally, all μCT imaging and initial analyses were performed by M.R. Allen (Anatomy & Cell Biology, Indiana University School of Medicine, Indianapolis, IN, USA).

Four month old Fisher-344 rats (n=42) were assigned into three groups, OVX (n=12), OVX+E2 (n=13), and INTACT (n=17). Both the OVX and OVX+E2 groups were subjected to ovariectomy; the OVX+E2 group also received a subcutaneous implant of two 0.05 mg 17-beta estradiol 60-day slow release pellets (Innovative Research; Novi, Michigan, USA). The INTACT group served as the age-matched control group. Rats were housed individually at 23º C and were maintained on a 12:12-h light-dark cycle. All rats were fed a phytoestrogen-free rat chow and water ad libitum. After 8 weeks all animals were sacrificed and the femurs were excised. All procedures were approved by the Institutional Animal Care and Use Committee at West Virginia University and conformed to the National Institutes of Health Guide for the Care and Use of Laboratory Animals (National Research Council, Washington D.C., Revised 1996).

Excised femurs were wrapped in gauze soaked with phosphate buffered saline (PBS), stored frozen, and shipped from West Virginia University (Morgantown, WV, USA) to Indiana University School of Medicine, (Indianapolis, IN, USA) for μCT imaging (n=36 of 42) and then to Texas A&M University (College Station, TX, USA) for pQCT imaging, specimen preparation, and mechanical testing (n=42). To further clarify, not all bones underwent μCT imaging; for OVX, 11 of 12, OVX+E2, 12 of 12, and for INTACT, 12 of 17, were imaged using μCT.

3.2 Computed Tomography

3.2.1 Micro-Computed Tomography (µCT)

Cancellous bone parameters of the distal femur metaphysis were assessed using microcomputed tomography (microCT; Skyscan 1172) by our collaborator, M.R. Allen. The procedure is widely used and well accepted by bone biologists. The details that follow were provided by M.R. Allen.[36] Bones were thawed to room temperature and wrapped in parafilm to prevent drying during the scanning. Scans were obtained using an x-ray source set at 60kV and 167 µA over an angular range of 180 degrees (rotational steps of 0.40 degrees) with a 12 µm pixel size. Projection images were reconstructed using standard Skyscan software. The trabecular bone compartment was segmented from the cortical shell for 50 slices in a region starting ~0.5 mm below the most proximal portion of the growth plate for each animal. Images were binarized (threshold of 100 on a 0-255 scale) and the following parameters were assessed for the three-dimensional volume: trabecular bone volume (BV/TV), trabecular number (Tb.N), trabecular thickness (Tb.Th), trabecular separation (Tb.Sp), and SMI. A phantom standard was scanned and reconstructed using the same parameters as above to allow conversion of gray scale values to density (mg/cm3).

The images and the results from the analysis described above were acquired from M.R. Allen and further analyzed using the Skyscan software installed in Dr. Harry Hogan's laboratory. The software allows for the analysis of a user defined region of interests (ROI) and the ability to convert the 2-dimensional slices to 3-dimensional models that correspond to the ROI's. As mentioned previously, anisotropy can have a large impact on the mechanical properties that are obtained from testing. The degree of anisotropy was quantified by the software using the mean intercept length and Eigen analysis. Furthermore, the scans were utilized to aid in the process of determining the optimal dimensions (length and diameter) for the specimens and their anatomical locations.

3.2.2 Peripheral Quantitative Computed Tomography (pQCT)

Each bone was also scanned using a Stratec XCT Research M (Stratec; Norland Corp. Fort Atkinson, WI) using a 0.071x0.071x0.5 mm voxel size. All bones were carefully positioned to be aligned axially with the machine with the bone resting on its anterior side. As seen in Figure 12, the distal metaphyseal region was scanned by 3 slices (0.5 mm thick) located 5.0, 5.5, and 6.0 mm proximal of the distal plateau, as determined in the scout view. These were analyzed using Stratec XCT 540 software using peel mode 4 and contour mode 3. These scan parameters were chosen to correspond with the existing lab protocols. Scanning the specimens with pQCT allowed for the comparison of this method with μCT. Also, it allows for laboratories with only pQCT available to compare the results from this study to evaluate whether the ICC method is applicable to their current study. The pQCT parameters evaluated were cancellous volumetric bone mineral density (vBMD) and total vBMD.
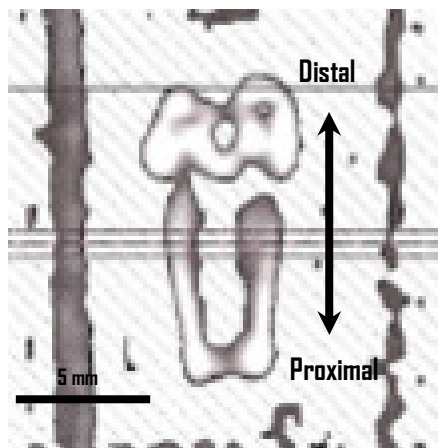
Figure 12: pQCT Scout View with Slice Locations Displayed

3.3 Specimen Size and Geometry Considerations

An image generated by μCT imaging of a rat femur is shown in Figure 13. The distal femur can be separated into three major sections, the epiphysis, growth plate, and

metaphysis. The epiphysis and metaphysis are separated by the growth plate, also called the physis, with the epiphysis located on the distal side. The metaphyseal cancellous bone is classified as either primary or secondary spongiosa. The primary spongiosa is characterized by axially oriented trabeculae that are protruding from the growth plate and consist of partially mineralized cartilaginous scaffolds. Secondary spongiosa is a matrix of trabeculae that are more randomly oriented forming a complex network of plates and rods and located proximal to the primary spongiosa.
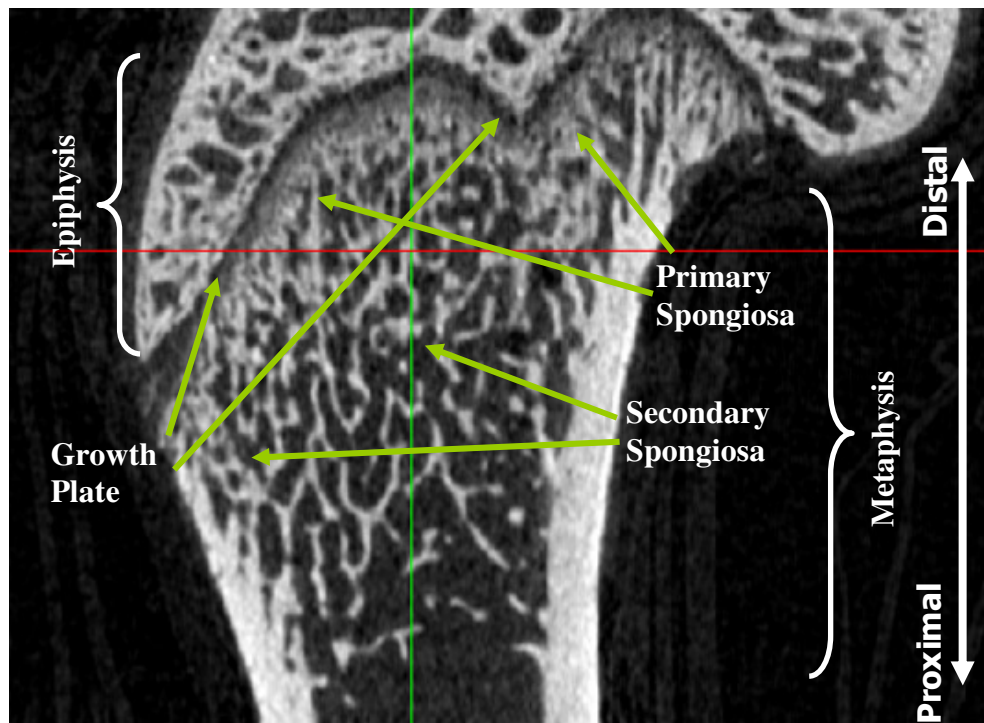
Figure 13: Distal Femur Anatomy in the Adult Female Rat

The cancellous region of bone that was evaluated is located in the distal end of the femur, just proximal to the growth plate and primary spongiosa. As seen in Figure 13, the amount of trabecular bone in the rat femur decreases as the distance from the growth plate increases. This area of bone can contain relatively dense or sparse amounts of cancellous bone, depending on the activity or hormonal status. Generally, the

osteopenic effects of disease tend to start in the cancellous bone located most proximal and central in the metaphysis and progress towards the growth plate. To further illustrate, consider the bone loss "weather front" as a cone starting at the proximal end of the cancellous region and moving towards the distal end.

In laboratory animal studies it is not unusual to have both ends of the density spectrum represented in a single study. In order to successfully extract specimens from animals having a wide range cancellous bone mass or trabecular networks, a critical task is determining the dimensions and anatomical location of the specimens. The method to be used for the preparing the specimens will be described in a later section, but the method produces a cylindrically shaped specimen. It is an exercise in optimization to determine the location and dimensions that allow for specimens to be successfully extracted. As previously mentioned, effects from buckling and friction play an important role in finding the optimal specimen geometry, and while they will be considered throughout the process, the most constraining factor geometrically is the amount of cancellous bone that is present in this metaphysis region.

The overarching goal is to have a robust method that can produce suitable specimens across a wide range of densities and micro-architectural parameters. The definition of "suitable" in this context is inherently subjective. Some basic considerations would be that the specimen can be cut without breaking apart, losing fragments, or being too fragile to handle and test. In addition, a reasonable level of connectivity would be desired along the peripheral edges of the cylindrical specimen. Obviously, lower density bone with provide the greatest challenges for producing suitable specimens.

3.3.1 Anatomic Location

The anatomic location of the cored specimen is an important factor due to the large variance in mechanical properties within a compartment of cancellous bone that has been demonstrated in other studies[20,21]. The four parameters that define the location of the core are: (1) the distance axially from the end of the bone (distal to proximal), (2) the location on the transverse plane, (3) the specimen length, and (4) the

specimen diameter. The second parameter is simply the center of the cancellous compartment. The first parameter requires a more in depth description and will be discussed in the next paragraph. The third and fourth parameters will be discussed in the following sections.

The general location of interest is the secondary spongiosa of the metaphysis region. Recall, in the rat's distal femur this location is proximal of the growth plate and the primary spongiosa, (see Figure 13). The μCT images were utilized to visualize this region in a number of specimens. From the images it was observed that the growth plate is not a flat transverse plane, but rather could be described topologically as a dome. The primary spongiosa follows the same contour. In general, this contour follows a dome-like form with the concave portion opening towards the proximal region. Thus, the location of the core's distal end was chosen to be just inside and proximal of this dome region. This location is distinguished on the transverse slice by using the triangular-shaped portion as an internal landmark, as seen in Figure 14.
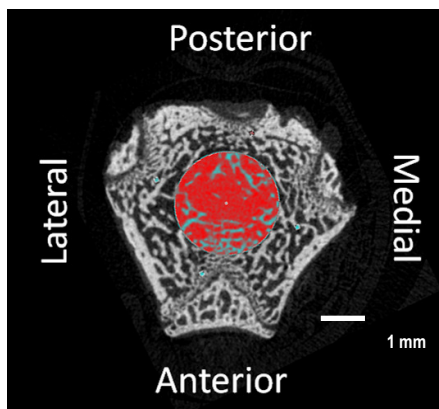
Figure 14: μCT Rendered Image of a Transverse Slice of the Rat Distal Femur: Illustrating the Location of the Distal End of the Typical Cored Specimen

Additionally, another consideration of the specimen size and location is how representative the cored specimen is of the region that is typically assessed through CT imaging. In this study, both the core specific CT region of interest and standard metaphyseal region of interest will be compared. Generally, the more proximal the

region of interest is selected the higher the expected change in bone content. Also, the bone is affected more at the central region. Considering these two factors it is hypothesized that the more proximally and centrally located cored specimen will be representative of the more distal standard metaphyseal region of interest. This will be addressed further in the discussion section.

3.3.2 Specimen Length Analysis

A brief pilot study was performed to evaluate the appropriate length of the specimen using μCT images. An initial review of the 2-dimensional μCT images placed the optimal length of the cylindrical specimen between 1.4 and 2 mm. Virtual cored specimens from six femurs in the lower density range across all three groups were constructed. The specimens were chosen because they would contain the least amount of bone mass to core. As illustrated in Figure 15 and Figure 16, disks of cancellous bone (0.1mm thick) corresponding with the cylindrical specimen's ROI were virtually sliced for the range of 1.4 to 2.0 mm (6 slices) with a diameter of 2.0 mm. Three-dimensional models were generated for the individual slices and for the entire cylindrical specimen and inspected visually. Additionally, these disks were evaluated by examining variations in micro-architecture and density parameters generated by the μCT analysis software. Specifically, BV/TV, vBMD, and trabecular bone pattern factor (Tb.Pf) were analyzed. The latter parameter is an indicator of connectivity of the trabecular rods and plates within the three-dimensional structure. The goal of the analysis was to evaluate parameters that could give insight into the "core-abilty" through a range of specimen lengths. Building the three-dimensional models allows for the specimen to be virtually cored and then inspected for connectivity and fullness of structure.
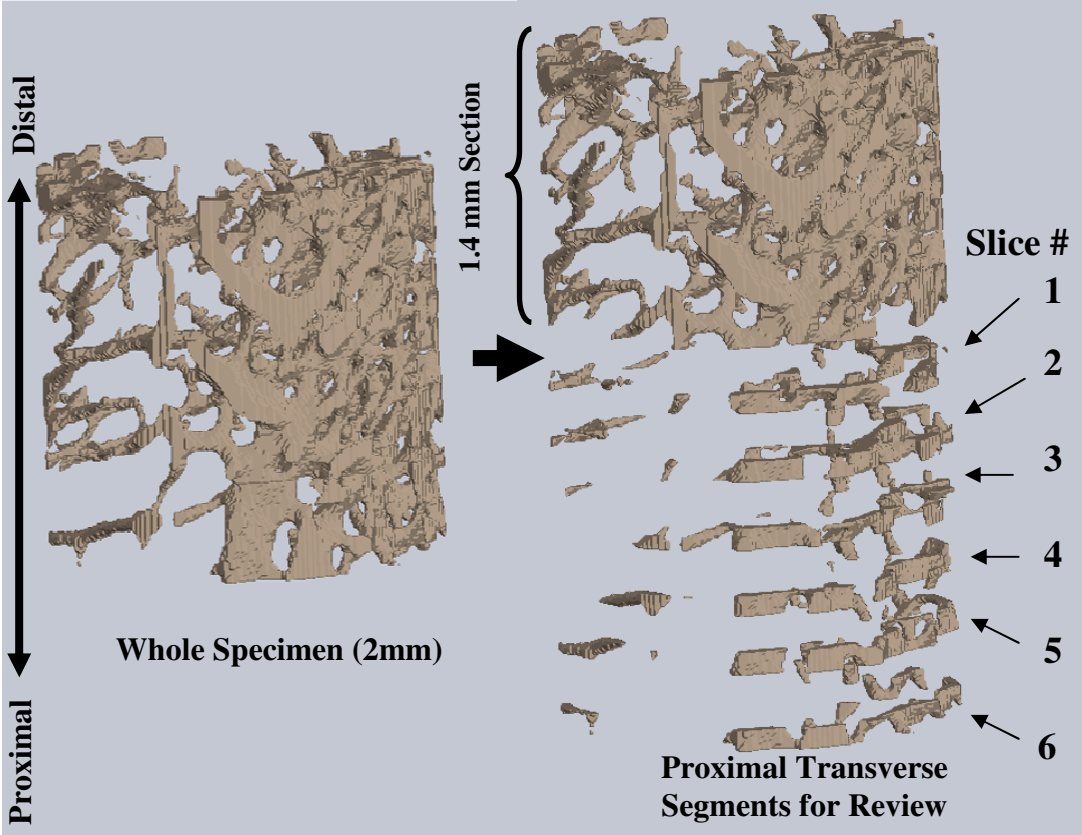
Figure 15: Perspective Views of 3-D Reconstruction
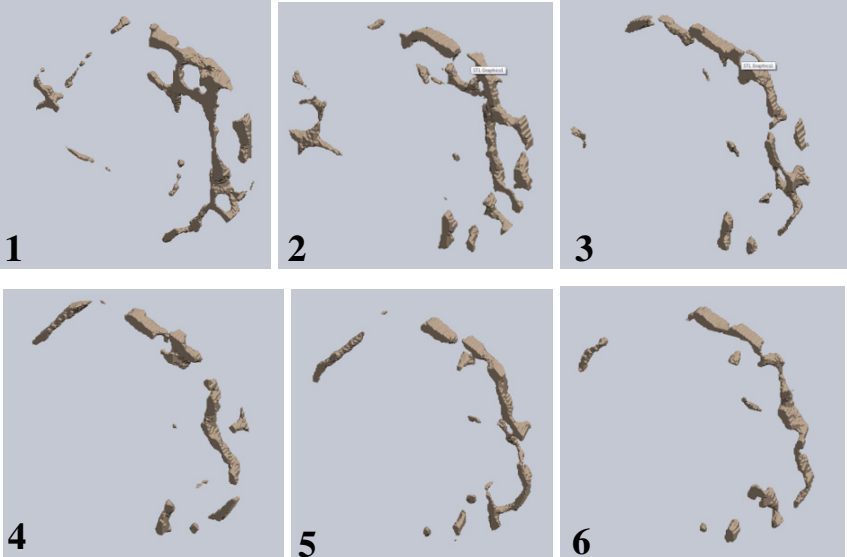
Figure 16: Cross Sectional Views

Visual inspection of virtual specimens proved to be the most useful tool for evaluating the possible core length. The sets of images for the six specimen can be found in Appendix A. The analysis of the bone parameters provided some useful insight, though Tb.Pf proved not as useful due to the small number and size of the trabeculae within the thin slices. To display the results this analysis graphically and quantitatively, each slice parameter value (BV/TV, vBMD) was represented as the percent of the corresponding value from the 1.4 mm distal section. These values were averaged for all six bones and are plotted in Figure 17 and Figure 18. The slice numbers on the graph correspond to those shown in Figure 15, thus slice 1 is portion of the cylindrical specimen from 1.4 to 1.5 mm. The results from the quantitative analysis did not show a clear drop in either vBMD or BV/TV only a trend towards lower values moving from distal to proximal. Considering both the visual inspection and these plots, a specimen height of 1.5 mm was chosen.
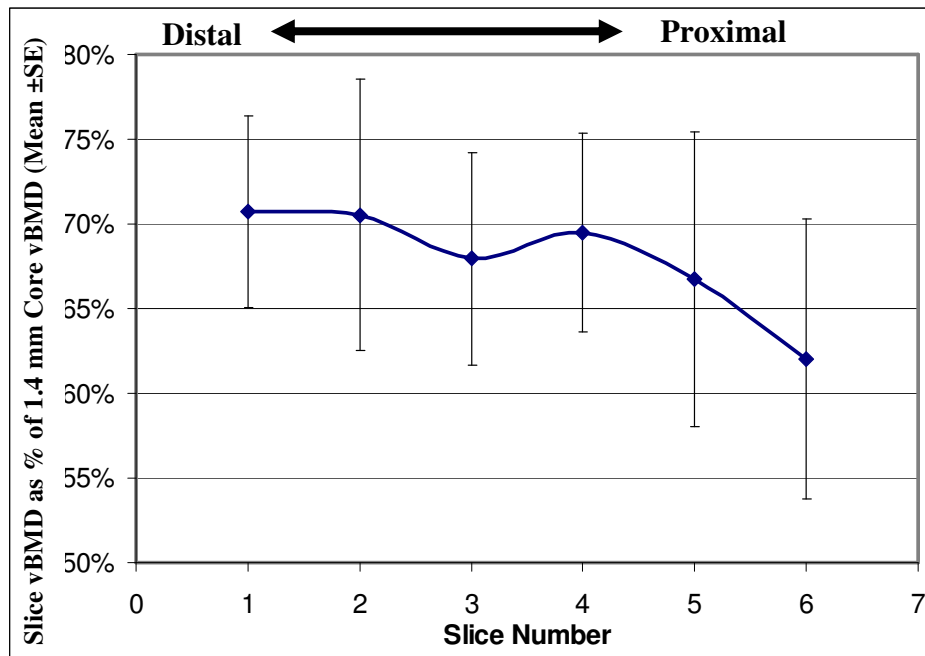
Figure 17: Normalized & Averaged BV/TV by Slice
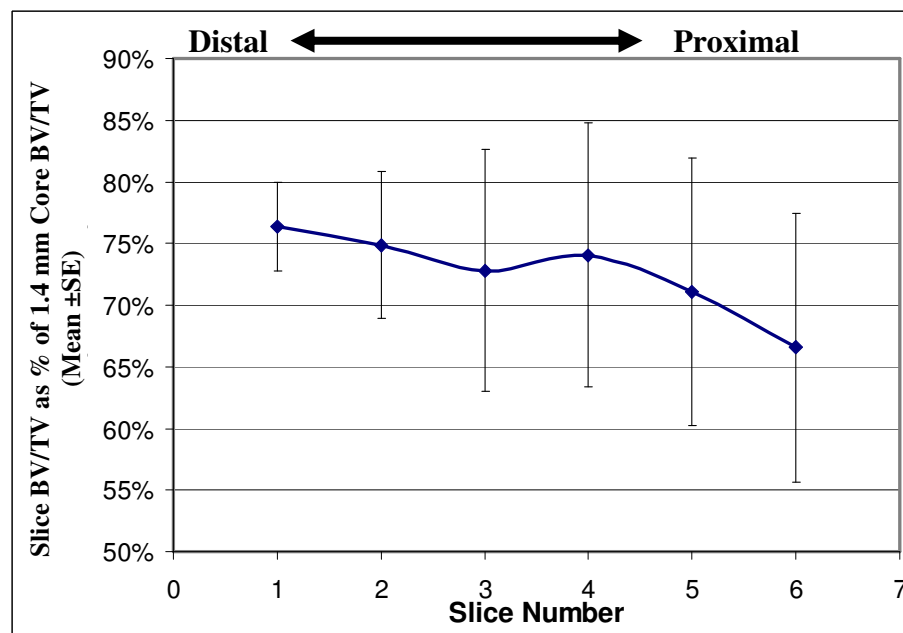
Figure 18: Normalized & Averaged vBMD by Slice

3.3.3 Specimen Diameter

Recall that in the RPC procedure the diameter of the platen is sized to the individual specimen. The cored specimen diameter for this project can also be customized to the individual femur's cancellous compartment and can be sized using similar imaging techniques; these procedures are described in the next section. The advantages and disadvantages of using a fixed diameter versus a specimen-specific diameter will be assessed briefly.

A fixed diameter allows for direct comparison of extrinsic properties between specimens. It also reduces the time and complexity required in the coring procedure. The benefit of using the specimen-specific diameter is that it reduces the systematic error introduced by using a uniform specimen core diameter on slices with a larger endocortical diameter. The center of the cancellous compartment is least dense, with the density of trabeculae generally increasing towards the cortical shell. Hence, if a fixed diameter is used the cores of specimens with larger endocortical diameters will be taken from a relatively lower density region, thereby systematically biasing the results. It should also be noted that in the literature review not a single reference was found that scaled the specimen size in the testing of cancellous bone from large animals and human cadavers based on the size of the cancellous compartment. The RPC method is the only method presented that scales the testing specimen (platen size) to the size of the cancellous compartment. The scaling of the specimens may be more applicable to the RPC method because of the confounding influence of the load sharing of the cortical shell. This is based on the intuitive assumption that the closer the outer edge of the platen is to the cortical wall, the larger the amount of the load sharing by the cortical wall. This is supported by the finite element modeling of the RPC method.[37]

It was found during the imaging of the specimens that the endocortical circle (EC) diameters for the specimens did not vary as much as expected. (See Appendix B) This unexpected finding, combined with all of the considerations listed above, factored in to the author's decision to use a fixed diameter of 2.3 mm, 80% of the average EC diameter (Figure 19). The variability of the EC diameter was minimal enough that even the specimen with the smallest EC diameter allowed for the cancellous core to machined

properly (i.e., the smallest EC diameter was sufficiently larger that the 2.3 mm core diameter). In studies with comparisons over large differences in animal age, the specimen-specific diameter might be more applicable.

3.4 Specimen Preparation Methods

A diamond wire saw (Well Diamond Wire Saws, Norcross, GA, USA) was utilized to cut the specimens. The diamond wire had a diameter of 130 microns with embedded 20 micron diamonds. Custom designed and fabricated fixtures were used in concert with the saw to core cancellous specimens from the distal metaphysis of the rat femur. These fixtures were designed using SolidWorks 2008 (SolidWorks Corporation, Concord, MA, USA). The engineering drawings can be found in Appendix C. The high precision machining tolerances, specified on the drawings, were required to provide a high level of precision in the coring method. The fixtures were fabricated by the Physics Department machine shop at Texas A&M University.

The first step in the procedure was to cut the transverse 1.5 mm thick section with the diamond wire saw from the metaphysis region. The first cut was taken 3.75 mm proximal from the distal end and the distinctive triangular-shape portion at the anterior edge was used to verify correct axial location as described in Section 3.3.1. If an additional cut was required the μCT images were utilized to determine the additional amount of bone to be removed. These slices were made carefully to ensure the orientation remained consistent between specimens. The thickness of the slice was measured using digital calipers. Then both the distal and proximal surfaces of each slice were photographed with a high resolution SLR camera and macroscopic lens (Nikon, Tokyo, Japan). The image was then analyzed to find the diameter of the largest possible endocortical circle (EC) (Figure 19) using a free software called GIMP GNU Image Manipulation Program version 2.6 (www.gimp.org). This process was completed for the entire batch of bones and then the EC diameters were averaged and the diameter of the cored specimens was calculated (i.e., 80% of the EC diameter).
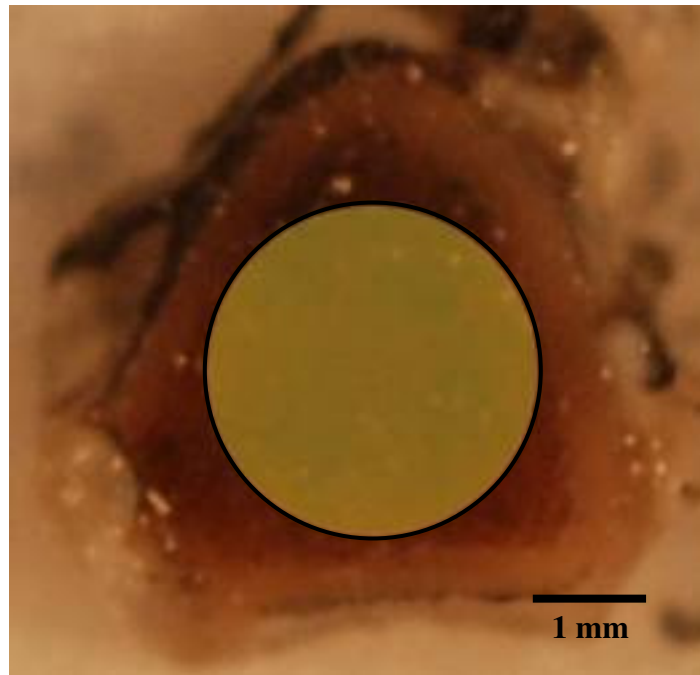
Figure 19: Endocortical Circle on the Proximal Face of the Rat Distal Femur

The next step in the isolated cancellous coring (ICC) process was to cut cylindrical core specimens from each 1.5mm thick slice. A major effort in this research was the design and fabrication of the fixtures for securing the specimen to allow accurate cutting of the cylindrical core. Equally important were the procedures for interfacing with the diamond wire saw to permit successful coring. The two main components of the coring system are the Specimen Holder and the Coring Fixture. The general coring set-up is shown in Figure 20. The bone slice is centered and clamped in the Specimen Holder with the securing pressure being applied to the cortical shell (Figure 21). The Specimen Holder is then placed in the Coring Fixture that is affixed to and aligned on the diamond wire saw micrometer table. The CAD assembly model of the coring system is shown in Figure 22. The Coring Fixture holds the Specimen Holder in such a way that ensures the cutting wire is a fixed distance from the center of the Specimen Holder and hence the specimen. As the Specimen Holder is moved into position the diamond wire cuts through the cortical shell of the bone. Once the wire has cut through the cortical shell it is in position, located at a distance equal to the radius of the core plus one-half of

the wire radius from the center. The Sliding Snugger is then moved into position to restrain the motion of the Specimen Holder to rotation only, as shown in Figure 20. The Specimen Holder is then rotated slowly by hand as the wire cuts a cylindrical specimen from the cancellous compartment of the bone. A Specimen Constraint (Fig. 17) is used to manually capture the cylindrical core to prevent it from being damaged when the cutting finishes and the cylindrical core is completely separated. Following the coring, the specimen is removed and the core is removed from the slice. The core and the remaining cortical shell were photographed and the diameter of each core was measured using the same method as previously described for the EC circle. Detailed procedures can be found in Appendix D.
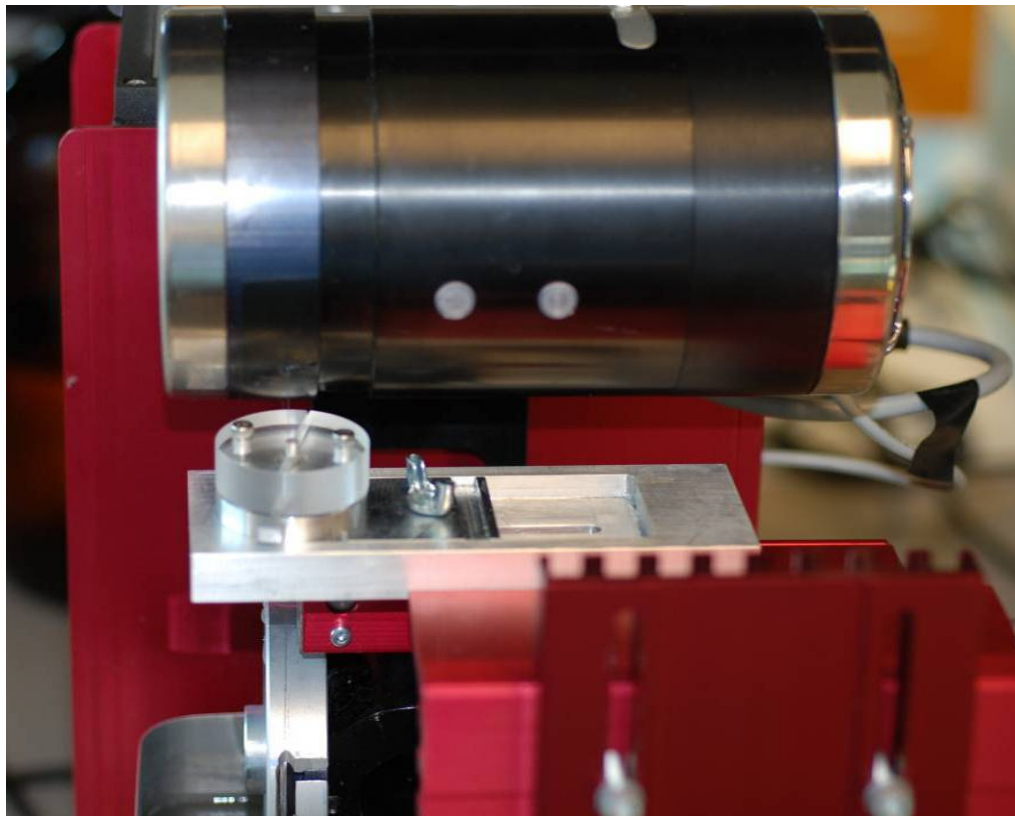
Figure 20: Diamond Wire Saw and Coring Fixture Assembly
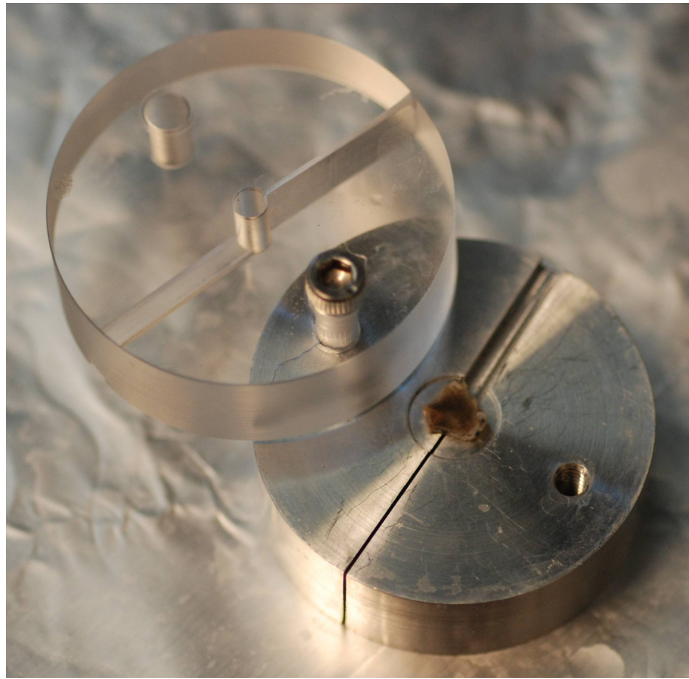
Figure 21: Specimen Holder with Machined Specimen Section Positioned in the Center
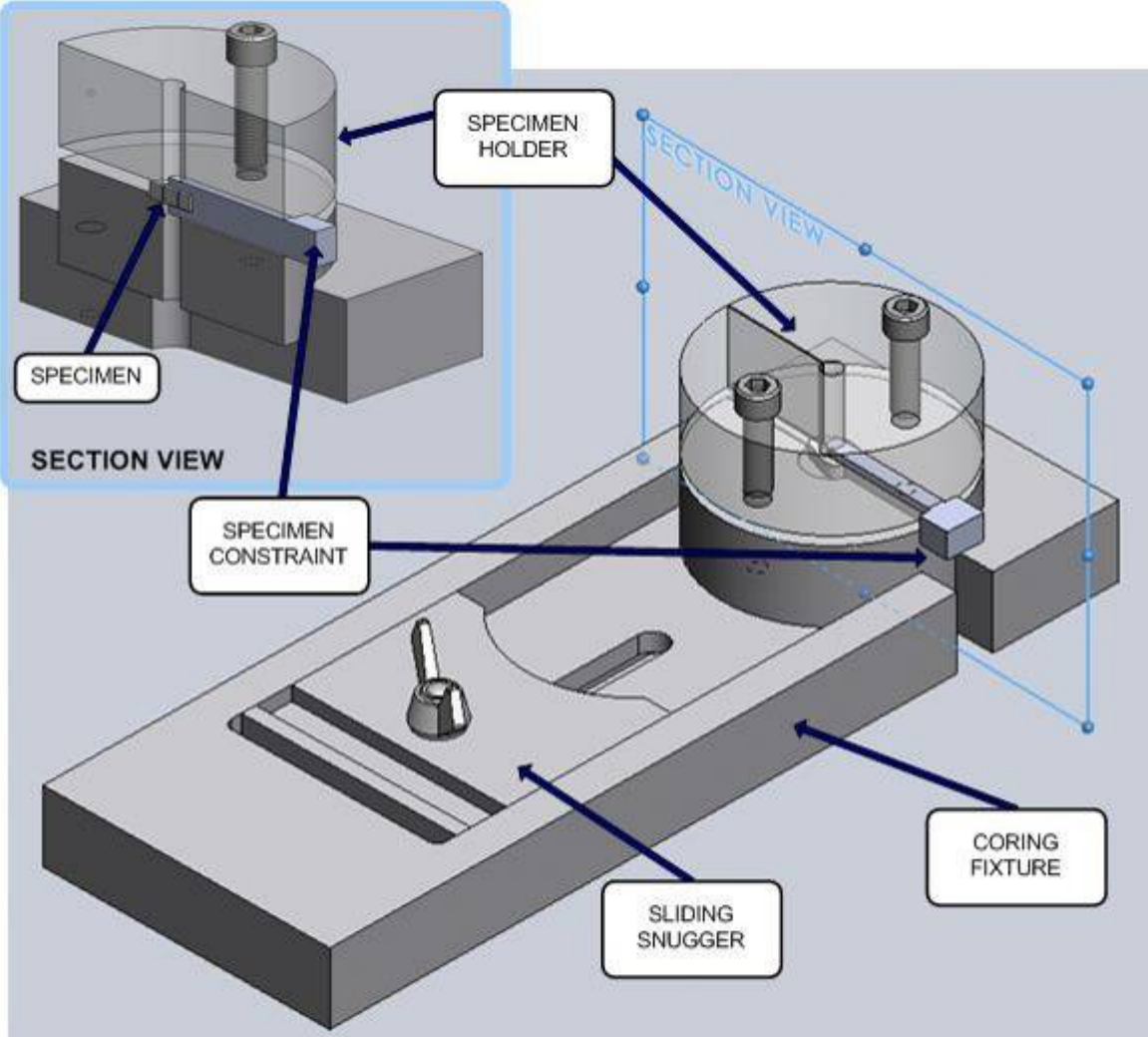
Figure 22: Coring Fixtures
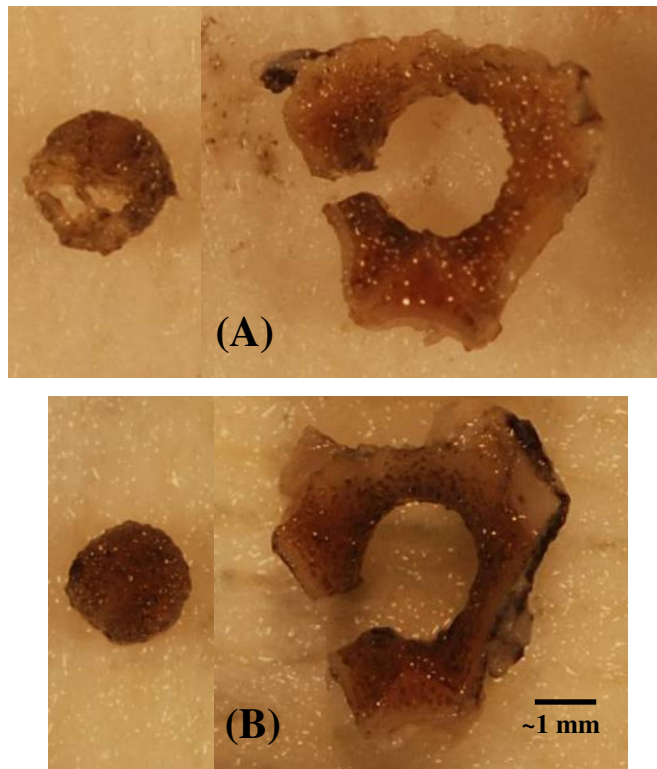
Figure 23: Representative Low (A) and High (B) Density Isolated Cancellous Cores

3.5 Compression Testing Method

The cylindrical specimens were tested under direct axial compression using an Instron 3345 mechanical testing machine and Instron Bluehill software (Instron, Norwood, MA, USA). A diagram of the testing set up is shown in Figure 24. The apparatus consists of two plano-parallel platens, a linearly variable displacement transducer (LVDT) directly attached to the platens to measure displacement, and a 100-N load cell that records the force. A low viscosity mineral oil lubricant is applied to the surfaces of the platens to reduce contact friction with the specimen. The specimen is centered on the lower platen with a surgical spatula. The test begins with a pre-load of 0.2 N, which is considered the zero-strain point. Next, cyclic loading is used to precondition the specimen. The cyclic loading is a triangular waveform loading to 0.3% strain for 5 cycles at a displacement rate of 0.015 mm/s (1 %/s). Following the preconditioning the specimen is loaded to failure at a displacement rate of 0.015 mm/s (1

%/s).   This test method was developed using Instron Bluehill software.   The displacement rate is considered to be both quasi-static and physiological.[30]   The specimen was kept hydrated with distilled water through the entire testing process.
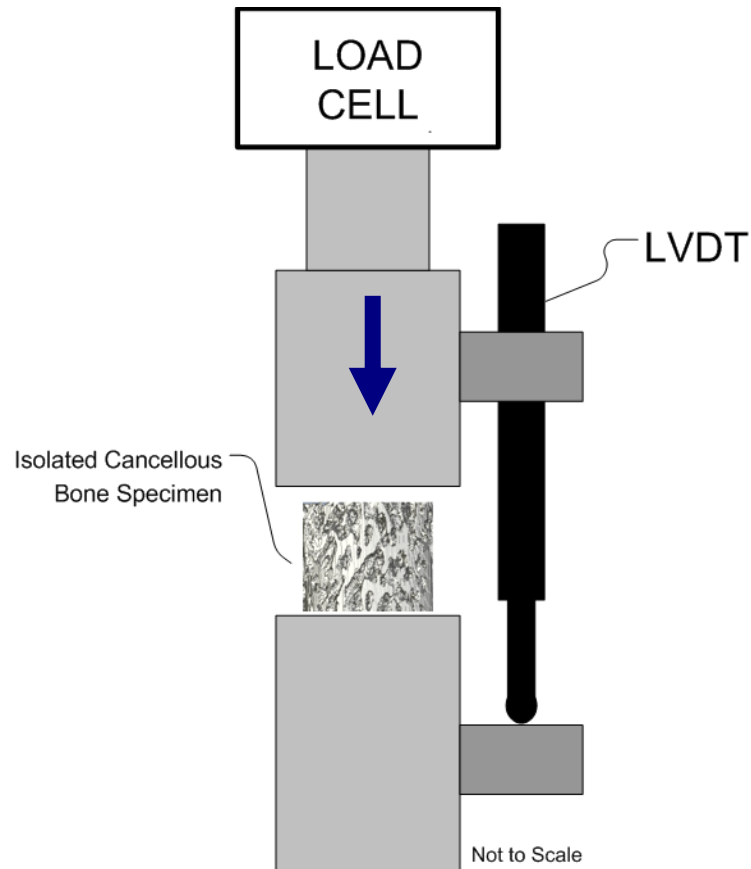
Figure 24: Mechanical Testing Set-Up

3.6 Apparent Density

Following mechanical testing, the wet mass (m_w) of each cored specimen was measured. The bulk volume, V_B, of the cube was determined from the diameter obtained through the image analysis and the height measured by the digital calipers.   Apparent density, ρ_A, was calculated by Equation 3.

$$\rho_A = \frac{m_w}{V_B} \qquad (3)$$

3.7 Analysis

3.7.1 Analysis of Mechanical Testing Data

      The extrinsic mechanical properties were calculated from the load-displacement curves generated by the testing. A typical force-deflection (F-D) curve can be seen in Figure 25 with the extrinsic properties labeled. The yield point was determined by a 95% of the stiffness slope method.   In this method, 95% of the slope of the linear portion of the F-D curve (i.e. stiffness) is calculated and a new line is using this slope (95% of stiffness) and the original x-intercept is drawn. The location where this new line crossed the F-D curve is the chosen as the yield point. The first local minimum on the load-deflection curve after the ultimate load was considered to be the end of the test. The extrinsic properties include stiffness (k ; N/mm), ultimate force (F_u ; N), yield force (F_y ; N), resilience (energy to yield) (W_y ; N-mm), energy to ultimate force (W_u ; N-mm), and energy to the first minimum, or end of test (W_f ; N-mm). All analyses were performed using Microsoft Excel and *DATMeT 3.0*, a custom MATLAB analysis program developed by S. Bouse.[38] For three of the compression tests, the yield point calculated by the 95% method was located after the ultimate force on the F-D curve. For these three instances, the values at the ultimate force were assumed to be also the yield values.

      From the extrinsic properties aforementioned the intrinsic properties are calculated. These include elastic modulus (E; MPa), ultimate stress (σ_u ; MPa), yield stress (σ_y ; MPa), strain at ultimate (ε_u ; mm/mm) and yield (ε_y ; mm/mm), toughness to yield (T_y ; N/mm^2), and toughness to ultimate stress (T_u ; N/mm^2). Toughness is also referred to as Strain Energy Density (SED). These properties account for the slight area and height differences between the specimens. The formulas are given in equations 4-9, where *h* is height, *A* is bulk area, and *V* is bulk volume (*V=hA*) of the specimen.
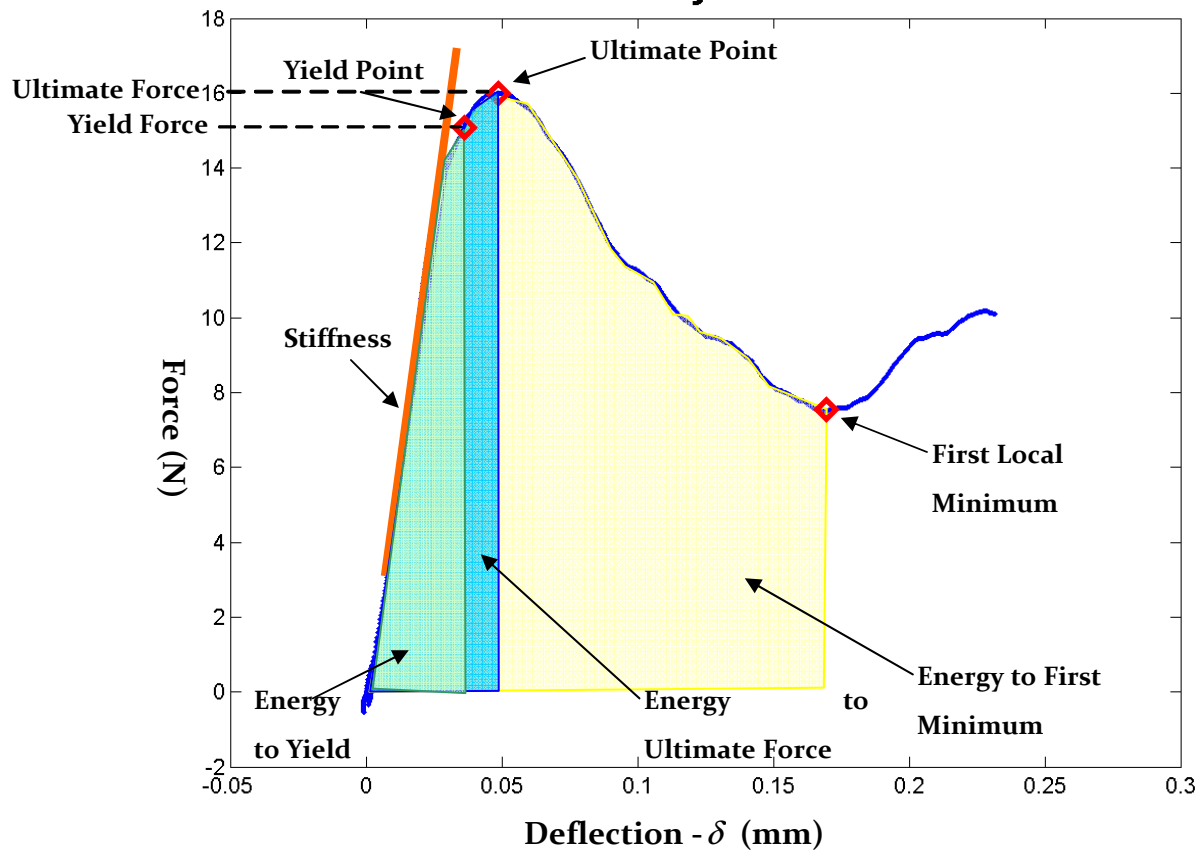
Figure 25: Typical ICC Force Deflection Plot from Compression Testing of Cored Cancellous Specimen from the Rat Distal Femur.

$$E = \frac{kh}{A} \quad (4)$$

$$\sigma_u = \frac{F_u}{A} \quad (5)$$

$$\sigma_y = \frac{F_y}{A} \quad (6)$$

$$\varepsilon = \frac{\delta}{h} \quad (7)$$

$$T_y = \frac{W_y}{V} \quad (8)$$

$$T_u = \frac{W_u}{V} \quad (9)$$

In this context, the intrinsic properties can be considered as properties of the effective or bulk material, which in effect is a highly porous material comprised of solid trabecular material and the void spaces in between.

3.7.2 Material Properties

An additional approach used by some investigators to assess mechanical properties of cancellous bone is to normalize by BV/TV. These material level properties were determined for stress, elastic modulus, and toughness for each individual specimen. Essentially, by dividing each value by BV/TV, the bulk cross sectional area, *A*, used in Equations 4-6 and 8-9 is replaced by the average bone area. Therefore, this approach provides an averaged estimate of the properties of the solid-phase or mineralized cancellous bone tissue.

3.7.3 Core-Specific μCT Analysis

Standard μCT analysis of the metaphyseal cancellous bone was conducted by M.R. Allen, as described previously (Section 3.2.1). In addition μCT analysis was also conducted for an ROI that matched, as closely as possible, the cored specimen. This was done in order to: (1) ensure that the specimens were taken from a location that was representative of the overall cancellous region and (2) to have specimen-specific values to compare with the mechanical testing results. This ROI-matching process was done utilizing the photographs taken before and after coring of the distal and proximal transverse faces of the slices and the measured dimensions of the core to define the core-specific ROI (Figure 26). The detailed procedure for this analysis is in Appendix E.

(A)
Photograph of section after
removal of the core.

(B)
Corresponding µCT rendering
with ROI highlighted in red.
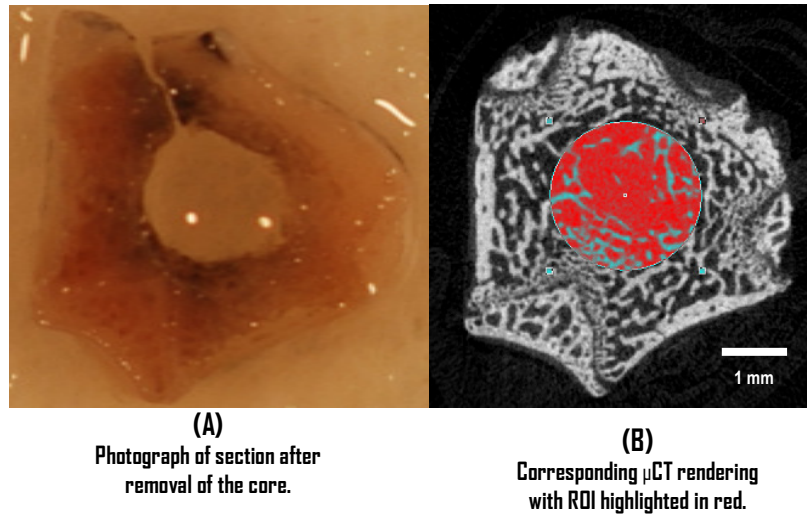
Figure 26: Example of Core-Specific ROI Selection

3.7.4 Statistical Analyses and Regressions

All statistical analysis was performed using SigmaStat (Systat, San Jose, CA). Comparisons were made between group means using unpaired t-tests if normality or equal variance assumptions were satisfied; if not, then a Mann-Whitney Rank Sum Test was performed. Statistical significance was defined by p<0.05. Also, one-way Fisher LSD ANOVA's were used to compare all three groups, the results of this analysis can be found in Appendix F. Chauvenet's criterion was used to exclude outliers in the mechanical testing data. Power law regressions were also performed in SigmaStat using a custom written non-linear regression function to correlate mechanical properties with density and micro-architectural parameters. Linear regressions were also performed. Additionally, multiple regressions that correlated mechanical testing results such as ultimate strength or elastic modulus as the dependent variable with multiple independent variables such as BV/TV, anisotropy, or BMD were found using custom non-linear power law regression functions. For the regressions, the standard error of estimation is given by equation 10, where P_i is the predicted value and O_i is the observed value.

$$SE_{Est.} = \sqrt{\frac{1}{n-2}\sum_{i=1}^{n}\left(P_i - O_i\right)^2} \quad (10)$$

4. RESULTS

4.1 Specimen Preparation

Forty-one out of forty-two specimens were successfully cored. The failed specimen was an extra bone (lacking a μCT image) from the OVX group. Since the bone had a pQCT cancellous BMD of 239.5 mg/cm3, the highest in OVX group, the failure was attributed to human error. It was assumed that the specimens that failed to be cored would be from the lowest density bones, but this was not the case. The range of applicability for coring the specimens in terms of the pQCT and μCT parameters is given in Table 1. The target dimensions were a diameter of 2.3 mm and a height of 1.5mm. The actual dimensions (Figure 27) varied slightly with averages ± S.D. of 2.29 ± 0.064 mm for the diameter, 1.53 ± 0.048 mm for the height, and a resulting 4.12 ± 0.22 mm^2 for the area. The coefficients of variance are 2.8%, 3.13%, and 5.49% for the diameter, height, and area, respectively.   One specimen in the OVX+E2 group was inadvertently cut too close to the growth plate and was not used. For each specimen the distance from the distal end of the bone to the slice location is given in Appendix G.
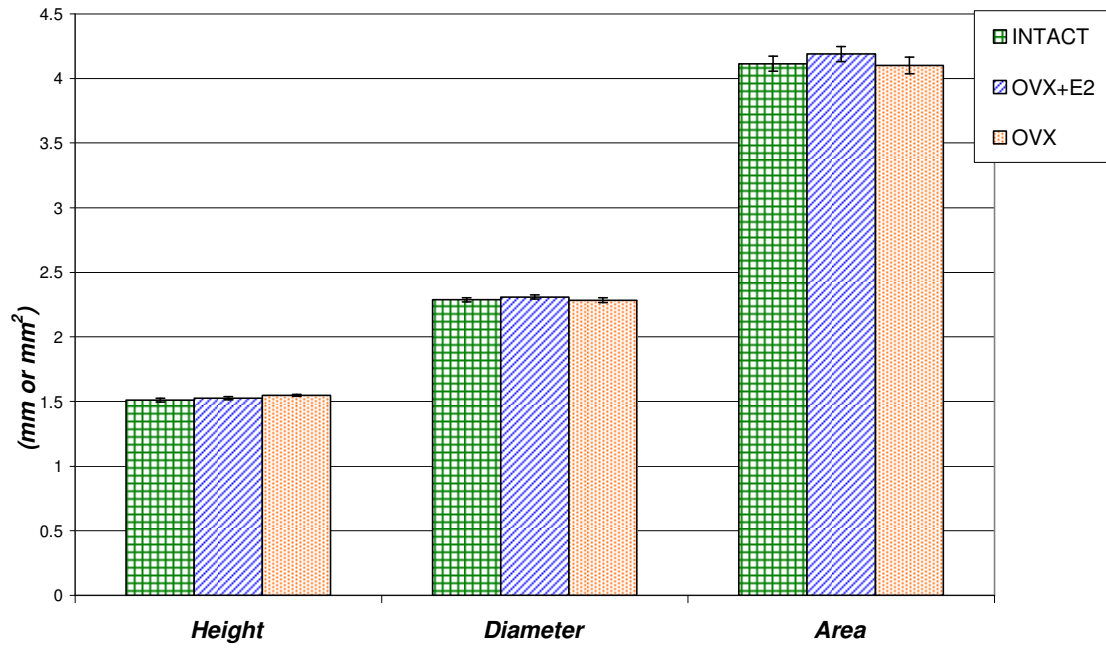
Figure 27: Cored Specimen Geometry of Samples from the Rat Distal Femur

Table 1: Range of Applicability for the Coring Method

Metaphyseal µCT Parameters	RANGE
BV/TV, %	10.5 - 43.3
Trabecular Thickness, mm	0.09 - 0.11
Trabecular number, 1/mm	1.22 - 4.33
Trabecular separation, mm	0.16 - 0.37
Trabecular Pattern Factor, 1/mm	0.88 - 15.99
Structural Model Index	0.90 - 2.21
vBMD, mg/cm^3	119.9 - 456.6
Core Specific µCT Parameters	
BV/TV, %	9.8 - 42.7
Trabecular Thickness, mm	0.08 - 0.11
Trabecular number, 1/mm	1.14 - 4.23
Trabecular separation, mm	0.16 - 0.60
Trabecular Pattern Factor, 1/mm	-4.79 - 15.87
Structural Model Index	0.30 - 2.23
vBMD, mg/cm^3	74.4 - 440.1
pQCT Parameters	
Cancellous vBMD, mg/cm^3	104.6 - 452.9
Total vBMD, mg/cm^3	539.7 - 723.8
Other	
Apparent Density (g/cm^3)	0.3 - 1.3

4.2 Computed Tomography (CT) Results

Table 2, the results from the metaphyseal cancellous µCT analysis performed by M. Allen are presented. The properties from the OVX+E2 and INTACT groups are not significantly different. Across all groups there is no significant difference in trabecular

thickness (Tb.Th.). Considering OVX in comparison to INTACT and OVX+E2 there is a significant difference in all properties, with the exception of Tb.Th. OVX is characterized with a higher SMI indicating a more rod-like structure. Also, OVX has a much lower vBMD (-37.3%) and BV/TV (-43.1%) compared to INTACT.

Table 2: Metaphyseal μCT Results (M. Allen)

	INTACT (n=12)	OVX (n=11)	OVX+E2 (n=13)	INTACT-OVX+E2	OVX+E2-OVX	INTACT-OVX
BV/TV, (%)	28.67 ± 1.64	16.32 ± 0.91 (-43.1%)	25.67 ± 1.42 (-10.5%)	N.S.	p=<0.001	p=<0.001
Tb.Th (mm)	0.093 ± 0.001	0.094 ± 0.002 (1.8%)	0.093 ± 0.002 (0.2%)	N.S.	N.S.	N.S.
Tb.N (1/mm)	3.10 ± 0.16	1.73 ± 0.09 (-44.0%)	2.75 ± 0.12 (-11.0%)	*p=0.088*	p=<0.001	p=<0.001
Tb.Sp (mm)	0.22 ± 0.01	0.33 ± 0.01 (51.0%)	0.24 ± 0.01 (11.4%)	*p=0.088*	p=<0.001	p=<0.001
Tb.Pf (1/mm)	7.49 ± 0.69	12.64 ± 0.44 (68.8%)	8.45 ± 0.68 (12.8%)	N.S.	p=<0.001	p=<0.001
SMI	1.53 ± 0.06	2.04 ± 0.03 (32.8%)	1.59 ± 0.05 (3.8%)	N.S.	p=<0.001	p=<0.001
vBMD (mg/cm3)	337.10 ± 14.80	211.33 ± 11.95 (-37.3%)	304.24 ± 14.17 (-9.7%)	p=0.03	p=<0.001	p=<0.001

Values given as Mean ± SE   N.S. - Not Significant, Values in *italics* are also not significant
Percents in parentheses are differences in the mean values with respect to INTACT

In order to obtain tomography data that were specific to the cores that were obtained through the ICC procedure, additional analysis was done as outlined in Section 3.7.3 (pg. 37). One specimen from the INTACT group was damaged in the testing set-up and is not included these results nor the mechanical testing results. The results of this analysis are presented in Table 3. This analysis is interrogating the central portion of the cancellous compartment and seemingly yields a more sensitive measurement of micro-architecture and density parameters than that of the metaphyseal μCT analysis. This higher sensitivity is indicated by larger percent differences between the INTACT and the OVX and OVX+E2 groups. The degree of anisotropy (DA) for the specimens did not significantly vary between the treatment groups for the core-specific μCT parameters. This is explained by two factors; one, anisotropy seems to be driven by the bone function and the loads applied to the bone, which would be similar between groups, and

two, care was taken to ensure the orientation of the slice taken was the same for all specimens. With the exception of Tb.Th and DA, the differences between all group properties were significant for the core-specific µCT parameters. The SMI shows a more plate-like structure for the INTACT group, with the OVX group being rod-like and OVX+E2 representing a mixture of rod and plate structure. The large difference in Tb.Pf indicates a much lower level connectivity in the OVX group with respect to the INTACT and a significantly lower, though not as drastic a difference, between the OVX+E2 and INTACT groups. The estrogen replacement seems to, at least partially, mitigate the losses in vBMD and BV/TV.

Table 3: Core Specific µCT Results

	INTACT (n=11)	OVX (n=11)	OVX+E2 (n=12)	INTACT-OVX+E2	OVX+E2-OVX	INTACT-OVX
BV/TV (%)	33.23 ± 1.99	13.69 ± 0.96 (-58.8%)	25.53 ± 1.70 (-23.2%)	p=0.008	p=<0.001	p=<0.001
Tb.Th (mm)	0.093 ± 0.002	0.091 ± 0.002 (-2.8%)	0.090 ± 0.002 (-3.4%)	N.S.	N.S.	N.S.
Tb.N (1/mm)	3.56 ± 0.18	1.50 ± 0.09 (-57.7%)	2.83 ± 0.16 (-20.5%)	p=0.007	p=<0.001	p=<0.001
Tb.Sp (mm)	0.20 ± 0.01	0.47 ± 0.02 (130.2%)	0.26 ± 0.01 (25.8%)	p=0.009	p=<0.001	p=<0.001
Tb.Pf (1/mm)	1.73 ± 1.18	12.39 ± 0.74 (616.9%)	5.46 ± 1.25 (216.0%)	p=0.042	p=<0.001	p=<0.001
SMI	0.93 ± 0.12	2.01 ± 0.05 (115.7%)	1.30 ± 0.11 (39.4%)	p=0.038	p=<0.001	p=<0.001
vBMD (mg/cm3)	362.39 ± 16.06	178.11 ± 15.00 (-50.8%)	290.85 ± 15.12 (-19.7%)	p=0.004	p=<0.001	p=<0.001
DA	1.87 ± 0.05	1.73 ± 0.06 (-7.2%)	1.84 ± 0.05 (-1.4%)	N.S.	N.S.	N.S.

Values given as Mean ± SE   N.S. - Not Significant, Values in *italics* are also not significant
Percents in parentheses are differences in the mean values with respect to INTACT

The results from the pQCT analysis are presented in Table 4. In contrast to the metaphyseal µCT analysis, there is a significant difference between the OVX+E2 and INTACT groups, with OVX+E2 being 14.4% lower. Recall, that these results include a larger number of specimens in INTACT group than the results from both the µCT analyses.

Table 4: Results from the pQCT Analysis

	INTACT (n=17)	OVX (n=11)	OVX+E2 (n=13)	INTACT-OVX+E2	OVX+E2-OVX	INTACT-OVX
Cancellous vBMD (mg/cm^3)	330.84 ± 17.86	163.08 ± 11.69 (-50.7%)	283.34 ± 9.70 (-14.4%)	p=0.03	p=<0.001	p=<0.001
Total vBMD (mg/cm^3)	673.99 ± 7.70	568.65 ± 8.33 (-15.6%)	656.65 ± 7.30 (-2.6%)	N.S.	p=<0.001	p=<0.001

Values given as Mean ± SE   N.S. - Not Significant, Values in *italics* are also not significant

Percents in parentheses are differences in the mean values with respect to INTACT

4.3 Mechanical Properties

The potential for end-artifact error was a concern as mentioned in Section 2.3.4.2, and cyclic loading and lubricated platens were used to try to minimize this error. Based on the visual inspection of the force-deflection curves only a small portion of the compression tests had the entrance toe and, in the cases that the toe existed, they appeared minimal. The extrinsic properties are presented Table 5 and the intrinsic properties in Table 6; results from the t-tests are given in the three right-most columns. The extrinsic properties are included for thoroughness and to show the similarity they exhibit with the intrinsic properties. The intrinsic properties account for the volume and area effects as defined in Equations 4-9, so these properties will be the focus of the following discussion. To better display the data visually, bar charts are included for the intrinsic properties in Figure 28 and Figure 29. The first minimum values represent the end of the test and provide insight into the post-yield behavior of the specimen. This first minimum could be considered the point where the specimens begin to compact causing the force to rise. It is interesting to note that the strain at first minimum is significantly larger in the OVX than both the INTACT and OVX+E2 groups. This could be due to the higher spacing between the trabeculae as seen by the μCT results in Table 3. This may be a factor of clinical relevance as tightly spaced trabeculae could possibly limit the degree of damage caused by a fracture. The strain at yield and max force are both fairly constant throughout the groups. For toughness, stress, and elastic modulus both the OVX+E2 and the OVX had significantly lower values than that of the INTACT group, with the exception of toughness to yield. The lower values were expected for the

OVX group, but the magnitude of the difference between the OVX+E2 group and the INTACT group was not expected based on the CT results.

Results for the solid-phase material properties, defined in Section 3.7.2 are summarized in Table 7. There seems to be very little difference between the OVX+E2 and OVX groups with surprisingly slightly higher non-significant material toughness values. The only significant difference found was in the toughness to max force between the OVX+E2 and INTACT groups. There seems to be a trend towards lower values for the OVX+E2 and OVX groups.

Table 5: Extrinsic Mechanical Properties

Extrinsic Property	INTACT (n=16)	OVX (n=11)	OVX+E2 (n=12)	INTACT-OVX+E2	OVX+E2-OVX	INTACT-OVX
Stiffness (N/mm)	822.60 ± 133.15	205.69 ± 48.62 (-75.0%)	413.67 ± 59.33 (-49.7%)	*p=0.082*	p=0.011	p=<0.001
Yield Force (N)	20.82 ± 2.51	6.41 ± 1.46 (-69.2%)	12.42 ± 1.13 (-40.3%)	N.S	p=0.003	p=<0.001
Ultimate Force (N)	24.314 ± 2.958	7.137 ± 1.582 (-70.6%)	13.979 ± 1.247 (-42.5%)	p=0.06	p=0.005	p=<0.001
First Minimum (N)	12.19 ± 1.45	3.62 ± 0.87 (-70.3%)	6.93 ± 1.12 (-43.1%)	*p=0.088*	p=0.007	p=<0.001
Yield Displacement (mm)	0.047 ± 0.005	0.047 ± 0.018 (-0.7%)	0.052 ± 0.006 (10.3%)	N.S	N.S.	N.S.
Disp. at Max Force (mm)	0.061 ± 0.003	0.061 ± 0.006 (-0.1%)	0.065 ± 0.005 (7.9%)	N.S	N.S.	N.S.
Disp. at First Minimum (mm)	0.135 ± 0.009	0.189 ± 0.016 (40.5%)	0.146 ± 0.009 (8.4%)	N.S	p=0.015	p=<0.001
Energy to Yield (mJ)	0.370 ± 0.049	0.907 ± 0.030 (145.0%)	0.252 ± 0.042 (-31.8%)	N.S	p=0.004	p=0.001
Energy to Max Force (mJ)	0.716 ± 0.075	0.231 ± 0.047 (-67.7%)	0.439 ± 0.053 (-38.7%)	p=0.017	p=0.005	p=<0.001
Energy to First Minimum (mJ)	2.07 ± 0.24	0.91 ± 0.20 (-56.3%)	1.35 ± 0.15 (-34.9%)	N.S	p=0.044	p=0.002

Values given as Mean ± SE   N.S. - Not Significant, Values in *italics* are also not significant
Percents in parentheses are differences in the mean values with respect to INTACT

Table 6: Intrinsic Mechanical Properties

Intrinsic Property	INTACT (n=16)	OVX (n=11)	OVX+E2 (n=12)	INTACT-OVX+E2	OVX+E2-OVX	INTACT-OVX
Elastic Modulus (MPa)	300.72 ± 48.23	76.92 ± 18.31 (-74.4%)	151.65 ± 20.73 (-49.6%)	p=0.032	p=0.015	p=<0.001
Yield Stress (MPa)	5.03 ± 0.58	1.56 ± 0.36 (-68.9%)	3.00 ± 0.27 (-40.3%)	p=0.015	p=0.005	p=<0.001
Ultimate Stress (MPa)	5.889 ± 0.689	1.740 ± 0.393 (-70.4%)	3.378 ± 0.301 (-42.6%)	p=0.013	p=0.003	p=<0.001
First Minimum Stress (MPa)	2.97 ± 0.35	0.89 ± 0.22 (-70.1%)	1.68 ± 0.27 (-43.4%)	p=0.011	p=0.018	p=<0.001
Strain at Yield (mm/mm)	0.0313 ± 0.003	0.0306 ± 0.004 (-2.4%)	0.034 ± 0.004 (9.5%)	N.S	N.S.	N.S.
Strain at Max Force (mm/mm)	0.040 ± 0.002	0.039 ± 0.004 (-2.5%)	0.043 ± 0.003 (6.4%)	N.S.	N.S.	N.S.
Strain at First Minimum (mm/mm)	0.089 ± 0.006	0.122 ± 0.011 (37.9%)	0.096 ± 0.006 (7.6%)	N.S.	p=0.032	p=0.002
Toughness to Yield (95%) (mJ/mm^3)	0.059 ± 0.007	0.021 ± 0.005 (-64.7%)	0.040 ± 0.007 (-31.6%)	*p=0.081*	p=0.004	p=<0.001
Toughness to Max Force (mJ/mm^3)	0.116 ± 0.012	0.037 ± 0.008 (-68.1%)	0.070 ± 0.008 (-40.0%)	p=0.022	p=0.009	p=<0.001
Toughness to First Minimum (mJ/mm^3)	0.33 ± 0.04	0.14 ± 0.03 (-56.8%)	0.21 ± 0.02 (-35.5%)	p=0.021	*p=0.093*	p=0.002

Values given as Mean ± SE   N.S. - Not Significant, Values in *italics* are also not significant
Percents in parentheses are differences in the mean values with respect to INTACT

Figure 28: Average Stress & Modulus Values
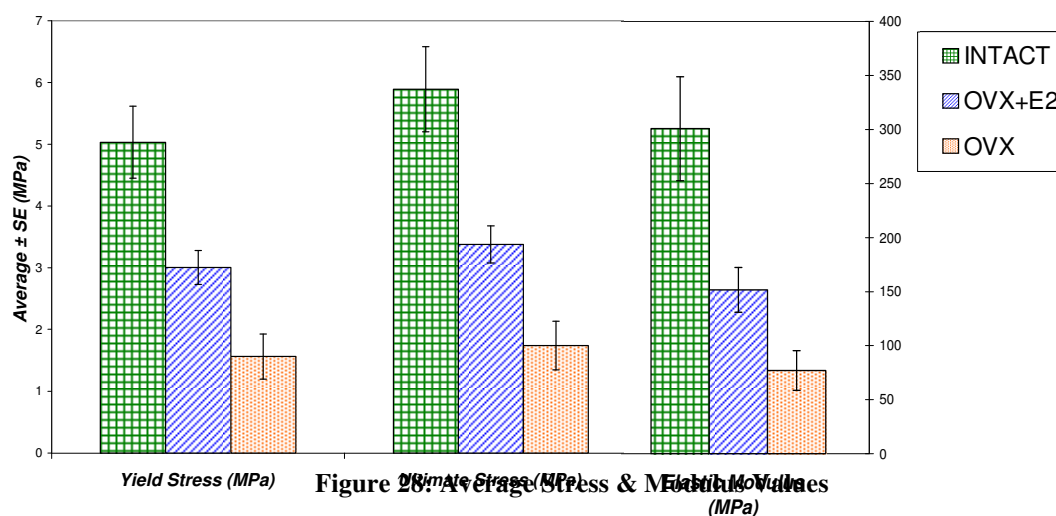
All group comparisons within mechanical property group are significantly different (p<0.05). See Table 6 for specific p-values.
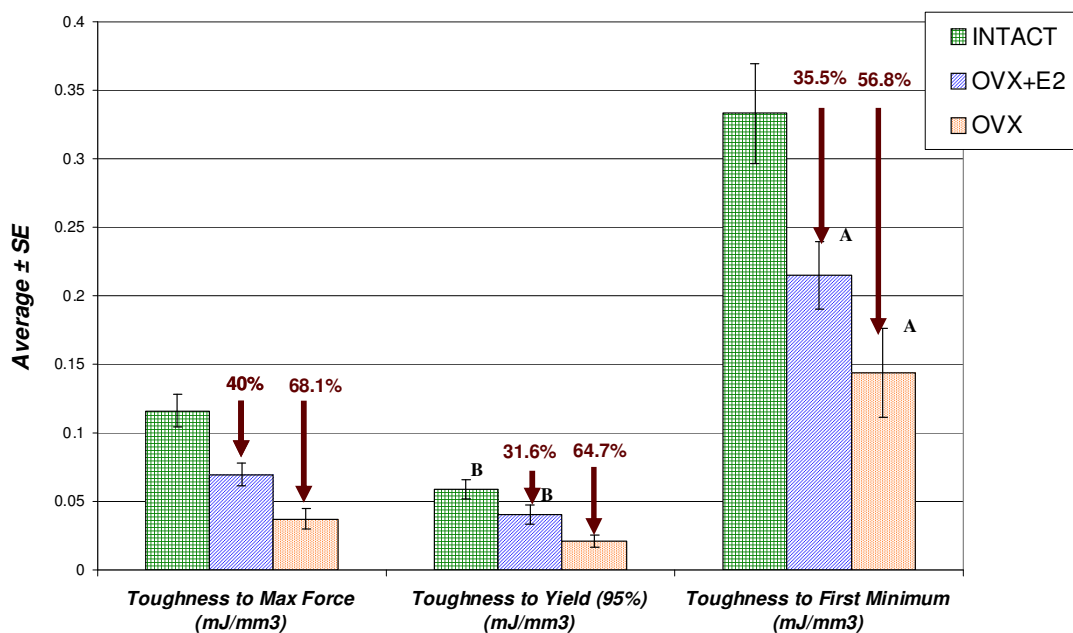
All group comparisons within mechanical property group are significantly different (p<0.05) except those with the same letter. See Table 6 for specific p-values.

Figure 29: Average Toughness Values

Table 7: Material Level Mechanical Properties

Material Property	INTACT (n=11)	OVX (n=11)	OVX+E2 (n=12)	INTACT-OVX+E2	OVX+E2-OVX	INTACT-OVX
Modulus/ [BV/TV] (MPa)	808.6 ± 204.1	556.3 ± 120.4 (-31.2%)	616.3 ± 89.9 (-23.8%)	N.S.	N.S.	N.S.
Yield Stress/ [BV/TV] (MPa)	15.06 ± 2.25	11.15 ± 2.01 (-26.0%)	11.80 ± 0.82 (-21.6%)	N.S.	N.S.	N.S.
Ultimate Stress / [BV/TV] (MPa)	17.91 ± 2.63	12.51 ± 2.28 (-30.1%)	13.28 ± 0.96 (-25.9%)	N.S.	N.S.	N.S.
First Minimum Stress / [BV/TV] (MPa)	8.94 ± 1.30	6.26 ± 1.12 (-30.0%)	6.32 ± 0.77 (-29.3%)	p=0.065	N.S.	N.S.
Toughness to Yield (95%) / [BV/TV] (mJ/mm^3)	0.184 ± 0.022	0.152 ± 0.027 (-17.4%)	0.151 ± 0.018 (-17.9%)	N.S.	N.S.	N.S.
Toughness to Max Force / [BV/TV] (mJ/mm^3)	0.370 ± 0.037	0.273 ± 0.049 (-26.1%)	0.265 ± 0.021 (-28.3%)	p=0.019	N.S.	N.S.
Toughness to First Minimum / [BV/TV] (mJ/mm^3)	1.059 ± 0.132	1.026 ± 0.205 (-3.2%)	0.846 ± 0.095 (-20.1%)	N.S.	N.S.	N.S.

Values given as Mean ± SE   N.S. - Not Significant, Values in *italics* are also not significant

Percents in parentheses are differences in the mean values with respect to INTACT

4.4 Correlation of Mechanical Strength to Elastic Modulus

It has been shown in the literature that there is a strong correlation of ultimate stress to elastic modulus in cancellous and cortical bone.[39,40] This inherently implies that the ultimate strain is relatively constant, meaning that the loaded bone reaches its peak load capacity at about the same strain. As this is the first study to test isolated cancellous bone from rats in a similar manner to that of larger animals it is of interest to investigate whether this general correlation is found from this study's results. On a clinical level this Modulus-to-Stress relationship is valuable because it is foreseeable that as technology improves measuring modulus in an in-vivo setting is possible. The linear correlation between stress and elastic modulus is presented in Figure 30. Additionally, the average strain at max force for our study was 3.3% +/- 0.3% (SE) with no significant difference between the groups. One must be careful in applying this correlation to any site other than the rat distal femur since Morgan, Kopperdahl, and Keaveny have shown that these stress-to-modulus correlations depend on anatomic site, direction of loading, and species.[41,42]

$$\sigma_u = 0.0158\,E + 1.0477$$
$$R^2 = 0.8868$$
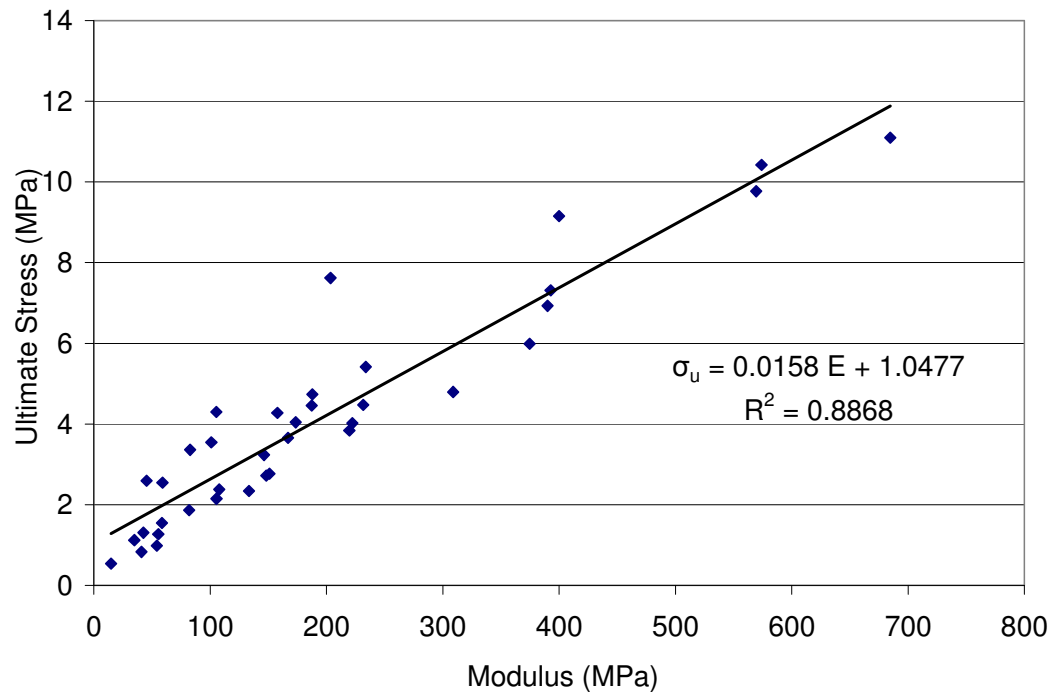
Figure 30: Correlation of Elastic Modulus and Ultimate Stress

4.5 Correlations between Mechanical Properties and Density and Micro-Architecture

Correlations between mechanical properties and density and micro-architecture are important on a clinical level because these can be measured by non-invasive methods and can be applied to partially assess the mechanical properties. Currently, bone mineral density is measured to diagnose osteoporosis and assess the fracture risk. In the future higher resolution scanners may be used to improve assessments of fracture by measuring micro-architecture parameters. Additionally, these correlations are of interest because they can be compared with other studies that have investigated similar relationships with human cancellous bone.

4.5.1 Correlations between Elastic Modulus and Density

Researchers consistently find a correlation between the elastic modulus and density in both human[41] and animal[43] cancellous bone. Generally, this correlation

seems to be best shown through a power law regression and in this study that was also the case. In Table 8, the results are shown for the regressions between elastic modulus and apparent density, the µCT core-specific vBMD, µCT cancellous vBMD, pQCT cancellous vBMD, and pQCT total vBMD. The first column in Table 8 indicates the specific density parameter; in column 2 the equation, is given for the regression, where E is elastic modulus and ρ is density variable from column 1. This notation and organization will be used throughout the remainder of the section. The best regression is with apparent density, yielding a coefficient of determination (R^2) of 0.53, interpreted as the apparent density accounting for up to 53% of the variation in elastic modulus. These data and the regression curve can be seen in Figure 31. The remaining regression plots can be found in Appendix H. An unexpected finding was that the pQCT vBMD values had stronger correlations with elastic modulus than did the µCT vBMD values, though there is little difference in the strength of correlation. This could be explained by the difference in the number of data points included in the regression, i.e., there were 5 specimens that did not have µCT data. The density parameter with the highest correlation for our study cannot be assessed by non-invasive methods, and measured vBMD can account for only 32.7% of the variation in elastic modulus. The power law regressions indicate that a small change in the independent variable, density, will yield a larger change in the dependent variable, elastic modulus.

Table 8: Power Law Regressions between Elastic Modulus and Density Parameters

Density Parameter (g/cm^3)	Equation	R Value	R^2 Value	Standard Error of Estimate	p-value
Apparent Density	$E=270.342\rho^{2.132}$	0.728	0.53	120.643	<0.001
µCT Core vBMD	$E=1205.5\rho^{1.5}$	0.522	0.273	144.89	0.002
µCT Cancellous vBMD	$E=1710\rho^{1.797}$	0.494	0.244	147.712	0.003
pQCT Cancellous vBMD	$E=1480\rho^{1.534}$	0.572	0.327	144.327	<0.001
pQCT Total vBMD	$E=3296\rho^{6.428}$	0.561	0.315	145.665	<0.001
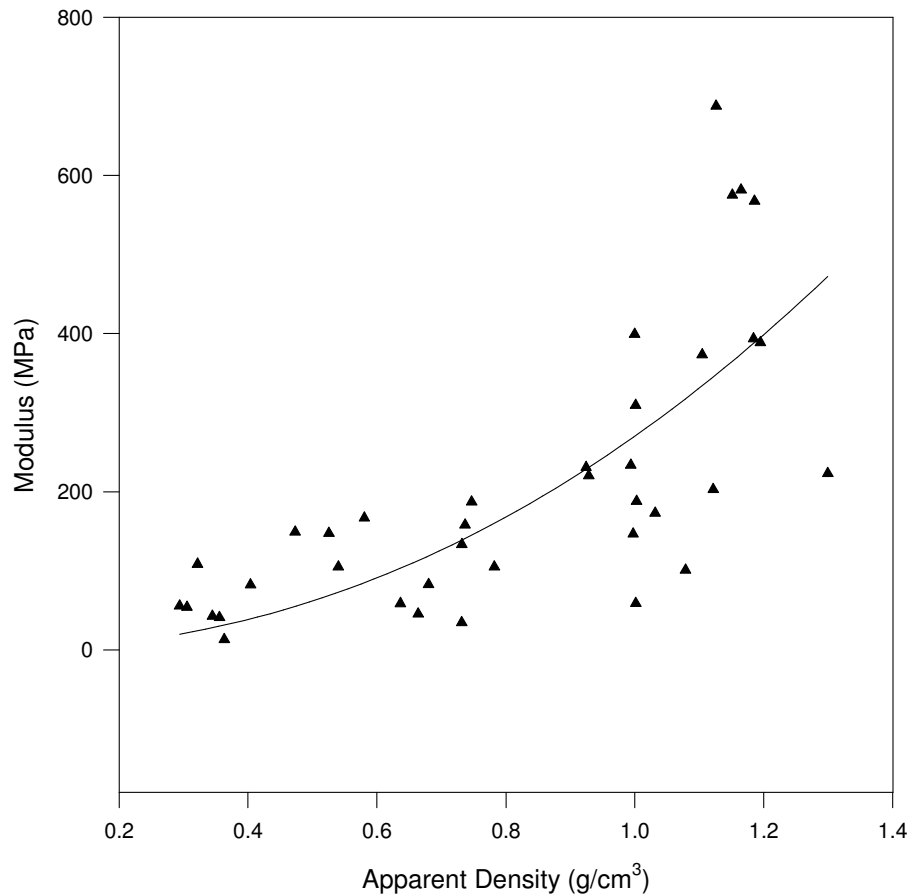
Figure 31: Elastic Modulus and Apparent Density Power Law Regression

4.5.2 Correlations between Strength and Density

The regressions in Table 9 look at the same density parameters as those listed in the previous section, but here they are correlated to ultimate stress. Comparing the modulus-to-density regressions to the strength-to-density regressions it is clear that density is a better predictor of strength than of modulus, based on the R^2 values. Also, unlike the modulus-to-density regressions, the μCT Core vBMD here produced the expected result of having the highest correlation value other than apparent density. In Figure 32, the correlation between strength and apparent density is plotted. The plots for the remainder of the stress-to-density regressions presented in Table 9 can be found in Appendix H.

Table 9: Power Law Regressions between Ultimate Stress and Density Parameters

Density Parameter (g/cm^3)	Equation	R Value	R^2 Value	Standard Error of Estimate	p-value
Apparent Density	$\sigma_u = 5.432\rho^{1.437}$	0.743	0.552	1.869	<0.001
µCT Core vBMD	$\sigma_u = 31.617\rho^{1.662}$	0.706	0.498	2.057	<0.001
µCT Cancellous vBMD	$\sigma_u = 42.83\rho^{1.915}$	0.662	0.438	2.177	<0.001
pQCT Cancellous vBMD	$\sigma_u = 25.01\rho^{1.378}$	0.652	0.426	2.117	<0.001
pQCT Total vBMD	$\sigma_u = 56.707\rho^{5.994}$	0.644	0.414	2.138	<0.001
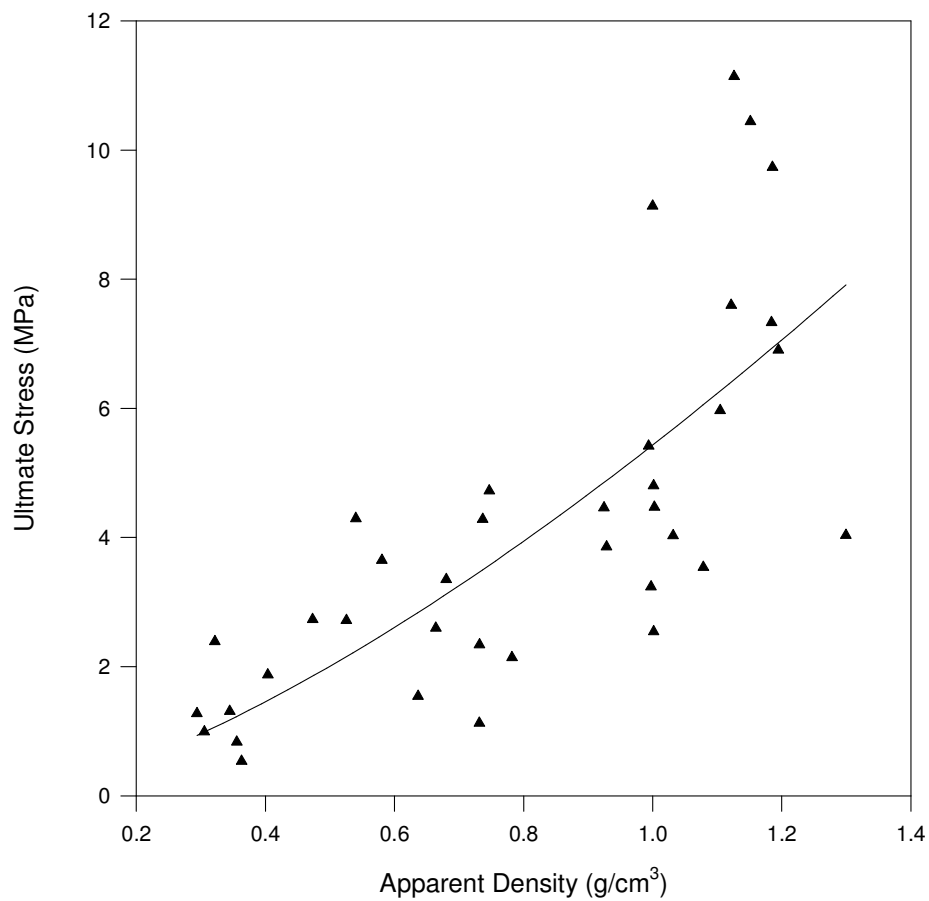
Figure 32: Ultimate Stress and Apparent Density Power Law Regression

4.5.3 Correlations Between Elastic Modulus and Micro-Architecture Parameters

Recently, as measurement techniques have improved and three dimensional micro-architecture properties have become easier to measure through the increased resolution of computed tomography, researchers have begun to take a closer look at the correlations between these micro-architecture properties and mechanical properties. Presented in this section are the correlations between elastic modulus and micro-architectural parameters measured in the core specific μCT analysis. Included in these correlations is the data from the specimens that had both μCT images and valid mechanical testing completed. Correlations using the metaphyseal μCT analysis results were not completed since they are not as representative of the cored specimen. The correlations between elastic modulus and micro-architecture parameters shown in Table 10 were lower than expected. BV/TV was the most predictive parameter for elastic modulus at 28.4% (Figure 33). The degree of anisotropy (DA) showed no correlation with elastic modulus, likely due to the fact that the DA did not vary much through the specimens since they were all taken along the same axis. If specimens were taken from along different axis or from different anatomical locations, the DA might show more of a correlation.

Table 10: Power Law Regressions between Elastic Modulus and Core Specific Micro-Architecture Parameters

Micro-Architecture Parameter	Equation	R Value	R^2 Value	Standard Error of Estimate	p-value
BV/TV (%)	$E=4.064(BV/TV)^{1.191}$	0.533	0.284	143.8	0.0001
Tb.Pf (1/mm)	$E=1322.5(Tb.Pf)^{-0.736}$	0.436	0.19	152.914	0.011
SMI	$E=202.546(SMI)^{-0.567}$	0.425	0.18	153.833	0.014
DA	$E=61.372(DA)^{1.850}$	0.184	0.0338	167.021	0.306
Tb.Th	$E=324335.6(Tb.Th)^{3.133}$	0.346	0.12	159.396	0.048
Tb.N	$E=50.460(Tb.N)^{1.298}$	0.517	0.267	145.496	0.002
Tb.Sp	$E=31.783(Tb.Sp)^{-1.295}$	0.491	0.241	148.023	0.0004
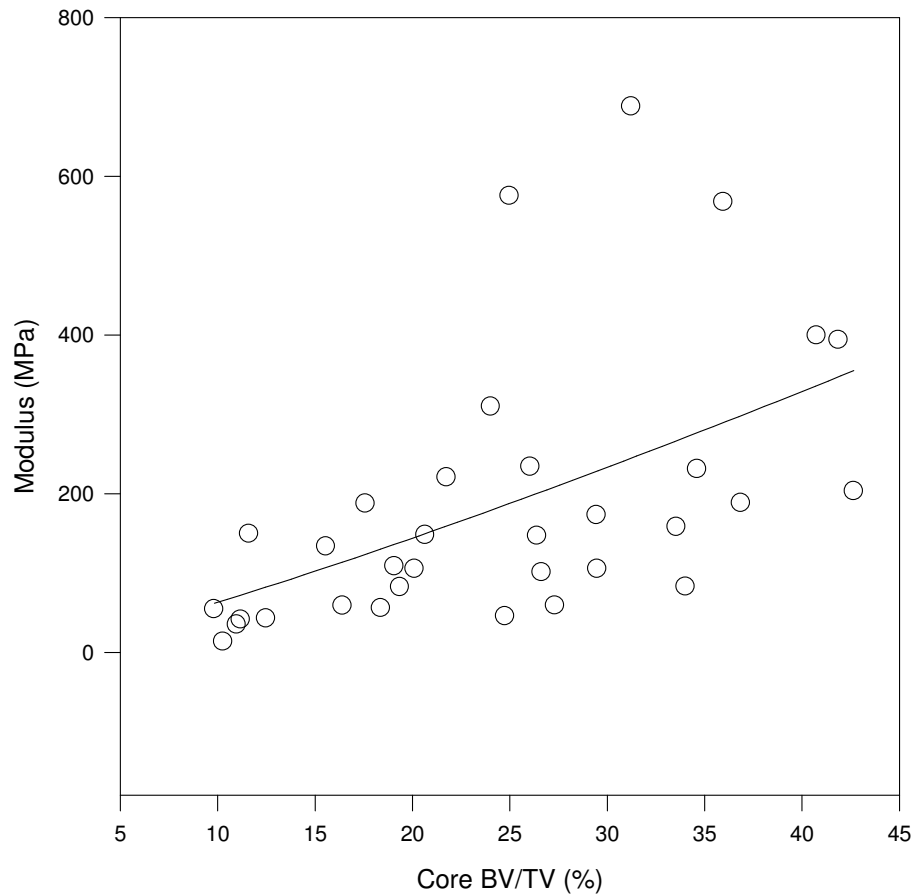
Figure 33: Elastic Modulus and Core Specific BV/TV Power Law Regression

4.5.4 Correlations Between Strength and Micro-Architecture Parameters

In the same manner as that presented in the previous section, the relationships between ultimate strength and micro-architecture parameters obtained from the core specific μCT analysis correlations were investigated. Table 11 contains the results from these correlations. BV/TV explained the highest amount of variation in the ultimate stress (Figure 34), followed by Trabecular Number (Tb.N) and Trabecular Spacing (Tb.Sp).

Table 11: Power Law Regressions between Ultimate Stress and Core Specific Micro-Architecture Parameters

Micro Architecture Parameter	Equation	R Value	R^2 Value	Standard Error of Estimate	p-value
BV/TV (%)	$\sigma_u=0.0655(BV/TV)^{1.281}$	0.711	0.506	2.042	<0.001
Tb.Pf (1/mm)	$\sigma_u=6.456(Tb.Pf)^{-0.223}$	0.444	0.197	2.603	0.01
SMI	$\sigma_u=4.426(SMI)^{-0.588}$	0.566	0.321	2.394	<0.001
DA	$\sigma_u=1.223(DA)^{1.99}$	0.251	0.0632	2.811	0.158
Tb.Th	$\sigma_u=745141.8(Tb.Th)^{5.08}$	0.537	0.288	2.45	0.001
Tb.N	$\sigma_u=1.045(Tb.N)^{1.345}$	0.674	0.455	2.145	<0.001
Tb.Sp	$\sigma_u=0.610(Tb.Sp)^{-1.382}$	0.655	0.43	2.193	<0.001
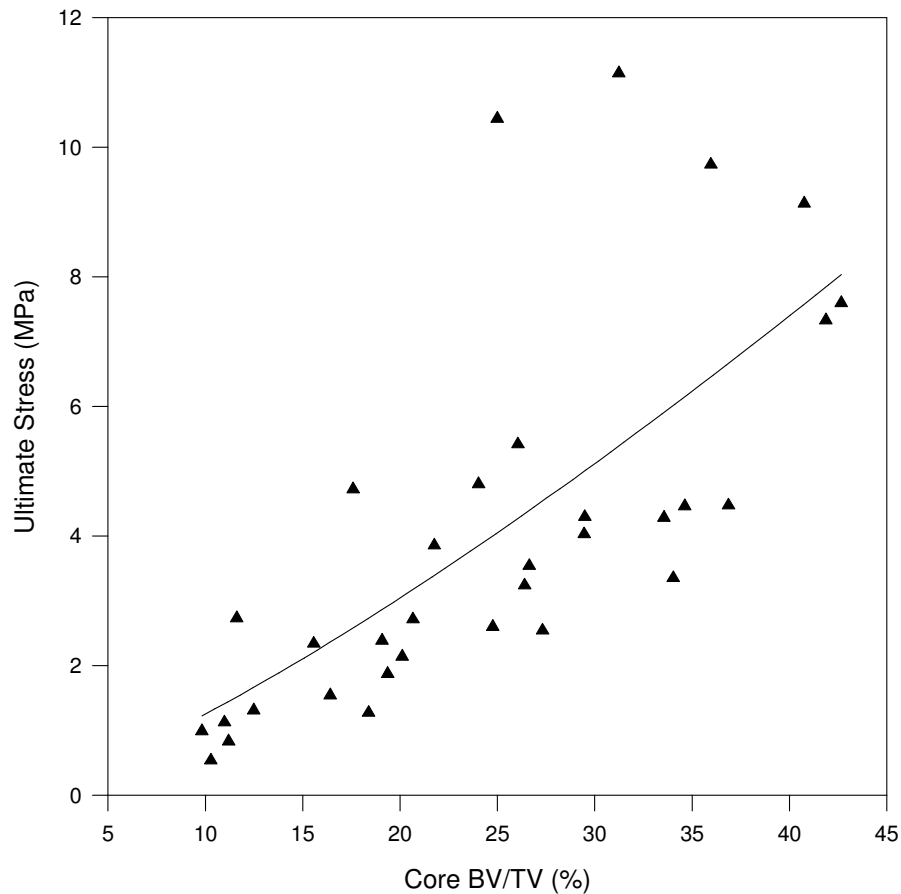
Figure 34: Ultimate Stress and Core Specific BV/TV Power Law Regression

4.5.5 Multiple Regressions

Nonlinear and linear regressions with multiple dependent variables using CT parameters were completed. Slightly higher basic regression coefficients (R^2 values) were found for the multiple variable regressions, though once these regression coefficients were adjusted to account for the number of dependent variables and the sample size they accounted for no more variation than some of the single non-linear regressions.

5. DISCUSSION AND CONCLUSION

5.1 Specimen Preparation

5.1.1 Specimen Sectioning

The slicing method presented in Section 3.4 could be further improved by two different means. First, the diameter of the wire could be increased to 220 microns versus the 130 micron wire used for this study. Although, this would slightly increase the minimum slice thickness that one could make from 0.25 mm to about 0.35 mm, including the kerf, it should decrease the cutting time and improve the plano-parallelness of the final specimen. Going to the larger diameter wire allows for more tension to be applied to the wire during cutting, reducing the potential for deflection in the wire. Secondly, μCT images that include the distal end of the bone would allow the direct selection of a first cut location.

During the process of slicing the bones, it was noticed that the base of the condyles on the posterior aspect of the bone may provide an anatomical marker for the first cut to be used in further studies, this location is shown in Figure 35. This could be further investigated through the use of μCT images and through additional experience slicing the bone.
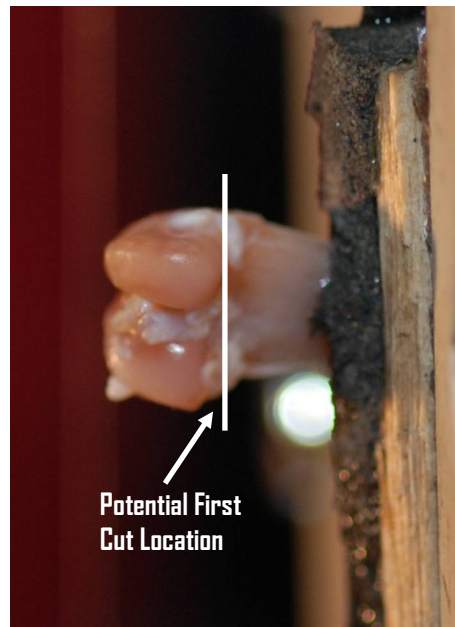
Figure 35: Anatomical Marker for First Cut Location

5.1.2 Specimen Coring

Ninety-seven percent of the specimens were cored successfully. The single specimen that failed to produce a core was in the lower range of the density spectrum, but not near the lowest value that was cored. One of the goals of this study was to quantify the lower limits of vBMD or BV/TV of specimens that could be successfully cored. There was indeed a very wide range of values of these parameters in the specimens studied and the results show that this method can be successfully applied to the entire range of specimens. Additionally, statistical comparisons between the core specific vBMD and the standard μCT cancellous vBMD and the pQCT Cancellous vBMD for each group (OVX+E2, OVX, INTACT) found no significant differences. This indicates that the cores are representative of their cancellous compartments and the standard metaphyseal region of interest in the μCT and pQCT analysis (Figure 36).
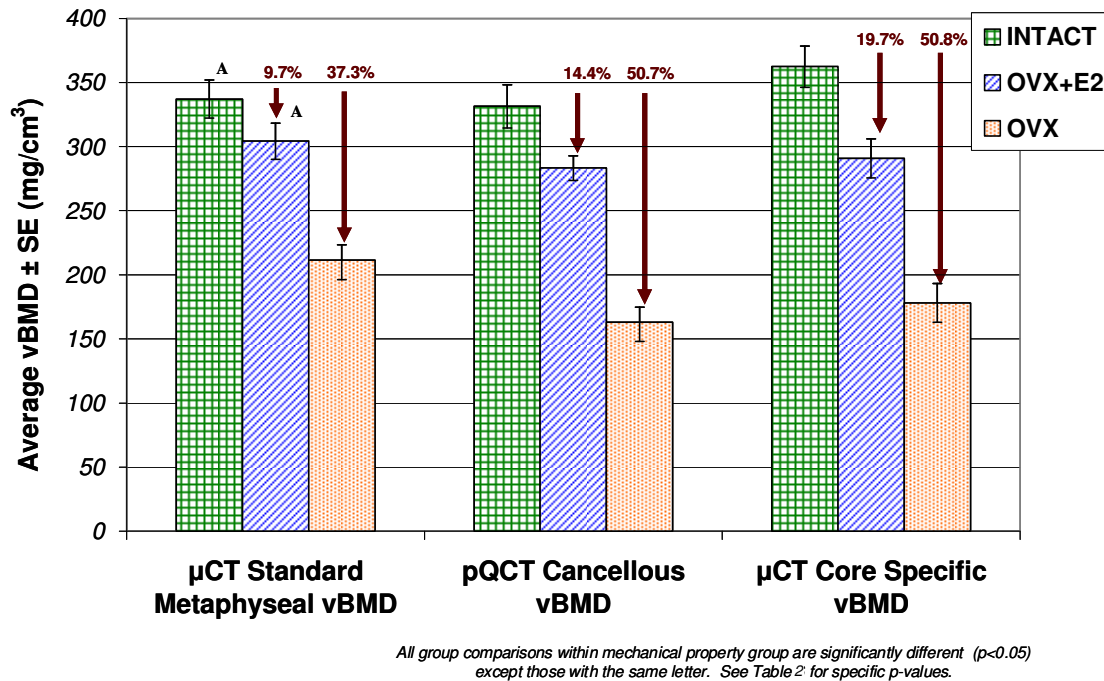
Figure 36: Group Average Values for Different Measures of Cancellous vBMD

Furthermore, automation of the coring process could possibly improve the preciseness of the cored specimens by eliminating some human involvement. This would also free the saw operator to prepare the next specimen.

5.2 μCT to pQCT Comparison

In an effort to allow the results of this study to be useable by labs with different CT capabilities, the bones were subject to both pQCT and μCT measurement techniques. The two methods were compared directly at assessing the cancellous vBMD in the metaphyseal region of the distal femur. Recall that the two different methods selected the regions of interest differently. The slice locations were specified axially by a set distance from the tibial plateau for pQCT and by anatomical location for the μCT method. Also, the cancellous compartment, sometimes referred to as marrow area, was

determined by visual inspection in the μCT method and by a computer algorithm in the pQCT method. It should be emphasized that the objective was not for the two methods to be identical with only different resolutions, but to use two standard methods to broaden the applicability and aid in determining the lower limits of the cancellous compartments from which specimens could be cored. In Figure 37, it can be seen that the average pQCT values are consistently lower than the μCT values. This could be explained by the location of the slices axially, suggesting that the fixed-distance method of the pQCT samples a region more distal, or it could be explained by the differences in defining the cancellous compartment, suggesting that the μCT's region includes more of the denser bone closer to the cortical wall. In Figure 38, the cancellous vBMD data points have been plotted and a linear regression has been applied. The R^2 value indicates a lower correlation between the two values than was expected. This could be explained by some differences in specimen alignment between the two methods.
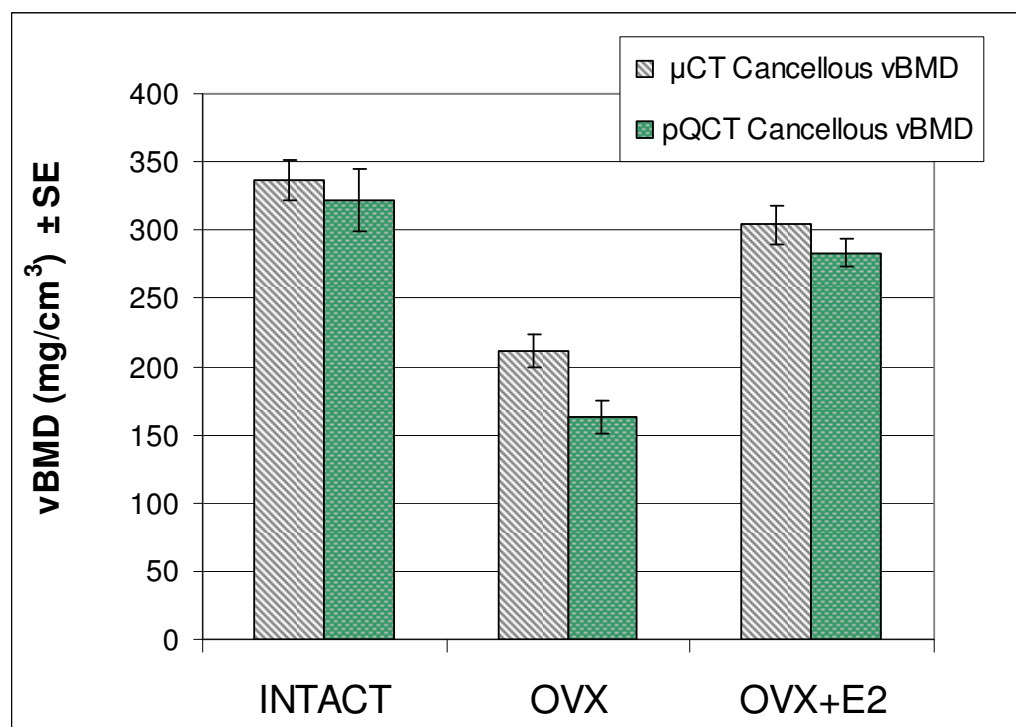
Figure 37: A Comparison of μCT and pQCT vBMD
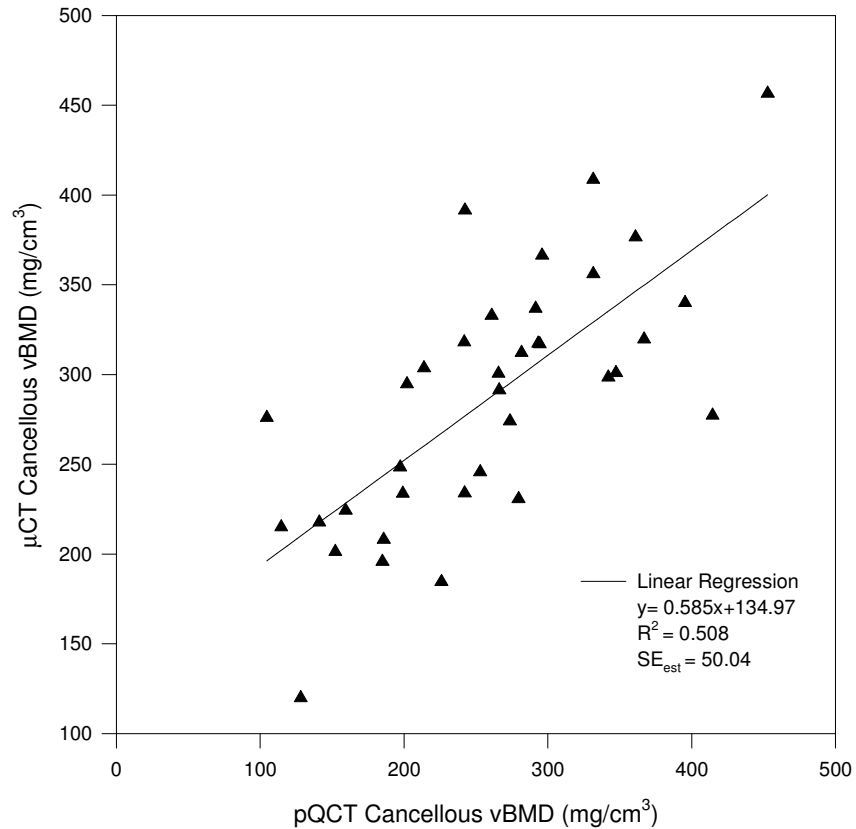
Figure 38: Linear Regression between pQCT Results and μCT Results

5.3 Summary of Correlations

In general, the apparent density of the cancellous core predicts the highest amount of variation with 55% and 52% for ultimate strength and elastic modulus, respectively. The apparent density is often presented and correlated with mechanical properties. Also, similar to our study, Mitton et al. found that apparent density was a better predictor of strength and modulus than was bone mineral density.[43] The limitation of this property, unlike that of the others, is that it cannot be measured with non-invasive tools.

In general, the ultimate strength was better predicted from the density and micro-architecture parameters than is elastic modulus.   Trabecular bone pattern factor showed only a slight difference in correlation coefficient for elastic modulus and stress.

The ranges of the isolated cancellous specimens' BV/TV, and Tb.Pf values (Table 1) are very similar to those that have been presented in human isolated cancellous bone studies.[45] The apparent density range is higher in the rat cancellous specimens than the human cancellous specimens, but similar to those in ewes.[41,42,43]   Also, the exponent values in the regression equations fell in the general range of those presented in other studies. [41,42,43,45]   Also, similar to our study, Mitton et al. found that apparent density was a better predictor of strength and modulus than bone mineral density.[43]

In other rat studies, researchers have found that about 60% of the variation in bone strength could be predicted using BMD and other morphology parameters in cortical and mixed bone sites.[44] In large animal and human isolated cancellous bone studies a larger percentage of the variation in modulus and bone strength can be explained by regressions. For instance, Perilli et al., after testing correlations between ultimate stress and BV/TV in cancellous cylinders from the proximal human femur, found an R^2 value of 0.84 using power law regressions and an R^2 of 0.95 when correlating to the minimum value of BV/TV.[45] In our study only 50% of the variation in bone strength for rodent cancellous bone could be predicted by densitometric or morphological variables.

5.4 Influence of Buckling and Friction

As mentioned previously, buckling and friction incurred during compression testing cause other forces and deflections that are not accounted for in purely axial compression theory. The influence of buckling and friction is proportional to L/D ratio. Given that the specimens were nominally 1.5 mm in length and 2.3 mm in diameter, the L/D ratio used for this study was 0.65. This L/D ratio was primarily chosen due to the geometric constraints of the cancellous compartment, but it is still important to understand what effects that buckling and friction may have on the mechanical testing

results. The L/D ratio is considered to be in the lower range, and thus the effects of buckling can be neglected. The frictional effects require further consideration.

Friction causes a non-homogenous stress distribution at the interface between the platen and the specimen. This stress distribution is given by [46]

$$\sigma = \sigma_o e^{(2f(D/2-r)/L)} \quad (11)$$

where σ_o is the yield stress, f is the Coulombic friction coefficient, and r is the distance from the center. Using equation 11, it can be shown that the stress at the center of the specimen and the max stress (σ_{max}) is given by

$$\sigma_{max} = \sigma_o e^{(2f(D/2)/L)} = \sigma_o e^{(f(L/D))} (12)$$

This stress distribution is shown in Figure 39.
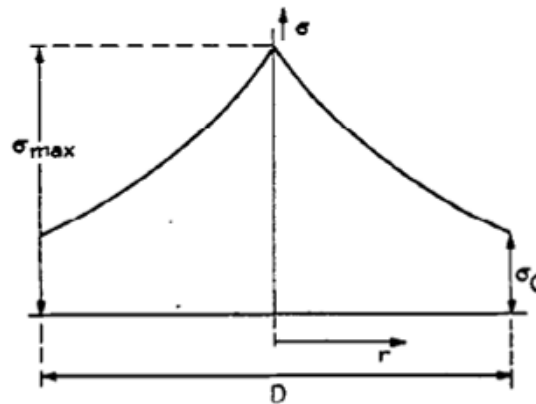
Figure 39: Distribution of Normal Stress in Compression Plates[26]

Our current set-up configuration incorporates polished platens, the use of low viscosity mineral oil for lubrication, and a specimen that has been cut using an abrasive fine diamond wire that is known to leave a very smooth surface. After reviewing the literature and finding no mention of a typical coefficient of friction for this lubricated interface, the coefficient of friction is estimated at 0.05. This could be a topic of further study. Vrijhoef and Driessens assumed the coefficient of friction to be 0.02 for dental material.[26] Shiraza-adl, Dammak, and Paiement found the coefficient of friction for

cancellous bone to a non-lubricated steel interface to be 0.42.[47] The coefficient of friction could be a topic of further study.

Incorporating the L/D ratio of 0.65 and a coefficient of friction of 0.05 into Equation 12 produces a max normal stress that is 1.08 times the yield stress. In other words, the normal stress is 8% higher at the center than at the edge of the specimen during testing. Based on this increased and uneven distribution of deformation pressure on the machined surface of the cored specimen, the mechanical properties would be underestimated slightly in our current testing procedure.

5.5 ICC to RPC Method Comparison

It has been seen throughout this thesis that the new ICC method is based upon the previously developed RPC method. The primary goal of this study was not to compare the values obtained by the ICC method with the RPC method, so a thorough results based comparison is not warranted. Thus this section must be prefaced by acknowledging that this comparison is primarily qualitative.

With all experimental testing methods the amount of time required complete the evaluation of the mechanical properties is something that should be considered. With respect to specimen preparation, the ICC method requires more time because of the coring step. This amounts to about 8-10 minutes per bone, though this process could be sped along by the automation of the coring device. For the mechanical testing aspect, the RPC method requires more time (~2-3 mins./bone) because of the higher difficulty in centering the specimen and the necessary changing of platens.

One of the issues with the current RPC slicing procedure is that if the first cut is taken too close to the growth plate then specimen will render invalid mechanical testing results. Using the Buehler Isomet Low Speed Saw (Buehler LTD., Lake Bluff, IL) allows only for one attempt to make the first cut due to the thickness of the blade (~0.5mm); a second cut would render the top of the specimen too far from the growth plate. The diamond wire saw alleviates this issue with its ability to produce a much thinner slice (~0.25 mm) and thus allowing for a second cut.

Based solely on the inherent cortical wall load sharing in the RPC method it can be concluded that the ICC method is better at assessing the actual mechanical properties of cancellous bone. In the RPC method, due to this load sharing nature, the mechanical loading creates three dimension stress state. Though, to assess the intrinsic mechanical properties it is assumed to be a simple uni-axial test. In the ICC method, the cancellous specimen has been removed from the cortical shell and the testing is uni-axial compression.

5.6 Biological Verification of the Testing Method

An important outcome of this study is to demonstrate the utility and value of the new testing method using the OVX rat model, a well accepted animal model for osteoporosis. The cancellous bone in the metaphysis has been shown to be a sensitive indicator of the changes in mechanical properties due to ovariectomy in rats through the RPC method.[14] The study by Hogan et al. used similar age animals (3.5 months) with a shorter duration of OVX (5 weeks) with Sprague-Dawley rats. Using the RPC method in the proximal tibia metaphysis with a platen size of 3mm it was found that the ultimate stress, elastic modulus, and energy to maximum force was 60.1%, 58.2%, and 58.6% less in the OVX than the INTACT group, respectively. In the current study, the percent differences are 70.5%, 74.4%, and 67.7% respectively. The two studies seem to be in general agreement; the larger difference in the current study could be attributed to many factors, including the smaller region tested, isolation of the cancellous bone, or the longer period post-ovariectomy.

As mentioned previously, Meng et al. conducted a similar study using rats of the same age (4 months) and found that six weeks post-OVX the load and stiffness were both diminished by 50% and 45%, respectively when the properties were assessed using indentation.[13] The current study found roughly a 25% higher percent difference. While this higher difference may be attributed to the longer period post-OVX, the smaller region tested by Meng et al. should have the opposite effect.

Comparisons with the previous published data seem to indicate that the ICC method may be a more sensitive indicator of changes in the properties of cancellous

bone than the indentation and RPC methods, though further investigation is required. This finding is expected since the load sharing of the cortical shell is eliminated in the current method. Additionally, since this source of error is removed the new method seemingly yields more truly accurate values. These findings clearly demonstrate the value and efficacy the ICC method as new and powerful method for ascertaining the mechanical properties of cancellous bone in the distal femur of the rat. Directly measuring the mechanical properties of cancellous bone is a strongly relevant functional outcome that is employed in many studies, but has been previously unavailable for studies using rats. This new method offers the ability to fill the gap in assessing cancellous bone in rats and may be applied to a broad range of bone-related ailments and treatments.

5.7 Effect of Estrogen on Tomographic and Mechanical Properties

Examining the study in a simplistic view there are three groups with different levels of estrogen: the INTACT group with normal levels of estrogen, the OVX group is estrogen deficient, and the OVX+E2 group has undergone ovariectomy, but is administered estrogen through slow release pellets. The latter two groups are representative of postmenopausal osteoporosis (OVX) and postmenopausal osteoporosis with estrogen treatment (OVX+E2), respectively. The results of these three groups and the statistical comparisons between them have been presented in Sections 4.2 and 4.3 (pg. 41). In this section, all three tomography methods will be compared and then these tomography results will be compared with the mechanical testing results.

The pQCT and metaphyseal µCT analyses were compared thoroughly in Section 5.2 in general terms, but here they will be discussed in terms of detecting the differences among treatment groups. The two tomographic methods are in general agreement (see Table 2; pg.42 and Table 4; pg.44), though the pQCT method yields a larger percent difference between the OVX+E2/OVX and INTACT groups. Also, between the OVX+E2 and INTACT a significant difference was only found for the pQCT results {Recap: INTACT vs. OVX+E2 - 10.5% (N.S) vs. 14.4% (Sig.); INTACT vs. OVX - 43.1% vs. 50.7% (both Sig.)}. As mentioned previously, the pQCT data includes five

extra bones in the INTACT group and this may have contributed to the difference found. Between the two sets of μCT analyses the core-specific analysis seems to be more sensitive to treatment, as the BV/TV for OVX+E2 was 23.2% lower and for OVX was 58.8% lower than the INTACT group. This is expected since this method analyzed the central region of the metaphysis, which generally responds more potently to treatment.

The estrogen treatment improves bone strength and elastic modulus, though the response is not as strong as what is suggested by changes in core-specific bone mineral density and other CT parameters (Table 12). The elastic modulus and strength were 42.6% and 49.6% lower respectively, for OVX+E2 when compared with INTACT, while the bone mineral density (vBMD) and BV/TV were only 19.7% and 23.2% lower, respectively. This can be partially explained by the normally assumed power law relationship between the mechanical property and CT parameter, but not completely. Additionally, the solid-phase material properties (Table 7, pg. 47) show very similar values for the OVX+E2 and OVX groups. While both of these groups are not significantly lower than INTACT, there is a trend toward a difference that might reach statistical significance by increasing the number of specimens tested. Comparing the material properties (Table 7, pg. 47) to the intrinsic properties (Table 6, pg. 41), it seems likely that the difference in intrinsic mechanical properties is due to the amount and micro-architectural properties of the cancellous bone. To further illustrate, the estrogen treatment is increasing the connectivity of the trabecular network and the amount of bone, but the material level quality of the bone is not being maintained. One factor that may contribute to this is the higher rate of bone turnover that is characteristic of estrogen deficiency. When the osteoclasts resorb bone, they leave small divot-like imperfections in the bone surface. The increase in bone turnover will be accompanied by an increase in bone resorption, and thereby increasing the number of small defects. This increase would negatively impact the strength of the bone. Additionally, the increase in bone turnover creates pockets of newer bone that may be less mineralized, and thus not as stiff as more mature mineralized bone.

Table 12: Summary of Comparisons for Key CT and Mechanical Properties, Differences in the Mean Values

	INTACT to OVX	INTACT to OVX+E2
μCT Standard Metaphyseal BV/TV (%)	-43.10%	-10.50%**
μCT Standard Metaphyseal vBMD (mg/cm3)	-37.30%	-9.70%
μCT Core Specific BV/TV (%)	-58.80%	-23.20%
μCT Core Specific vBMD (mg/cm3)	-50.80%	-19.70%
pQCT Cancellous vBMD (mg/cm3)	-50.70%	-14.40%
Ultimate Stress (MPa)	-70.40%	-42.60%
Elastic Modulus (MPa)	-74.40%	-49.60%

**Not Significant

Using similar aged animals, but with a longer period of ovariectomy and estrogen treatment, Jiang et al. looked at compressive strength and density parameters in the rat vertebra, a mixed cancellous and cortical bone site.[48] They showed that, while not significantly different, the estrogen treated group's compressive strength was about 20% lower and stiffness about 50% lower, while the density was less than 1% lower than the corresponding sham group. This trend corroborates the discordant strength to density findings in the study. In contrast, Chachra et al. reported that estrogen replacement therapy rescued bone density and strength completely in the rat vertebra.[49] This discordant relationship between BMD and mechanical properties with variations in estrogen status requires more investigation.

These results reiterate the importance of direct mechanical testing of small animal bone specimens and highlight the significance of the insight that is gained by testing isolated cancellous bone in rats using this new method.

5.8 Summary

The primary objective of this thesis was to develop a new method that would allow the testing of isolated cancellous bone from the distal femur metaphysis of rat bone. This objective was met and the results exceeded the initial expectations and proving that the ICC method can sucessfully produce cancellous cores from a group of bones with a wide range of density and micro-architecture parameters. Results also demonstrate that cancellous bone in the distal rat femur follows a strong linear stress to elastic modulus correlation, which has been consistently shown in bovine and human cancellous bone. Correlations between the mechanical properties of stress and modulus to density and micro-architectural properties were investigated, and it was found that apparent density explains the largest amount of variance in both mechanical properties. Additionally, these correlations follow the same power law regression with similar exponents and in some cases cover the same range micro-architecture properties as studied by other researchers investigating cancellous bone in larger animals and humans. The ICC method has been shown to be an effective method for detecting changes in the cancellous bone mechanical properties caused by ovariectomy and ovariectomy plus estrogen.

6. FUTURE WORKS

6.1 Automation of the Coring

Reduction of human error in the coring process could be obtained by automating the rotational motion of the specimen holder. By controlling and keeping the rotational speed constant, a more repeatable uniform circular core could be obtained. Also, this would free the operator to perform other tasks and thereby increase the efficiency of the process. The automation could be implemented using a small variable speed motor and either a gear or belt system.

6.2 Coring of Other Anatomical Locations

A next step in the development in the ICC method would be to apply it to other anatomical locations in the rat such as the proximal tibia metaphysis or the lumbar vertebrae. The first specimens cored were from old RPC specimens from the proximal tibia metaphysis. It has been shown that cancellous bone obtained from different anatomical locations has dissimilar micro-architectural and mechanical properties. With this in mind, it would be valuable to evaluate different anatomical locations to see which site in the adult rat best mimics human cancellous bone. The method could also be applied to other small laboratory animal models.

6.3 Identification of External Landmarks

For the current study, the base of the condyles on the posterior aspect of the bone seemed to provide an external landmark for the slice location. For this to be used in practice, further investigation would be required. Additionally, a large set of distal femurs that includes a large age range, various breeds, and both male and female rats and their corresponding μCT images could be used to further evaluate the validity of this external landmarker.

6.4 Repeatability Study

Using a group of rats with a wide range of age and bone mineral density, specimens could be obtained from contra-lateral femur pairs. Since in general the

properties of the right and left legs are considered to be the same, specimens could be cored and tested from each leg and the difference between the mechanical testing results would provide an assessment of the repeatability of the method.

6.5 Finite Element Analysis (FEA)

Finite Element Analysis is a tool that has been utilized by various researchers to attempt to model and better explain the mechanical properties of cancellous bone. Using the high resolution μCT images a 3 dimension solid model could be constructed and a Finite Element Software package could be utilized to implement the analysis. This analysis could be validated to the mechanical testing results from this study. Additionally, the model could be used to further assess the effects of friction at the cancellous bone to compression platen interface and the side-artifact effects.

6.6 Development of Criteria for the Transition from Primary to Secondary Spongiosa

Since the region of interest for the cancellous cores is in the secondary spongiosa, it would be advantageous to better define the transition zone from primary to secondary spongiosa. This is further warranted due to the seemingly complex contour of the growth plate and the adjacent primary spongiosa in the distal rat femur.

The transition from primary to secondary spongiosa might be determined using μCT analysis by looking at the bone mass per bone volume. Since the primary spongiosa is composed of partially mineralized cartilaginous tissue it would yield lower density values than the fully mineralized secondary spongiosa. The validity of the μCT analysis to find the transition zone could then be investigated through histology using a specific stain to identify the cartilaginous tissue. If the method for using μCT is validated then it could be applied to any specimen set to aid in finding the optimal location for the cancellous cores.

REFERENCES

1.   Martin RB, Burr DB, Sharkey NA 1998 Skeletal Tissue Mechanics, Springer-Verlag, New York.

2.   Baker C (Accessed March, 2009) Primary Tissues: Bone Ossification and Growth. https://courses.stu.qmul.ac.uk/-smd/kb/microanatomy/bone/images/line/femur2.gif

3.   Dempster DW 2006 Anatomy and Functions of the Adult Skeleton. In: ASBMR Primer on the Metabolic Bone Diseases and Disorders of Mineral Metabolism, 6th ed. ASBMR, Washington, DC. Pgs. 7-11

4.   Turner RT, Maran A, Lotinun S, Hefferan T, Evans GL, Zhang M, Sibonga JD 2001 Animal models for osteoporosis. Endocrine & Metabolic Disorders **2**:117-127

5.   Kalu DN 1991 The ovariectomized rat model of postmenopausal bone loss, Bone and Mineral, **15**: 175-192

6.   Osteoporosis Overview (Accessed January, 2009) http://www.niams.nih.gov , NIH National Institutes of Health Osteoporosis and Related Bone Diseases ~ National Resource Center

7.   Kharode YP, Sharp MC, Bodine PV 2008 Utility of the ovariectomized rat as a model for human osteoporosis in drug discovery. Methods Mol Biol. **455**:111-124

8.   Jämsa T, Tuukkanen J, Jalovaara, P 1998 Femoral neck strength of mouse in two loading configurations: Method evaluation and fracture characteristics J. Biomechanics, **31**:723-729

9.   Brouwers JEM, Ruchelsman M, Rietbergen Bv, Bouxsein ML 2008 Determination of rat vertebral bone compressive properties in untreated intact rats and zoledronic-acid-treated, ovariectomized rats. Osteoporosis Int. Published Online http://www.springerlink.com/content/4252320p58709nx5/fulltext.pdf

10. An YH, Zhang J, Kang Q, Friedman RJ 1997 Mechanical properties of rat epiphyseal cancellous bones studied by indentation testing. Journal of Material Science: Materials in Medicine **8**:497-495

11. Shen V, Birchman R, Xu R, Otter M, Wu D, Lindsay R, Dempster DW 1995 Effects of reciprocal treatment with estrogen and estrogen plus parathyroid hormone on bone structure and strength in ovariectomized rats. J Clin Invest **96**:2331-2338

12. Ke HZ, Shen VW, Qi H, Crawford DT, Wu DD, Liang XG, Chidsey-Frink KL, Pirie CM, Simmons HA, Thompson DD 1998 Prostaglandin E2 increases bone strength in intact rats and in ovariectomized rats with established osteopenia. Bone **23**:249-255

13. Meng XW, Liang XG, Birchman R, Wu DD, Dempster DW, Lindsay R, Shen V 1996 Temporal expression of the anabolic action of PTH in cancellous bone of ovariectomized rats. J Bone Min Res **11**:421-429

14. Hogan HA, Ruhmann SP, Sampson HW 2000 The mechanical properties of cancellous bone in the proximal tibia of ovariectomized rats. J Bone Min Res **15**(2):284-292

15. Ruhmann SP 1998 Methods for testing the strength of cancellous bone and tested method effects on cortical one in the ovariectiomized rat. MS thesis, Texas A&M University, College Station.

16. Oxlund H, Dalstra M, Ejersted C, Andreassen TT 2002 PTH induces formation of new cancellous bone with substantial mechanical strength at site where it had disappeared in old rats. European Journal of Endocrinology **146**:431-438

17. Sumner LR 2007 Osteogenic effect of optimized muscle stimulation as a countermeasure during hindlimb unloading. MS thesis, Texas A&M University, College Station.

18. Lemmon H 2004 Methods for reduced platen compression (RPC) test specimen cutting locations using micro-ct and planar radiographs. MS thesis, Texas A&M University, College Station.

19. Alcorn JD 2006 Osteogenic effect of electrical muscle stimulation as a countermeasure during hindlimb unloading. MS thesis, Texas A&M University, College Station.

20. Goldstein SA, Wilson DL, Sonstegard DA, Mathews LS 1983 The mechanical properties of human tibial trabecular bone as a function of metaphyseal location. J. Biomechanics, **16**:965-969

21. Brown TD, Ferguson AB 1980 Mechanical property distributions in the cancellous bone of the human proximal femur. Acta Orthop Scand **51**:429-437

22. Ohman C, Baleani M, Perilli E, Dall'Ara E, Tassani S, Baruffaldi F, Viceconti M 2007 Mechanical testing of cancellous bone from the femoral head: Experimental errors due to off-axis measurements. J. Biomechanics **40**:2426-2433

23. Geisen EBW, Ding M, Dalstra M, van Eijden TMGJ 2001 Mechanical properties of cancellous bone in the human mandibular condyle are anisotropic. J. Biomechanics **34**:799-803

24. Day JS, 2008 Bone quality: The mechanical effects of microarchitecture and matrix properties. Doctoral Thesis, Department of Orthopeadics, Erasmus MC, Rotterdam, The Netherlands

25. Ding M, Odgaard A, Danielsen CC, Hvid I 2002 Mutual associations among microstructural, physical and mechanical properties of human cancellous bone. J Bone Joint Surg [Br] **84-B**(6):900-907

26. Vrijhoef MMA, Driessens FCM 1971 On the interaction between specimen and testing machine in mechanical testing procedures. J. Biomechanics **4**:233-238

27. Linde F, Hvid I, Madsen, F 1992 The effect of specimen geometry on the mechanical behavior of trabecular bone specimens. J. Biomechanics **25** (4):359-368

28. Keaveny TM, Brchers RE, Gibson LJ, Hayes WC 1993 Trabecular bone modulus and strength can depend on specimen geometry. J. Biomechanics **26**(8):991-1000

29. Harrigan TP, Jasty M, Mann RW, Harris WH 1988 Limitations on the continuum assumption in cancellous bone. J. Biomechanics **21**(4):269-275

30. Turner CH, Burr DB 1993 Basic biomechanical measurement of bone: A tutorial. Bone **14**:595-608

31. Keaveny TM, Pinill TP, Crawford RP, Kopperdahl DL, Lou A 1997 Systematic and random errors in compression testing of trabecular bone. Journal of Orthopaedic Research **15**:101-110

32. Odgaard A, Linde F 1991 The underestimation of Young's modulus in compressive testing of cancellous bone specimens. J. Biomechanics **24**(8):691-698

33. Űn K, Bevill G, Keaveny TM 2006 The effects of side-artifacts on the elastic modulus of trabecular bone. J. Biomechanics **39**:1955-1963

34. Bevill G, Easely SK, Keaveny TM 2007 Side-artifact errors in yield strength and elastic modulus for human trabecular bone and their dependence on bone volume fraction and anatomic site. J. Biomechanics **40**:3381-3388

35. Linde F, Sorensen HC 1993 The effect of different storage methods on the mechanical properties of trabecular bone. J. Biomechanics **26**(10):1249-1252

36. Allen MR, Personal Communication, Jan. 13, 2009

37. Rogers W 2002 Methods and modeling for the reduced platen compression of cancellous bone in the rodent proximal tibia, MS thesis, Texas A&M University, College Station.

38. Bouse S 2009 Investigation of transfer function analysis as a means to predict strain on the rat tibiae from ankle torque waveforms. MS thesis, Texas A&M University, College Station.

39. Fyhrie DP, Vashishth D 2000 Bone stiffness predicts strength similarly for human vertebral cancellous bone in compression and for cortical bone in tension. Bone **26**(2):169-173,

40. Yeni YN, Dong XN, Fyhrie DP, Les CM 2004 The dependence between strength and stiffness of cancellous and cortical bone tissue for tension and compression: Extension of a unifying principle. Bio-Medical Materials and Engineering **14**:303-310

41. Morgan EF, Keaveny TM 2001 Dependence of yield strain of human trabecular bone on anatomic site. J. Biomechanics **34**:569-577

42. Kopperdahl DL, Keaveny TM 1998 Yield strain behavior of trabecular bone. J. Biomechanics **31**:601-608

43. Mitton D, Rumelhart C, Hans D, Meunier PJ 1997 The effects of density and test conditions on measured compression and shear strength of cancellous bone from the lumbar vertebrae of ewes. Med. Eng. Phys. **19**(5):464-474

44. Ammann P, Rizzoli R 2003 Bone strength and its determinants. Osteoporosis Int. **14**(Suppl. 3):S13-S18

45. Perilli E, Baleani M, Ohman C, Fognani R, Baruffaldi F, Viceconti M 2008 Dependence of mechanical compressive strength of local variations in microarchitecture in cancellous bone of proximal human femur. J. Biomechanics **41**:438-446

46. Dieter GE 1974 Mechanical Metallurgy, McGraw-Hill, New York.

47. Shiraza-adl A, Dammak M, Paiement G 1993 Experimental determination of friction characteristics at trabecular bone/porous-coated metal interface in cementless implants. J. of Biomedical Materials Research, **27**(2):167-175

48. Jiang Y, Zhao, J, Genant HK, Dequeker J, Geusens P 1996 Long-term changes in mone mineral and biomechanical properties of vertebrae and femur in aging, dietary calcium restricted, and/or estrogen-deprived/-replaced rats. J Bone Min Res **12**:820-831

49. Chachra D, Kasra M, Vanin CM, MacLusky NJ, Casper RF, Grynpas MD 1995 The effect of different hormone replacement therapy regimens on the mechanical properties of rat vertebrae. Calc. Tis. Int. **56**:130-134

APPENDIX A

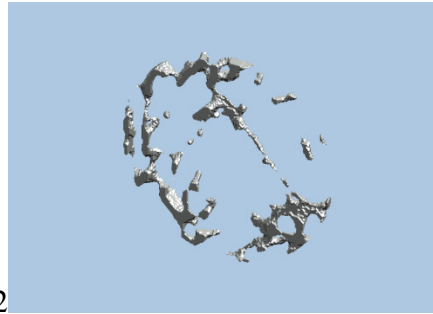# SPECIMEN HEIGHT ANALYSIS IMAGES

Bone: 10-30 / Group: OVX
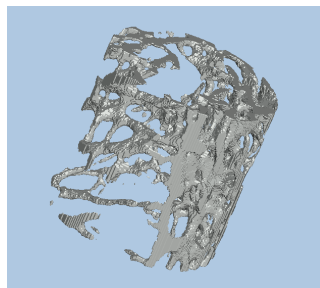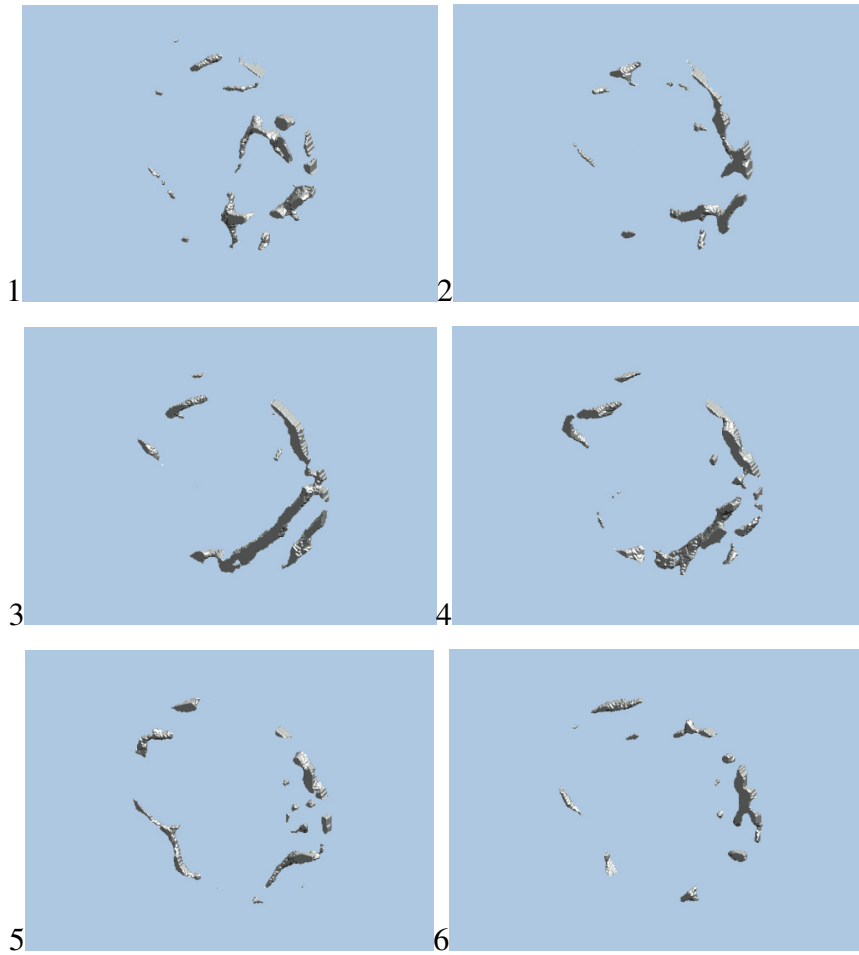
2mm Core

Bone: 2-6 / Group: OVX+E2

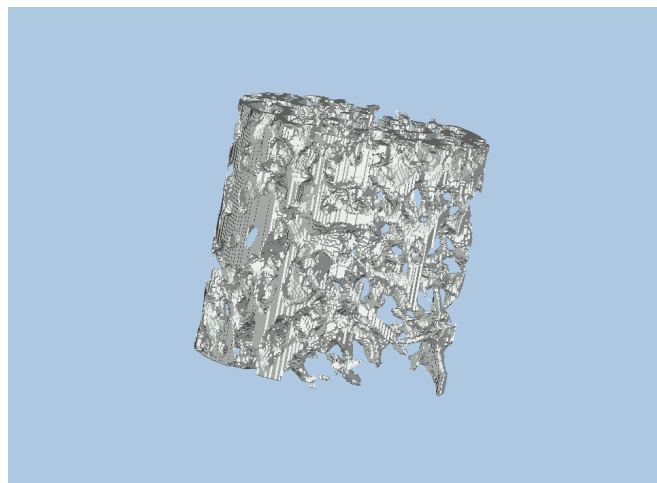1   (.stl failed)   2

3   4   (.stl failed)

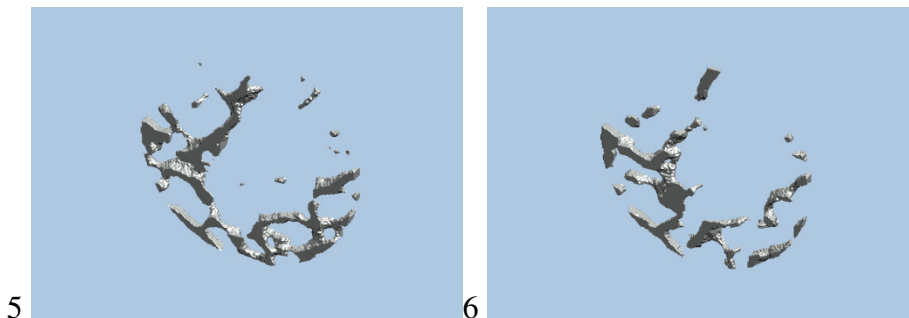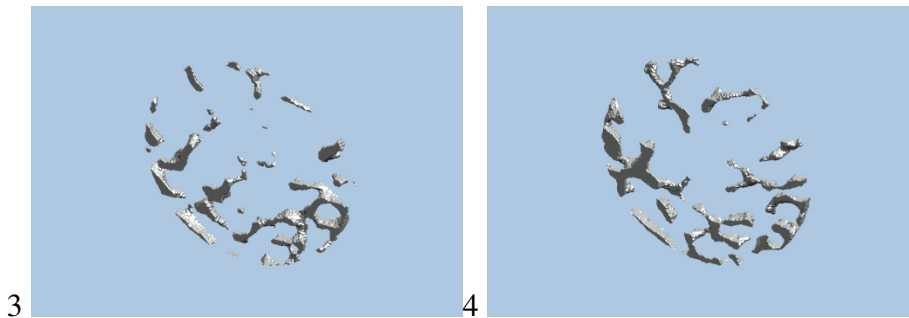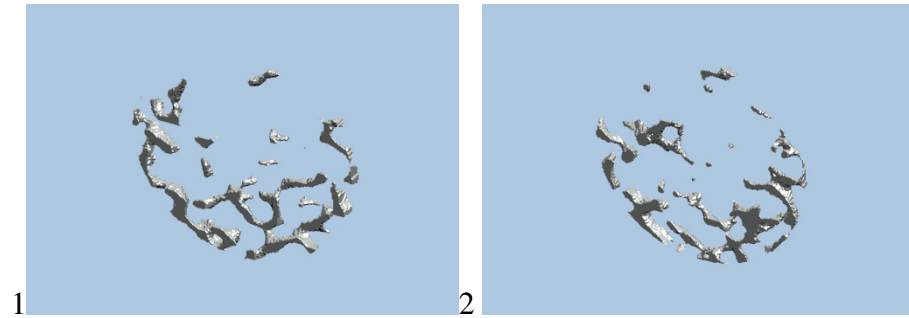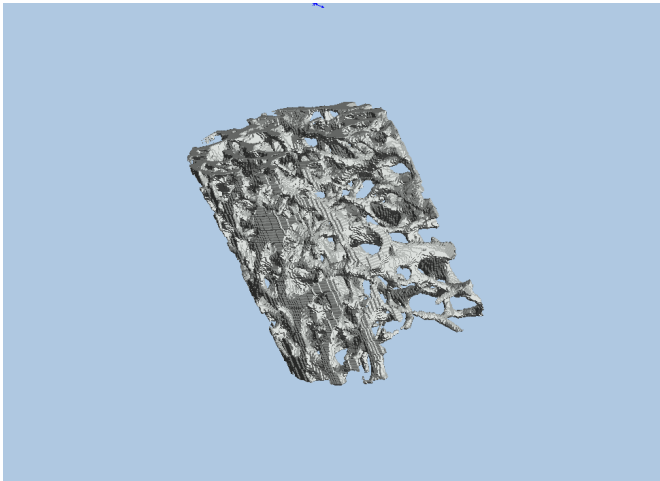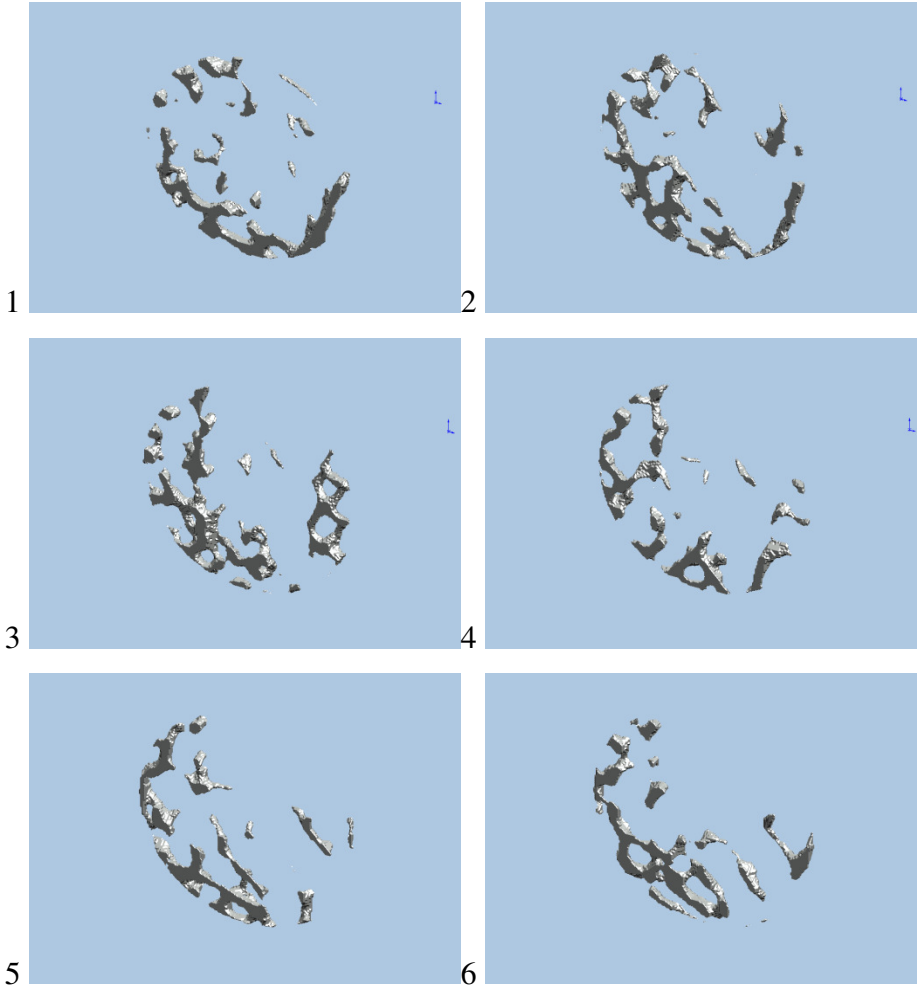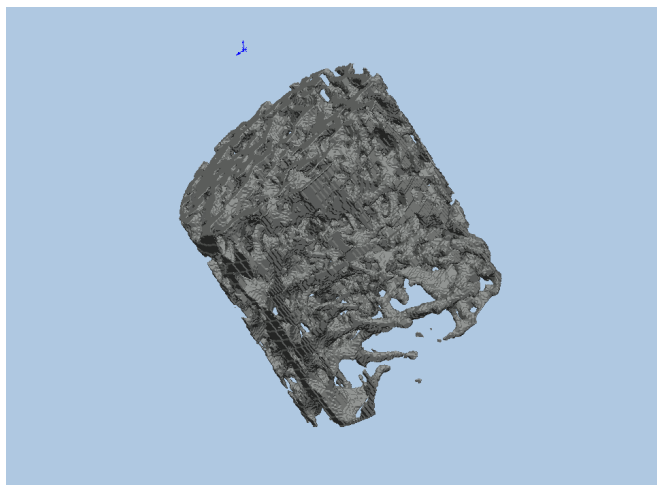5   6

2mm Core
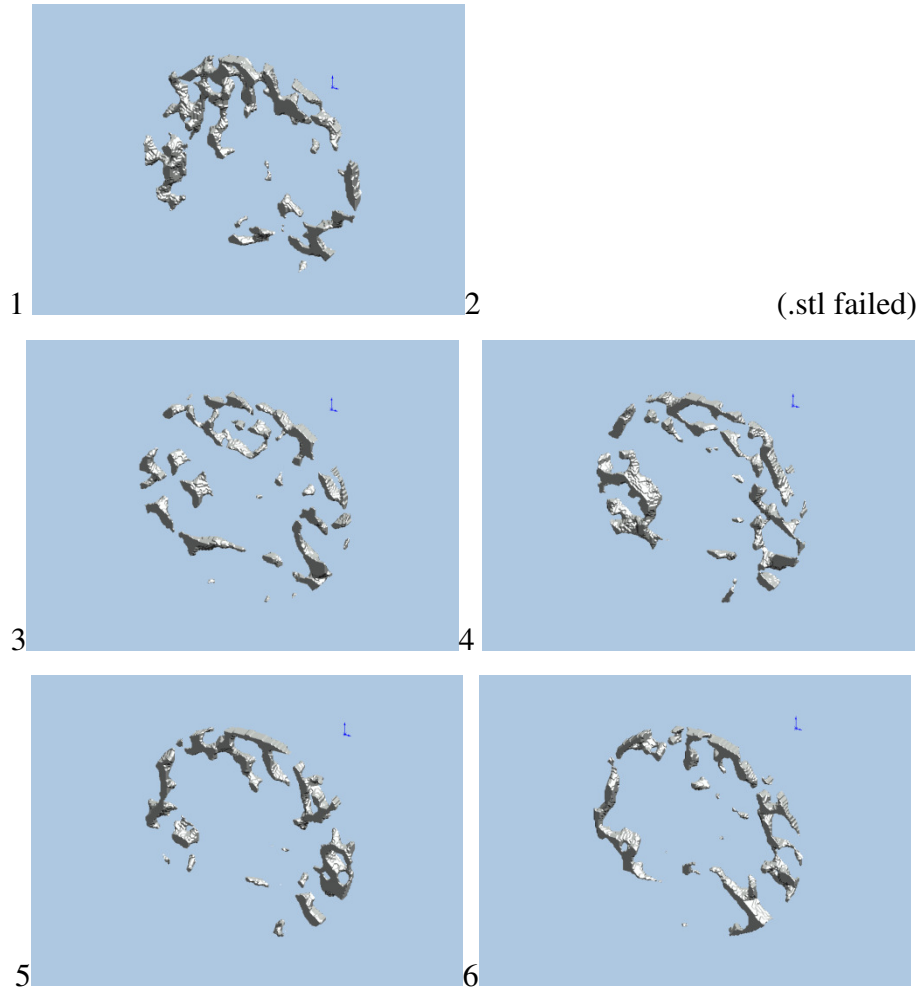
Bone: 2-8 / Group: OVX+E2
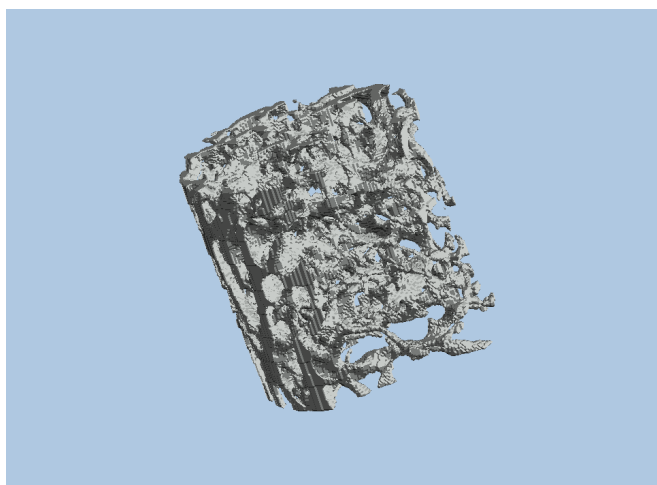
2mm Core

Bone: 1-4 / Group: INTACT

2mm Core

Bone: 8-21 / Group: INTACT
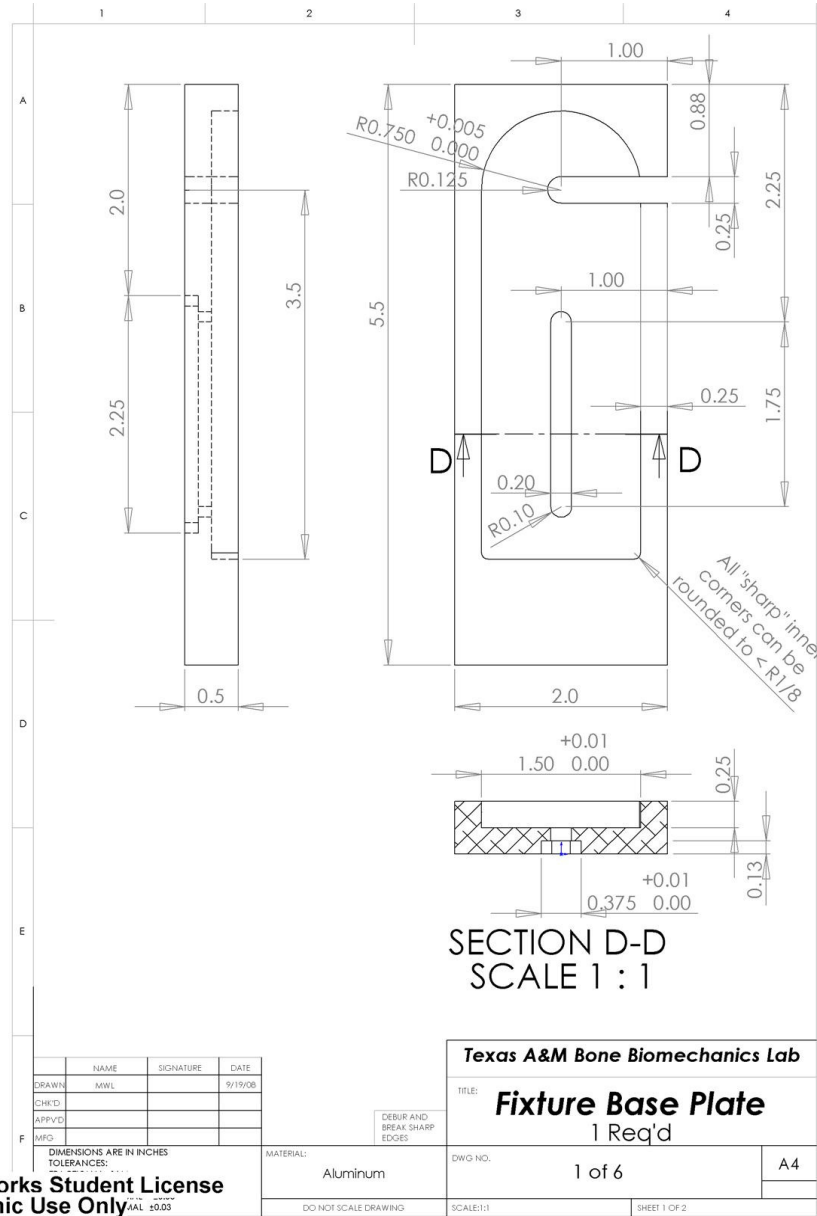

1   2   (.stl failed)

3   4

5   6

2mm Core

APPENDIX B

ENDOCORTICAL DIAMETER RAW DATA AND AVERAGES

Group	Animal #	Min. EC Diameter
CON	17-Aug	2.7500
CON	28-Aug	2.7447
CON	4-Sep	2.8478
CON	11-7B	2.9565
CON	11-7A	2.9111
CON	27-Aug	2.7660
CON	4-Jan	2.7292
CON	11-7C	2.7872
CON	22-Aug	2.7500
CON	21-Aug	2.5957
CON	29-Aug	3.1064
CON	23-Aug	2.8636
Extra	21-Jan	3.1458
Extra	23-Jan	2.8542
Extra	7-Mar	2.8750
Extra	12-Mar	2.9583
Extra	3-Oct	3.3830
Group Average		**2.8838**
Group Std. Error		**0.0457**
E2	1-Feb	2.9167
E2	4-Feb	3.1042
E2	8-Feb	2.9792
E2	6-Feb	2.7708
E2	13-Aug	2.9375
E2	5-Feb	2.9783
E2	18-Oct	2.5532
E2	30-Jan	2.9130
E2	22-Oct	2.9375
E2	24-Oct	2.9167
E2	14-Aug	2.8125
E2	28-Oct	2.8936
E2	25-Oct	2.6596
Group Average		**2.8748**
Group Std. Error		**0.0402**
OVX	31-Oct	2.9375
OVX	25-Jan	2.9375
OVX	7-Aug	2.9348
OVX	29-Oct	2.8478
OVX	30-Oct	2.8043
OVX	28-Jan	2.8936
OVX	24-Jan	2.8511
OVX	1-Aug	2.9149
OVX	2-Nov	2.7447
OVX	6-Aug	2.7083
OVX	29-Jan	2.8511
Extra	16-Aug	2.8542
Group Average		**2.8566**
Group Std. Error		**0.0207**
Total Average		**2.8733**
Total Std. Error		**0.0227**
80% of Total Average		**2.2986**

APPENDIX C

ICC FIXTURE ENGINEERING DRAWINGS

0.25
0.15

Ø0.20
R0.75
0.5
0.35
0.1
0.00
1.50 − 0.02
0.75
0.63
1.5

UNLESS OTHERWISE SPECIFIED:

DIMENSIONS ARE IN INCHES
TOLERANCES:
FRACTIONAL ±1/64
ANGULAR: MACH ±1   BEND ±1
ONE PLACE DECIMAL ±0.05
TWO PLACE DECIMAL ±0.03

	NAME	DATE
DRAWN	MWL	9/19/08
CHECKED		
ENG APPR.		
MFG APPR.		
Q.A.		
COMMENTS:		

MATERIAL
Aluminum

FINISH

DO NOT SCALE DRAWING

TEXAS A&M UNIVERSITY
BONE BIOMECHANICS LAB

TITLE:

Sliding Snugger
1 Req'd

SIZE A   DWG. NO. 2 of 6   REV

SCALE: 2:1   SHEET 1 OF 1

0.01 (0.3mm) Will be cut with DWS

See Table

∅ 0.147 Thru 2X

R0.75

+0.005
0.10 - 0.005

0.05 +0.003 -0.003

0.5

Center Hole		
Small ∅ (2 Req'd)	2.8 +/_ 0.03 mm	
Large ∅ (2 Req'd)	3.3 mm +/_ 0.03 mm	

UNLESS OTHERWISE SPECIFIED:

DIMENSIONS ARE IN INCHES
TOLERANCES:
FRACTIONAL: ±1/64
ANGULAR: MACH ±1   BEND ±1
ONE PLACE DECIMAL   ±0.05
TWO PLACE DECIMAL   ±0.03

MATERIAL
Clear Plastic
FINISH

DO NOT SCALE DRAWING

	NAME	DATE
DRAWN	MWL	9/19/08
CHECKED		
ENG APPR.		
MFG APPR.		
Q.A.		
COMMENTS:		

Texas A&M University
Bone Biomechanics Lab

TITLE:

Specimen Holder Top
4 Total Req'd

SIZE **A**   DWG. NO. **3 OF 6**   REV

SCALE: 2:1   SHEET 1 OF 1

0.01 (0.3mm) Will be done with DWS

R0.17 V 0.02

#6-32 Drill 2X Thru &
Tap Thru 2X

R0.75 - 0.000
- 0.003

See Table

0.50

+0.005
0.100 - 0.005

0.069 - 0.003
+0.003

0.5

Center Hole		
Small ⌀ (2 Req'd)	2.8 +/- 0.03 mm	
Large ⌀ (2 Req'd)	3.3 +/- 0.03 mm	

UNLESS OTHERWISE SPECIFIED:

DIMENSIONS ARE IN INCHES
TOLERANCES:
FRACTIONAL ±1/64
ANGULAR: MACH ± 1   BEND ±1
ONE PLACE DECIMAL ±0.05
TWO PLACE DECIMAL ±0.03

MATERIAL
Aluminum

FINISH

DO NOT SCALE DRAWING

	NAME	DATE
DRAWN	MWL	9/19/08
CHECKED		
ENG APPR.		
MFG APPR.		
Q.A.		
COMMENTS:		

TEXAS A&M UNIVERSITY
BONE BIOMECHANICS LAB

TITLE:

Specimen Holder Base
4 Total Req'd

SIZE **A**   DWG. NO.   **4 OF 6**   REV

SCALE: 2:1   SHEET 1 OF 1

SolidWorks Student License
Academic Use Only

0.000
0.095 -0.005

0.075

R0.05

0.93

0.20

0.25

0.17

0.044

+0.003
0.08 0.000

0.16

UNLESS OTHERWISE SPECIFIED:

DIMENSIONS ARE IN INCHES
TOLERANCES:
FRACTIONAL ±1/64
ANGULAR: MACH± 1   BEND ±1
ONE PLACE DECIMAL   ±0.05
TWO PLACE DECIMAL   ±0.03
THREE PLACE DECIMAL ±0.005

MATERIAL
Stainless 304

FINISH

DO NOT SCALE DRAWING

	NAME	DATE
DRAWN	MWL	9/19/08
CHECKED		
ENG APPR.		
MFG APPR.		
Q.A.		
COMMENTS:		

TEXAS A&M UNIVERSITY
BONE BIOMECHANICS LAB

TITLE:
Cylindical Plug
Retainer (2 Req'd)
Fabricate Last

SIZE **A**   DWG. NO. **5 of 6**   REV

SCALE: 4:1   SHEET 1 OF 1

2   1

0.5

To be cut with DWS

R0.75 - 0.003 / 0.000

R0.010

UNLESS OTHERWISE SPECIFIED:		NAME	DATE		TEXAS A&M UNIVERSITY
DIMENSIONS ARE IN INCHES					BONE BIOMECHANICS LAB
TOLERANCES:	DRAWN	MWL	9/20/08	TITLE:	
FRACTIONAL: ±1/64	CHECKED				
ANGULAR: MACH ±1 BEND ±1	ENG APPR.				Alignment Tool
ONE PLACE DECIMAL ±0.05	MFG APPR.				(1 Req'd)
TWO PLACE DECIMAL ±0.03					
THREE PLACE DECIMAL ±0.005	Q.A.				
INTERPRET GEOMETRIC	COMMENTS:			SIZE	DWG. NO.	REV
TOLERANCING PER:				A	6 of 6	
MATERIAL					
Aluminum					
FINISH				SCALE: 2:1	SHEET 1 OF 1

PROPRIETARY AND CONFIDENTIAL

THE INFORMATION CONTAINED IN THIS DRAWING IS THE SOLE PROPERTY OF MWL. ANY REPRODUCTION IN PART OR AS A WHOLE WITHOUT THE WRITTEN PERMISSION OF MWL IS PROHIBITED.

DO NOT SCALE DRAWING

APPENDIX D

ISOLATED CANCELLOUS CORING PROCEDURES (ICC)

(Distal Femur)

Slicing:

1. The bone will have normally undergone 3-pt bending prior to coring and will be in two pieces. If it has not, cut the bone in half.

2. Place the mid-diaphyseal portion (small end) of the bone in the fixture and clamp securely with the bone perpendicular to the fixture.   (See Figure 1)

Figure D1: Bone Slicing Alignment

3. Adjust the position of the bone with the micrometer so that diamond wire will cut just rub/pass the end of the bone. Record the micrometer measurement.

4. Move the bone a set distance that should be determined by the age/treatment of the rat. For four month old rats 3.75 mm works well.

5. Turn on the saw to speed 8 and make the first cut.

6. Check to make sure that the cut has been made in the proper location. If it is too distal there will be a sharp "V" protruding to the center. A distal cut and a proper cut are shown in Figure 2. If the cut was to distal move the bone a minimum of .25mm and make the next cut. (Ideal cut distances can be found using micro-CT images, or if these are not available the move distance can be based on previous experience.)
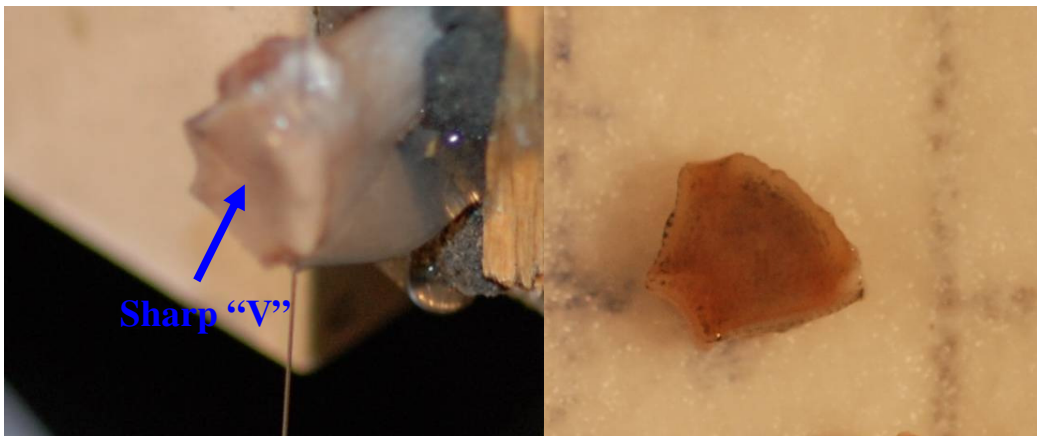
Figure D2: Left- First cut too distal, Right - Correct cut location

7. For a 1.5 mm slice move the specimen 1.5 mm plus the diameter of the wire using the micrometer table. (If the diameter is .13 mm add .16 mm. this is needed to account for the embedded diamonds.)

8. The second cut should be made starting on the posterior side of the bone. Watch the specimen as the cut finishes. (Sometimes it stays attached with tissue other times it may drop)

Imaging for Core Diameter:

1. Using the camera stand and the macroscopic lens photograph both of the plano-parallel faces of the metaphyseal slice with a ruler in the picture. (See below)   Be sure to record the picture numbers and their corresponding bone numbers.
2. Open the picture of the smaller diameter end in Photoshop.
3. In PhotoShop draw a 5-mm diameter circle (from one edge of the line on the ruler to the same edge on the fifth line) and use the circle's diameter in pixels to find the mm to pixel ratio (record).
4. Draw a circle that touches inside edges of the cortical bone (Endocortical, EC) and find the EC pixel diameter (record).
5. Use the pixel diameter and the mm to pixel ratio to find the EC diameter in mm. (Excel can speed this process along.)
6. Calculate the 80% EC diameter. This is the diameter of the core to be taken from the specimen. For the OVX study the 80% of the average minimum EC was used.

Coring:

1. Set up the diamond wire coring fixtures as shown below in Figure 3.

Figure D3: Coring Set Up with Alignment Block

2. Use the alignment block to find the center location for the coring fixture by using the micrometer table and setting a stop on the lower right hand side.

3. Move the fixture using the micrometer table to the desired location. (For a diameter of 2 mm move 1mm + 1/2 diameter of the wire)

4. Place the specimen in the clamping fixture and center it. It seems best to get the specimen in about the center, snug the top disk down lightly, and then make fine tune adjustments. To minimize the cutting time it's best to orient the specimen so that a minimal amount of cortical shell must be cut. The medial or lateral sides seem to be the best to cut through. To ensure that the fixture is set up correctly it is important to do a make a test core. (Styrofoam works well.)

5. Reinspect to make sure that the specimen is properly centered and place it in the coring fixture.

6. Start the machine. (Speed=7.5)

7. Gently slide the specimen fixture into the wire cutting the cortical shell of the bone. Make sure that the wire is completely through the cortical shell and vertical.

8. Turn the fixture ~270 degrees slowly allowing the wire to cut through the cancellous bone.

9. Place specimen retainer in the slotted entry to trap the specimen and then finish rotating the specimen fixture the 360 degrees. Make sure to completely

10. When the coring is complete slide the specimen fixture to the right and remove the specimen.

11. Image the specimens to be analyzed to determine the diameter.

12. Place the new cored specimen in gauze and PBS and stored in a newly labeled tube. Place all other bone remnants back in the original tube.

APPENDIX E

µCT DISTAL FEMUR ISOLATED CANCELLOUS CORE ANALYSIS

(Adapted from the standard analysis procedure from Matt Allen)

OPEN Folder with photo images of the distal and proximal ends of the slices before and after coring.

OPEN CtAn icon (CT analyze) → FILES → OPEN

OPEN any file with a paint brush icon: i.e., a sample ID_rec# (rec=reconstruction)

PRINT the diameter and height measurements from the specimens.

Region of Interest Selection

Toolbar at top of page. Go to:
→ Icon 1: Raw Image Icon.

- ➢ Scroll through Raw Image file window to find the starting point for the scan i.e., the point which the scan matches the corresponding image. The most distinguishing marker is the triangular portion on the posterior side of the bone. See the images to the right..
- ➢ Right Click & SET BOTTOM OF SELECTION. Everything above the line in green is excluded.
- ➢ RECORD starting position & line
- ➢ Scroll downwards through Raw Image file again to find the closest image that is the height of the cored specimen.
- ➢ below the starting position.
- ➢ Right Click & SET TOP OF SELECTION.
- ➢ RECORD top position and line
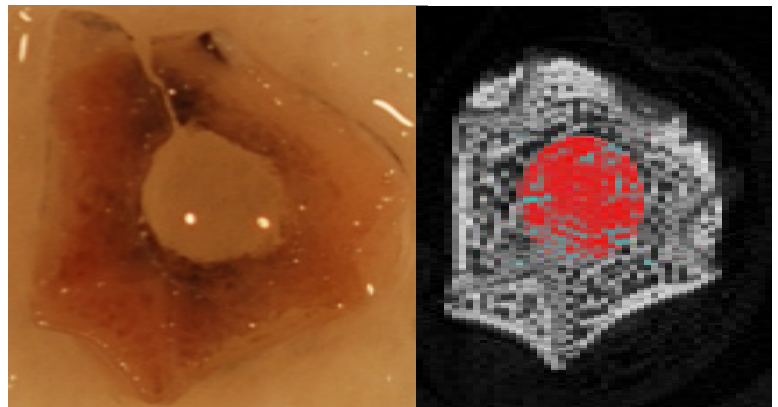
→ Icon 2: Region of Interest Icon.
 ➢ Files with yellow icons in the ROI window indicate slices that are in the selected ROI (area *not* shaded green).
 ➢ Click on the bottom most image of interest.
 ➢ The image of the bone will be entirely red until you start drawing the ROI.
 ➢ Click the …. And select the circular ROI.
 ➢ Size the ROI circle by dragging a corner. The dimension is shown on the bottom right portion of the screen. Place the ROI circle in the location corresponding to the core. See images above.
 ➢ Scroll to the top and click the … and select the circular ROI. This should give you the ability to move the existing ROI.
 ➢ Place this top (proximal) ROI using the distal cored image. (Remember that the image will be essentially be inverted since the photo is coming from the opposite side.)
 **Note: to reset all ROI's & start over, go to "Region of Interest" located in a tab at the top of the screen and select "Reset All".

→ Icon 3: Binary Images Icon.
 - in the Histogram Box window make sure the Index axis of the Histogram is set to 100 (the selected threshold)
 - Click on tab that indicates FROM SELECTION
 - Wait while the program does histogram calculations.
 - In the window under the histogram the grayscale images tab should be selected.
 - Scroll down to below 100%, here you will need to RECORD three things:
     o Mean (total)
     o Mean
     o Number of Voxels

 - in the histogram window left click on the 2nd icon: SAVE HISTO   to the default file_CORE.

 - Click and SAVE the 3-D model   to the default file_CORE.

→ Icon 4: Processed Image Icon.
 - in the Analysis window left click on the 3rd icon: SAVE 3D ANALYSIS RESULTS
 - A 3D analysis box will appear, make sure checked items include:
     ☑ all Base Values
     ☑ all Additional Values
     ☑ Auto Save
     ☉text table
 - Click Continue
 - Will have to wait while the program generates the data

- When a window opens with 3D analysis you can CLOSE it because it was automatically saved.

IMPORT µCT data into an Excel Spreadsheet

Click On:
 → START
 → ALL PROGRAMS
 → Microsoft Office
 → Microsoft Excel
 → OPEN FILE
 → Select the file with the data you want to import (Make sure File Type Selected is ALL FILES)
 → OPEN
 → ⊙ Delimited should be checked → NEXT
 → Make sure these boxes are checked: ☑Tab ☑Comma → NEXT
 → FINISH

APPENDIX F

ANOVA STATISTICAL ANALYSIS

One way ANOVAs were performed as shown below using the Fisher LSD method.

Metaphyseal Micro-CT			
	SHAM-OVE	**OVE-OVX**	**SHAM-OVX**
BV/TV, (%)	N.S.	p=<0.001	p=<0.001
Tb.Th (mm)	N.S.	N.S.	N.S.
Tb.N (1/mm)	p=0.175	p=<0.001	p=<0.001
Tb.Sp (mm)	p=0.175	p=<0.001	p=<0.001
Tb.Pf (1/mm)	N.S.	p=<0.001	p=<0.001
SMI	N.S.	p=<0.001	p=<0.001
vBMD (mg/cm3)	N.S.	p=<0.001	p=<0.001

pQCT			
	SHAM-OVE	**OVE-OVX**	**SHAM-OVX**
Cancellous vBMD	p=0.054	p=<0.001	p=<0.001
Total vBMD	N.S.	p=<0.001	p=<0.001

Core Specific Micro-CT			
	SHAM-OVE	**OVE-OVX**	**SHAM-OVX**
BV/TV (%)	p=0.007	p=<0.001	p=<0.001
Tb.Th (mm)	N.S.	N.S.	N.S.
Tb.N (1/mm)	p=0.005	p=<0.001	p=<0.001
Tb.Sp (mm)	p=0.093	p=<0.001	p=<0.001
Tb.Pf (1/mm)	p=0.062	p=<0.001	p=<0.001
SMI	p=0.044	p=<0.001	p=<0.001
vBMD (mg/cm3)	p=0.007	p=<0.001	p=<0.001
DA	N.S.	N.S.	N.S.

Intrinsic Properties			
Mechanical Property	**SHAM-OVE**	**OVE-OVX**	**SHAM-OVX**
Modulus (MPa)	N.S.	N.S.	p<0.05
Yield Stress (MPa)	N.S.	N.S.	p<0.05
Ultimate Stress (MPa)	N.S.	N.S.	p<0.05
First Minimum Stress (MPa)	N.S.	N.S.	p<0.05
Strain at Yield (mm/mm)	N.S	N.S.	N.S.
Strain at Max Force (mm/mm)	N.S.	N.S.	N.S.
Strain at First Minimum (mm/mm)	N.S.	p=0.039	p=0.002
Toughness to Yield (95%) (N/mm2)	N.S.	N.S.	p<0.05
Toughness to Max Force (N/mm2)	N.S.	N.S.	p<0.05
Toughness to First Minimum (N/mm2)	p=0.021	N.S.	p=0.002

Extrinsic Properties			
Mechanical Property	**SHAM-OVE**	**OVE-OVX**	**SHAM-OVX**
Stiffness (N/mm)	N.S.	N.S.	p<0.05
Yield Force (N)	N.S.	N.S.	p<0.05
Ultimate Force (N)	N.S.	N.S.	p<0.05
First Minimum (N)	N.S.	N.S.	p<0.05
Yield Displacement (mm)	N.S	N.S.	N.S.
Disp. at Max Force (mm)	N.S	N.S.	N.S.
Disp. at First Minimum (mm)	N.S	p=0.030	p=<0.001
Energy to Yield (N-mm)	N.S.	N.S.	p<0.05
Energy to Max Force (N-mm)	N.S.	N.S.	p<0.05
Energy to First Minimum (N-mm)	N.S.	N.S.	p<0.05

No Significant Differences were found using ANOVA for the Material Properties

APPENDIX G

DISTANCE FROM THE DISTAL END OF THE BONE TO THE PROXIMAL FACE OF THE SLICE

Order of Slicing	Bone Number	Group	Distance (mm)
14	29-Aug	Con	3.92
15	17-Aug	Con	4.3
16	28-Aug	Con	3.75
18	4-Sep	Con	3.78
20	23-Aug	Con	4.16
28	11-7B	Con	3.8
29	11-7A	Con	3.72
32	27-Aug	Con	3.72
33	4-Jan	Con	4.04
36	11-7C	Con	3.65
39	22-Aug	Con	3.87
41	21-Aug	Con	4.05
7	13-Aug	E2	3.91
8	8-Feb	E2	3.8
9	4-Feb	E2	3.77
11	1-Feb	E2	4
12	6-Feb	E2	4.35
22	5-Feb	E2	4.37
24	18-Oct	E2	3.66
26	30-Jan	E2	4.11
27	22-Oct	E2	3.77
31	24-Oct	E2	4.45
34	14-Aug	E2	4.55
38	28-Oct	E2	4.67
42	25-Oct	E2	4.23
1	3-Oct	Extra	4.07
2	21-Jan	Extra	3.7
3	23-Jan	Extra	3.8
4	12-Mar	Extra	3.93
5	7-Mar	Extra	3.9
6	16-Aug	Extra	3.84
10	31-Oct	OVX	3.9
13	25-Jan	OVX	3.85
17	7-Aug	OVX	4.36
19	29-Oct	OVX	4.27
21	30-Oct	OVX	4.15
23	28-Jan	OVX	4.15
25	24-Jan	OVX	4.15
30	1-Aug	OVX	3.59
35	2-Nov	OVX	4.25
37	6-Aug	OVX	3.99
40	29-Jan	OVX	4.02

	SHAM	OVX	OVX+E2
Average	3.892	4.043	4.126
Standard Deviation	0.181	0.221	0.334
Standard Error	0.044	0.064	0.093

No significant differences were found between groups using either t-test or ANOVA comparison methods.

APPENDIX H

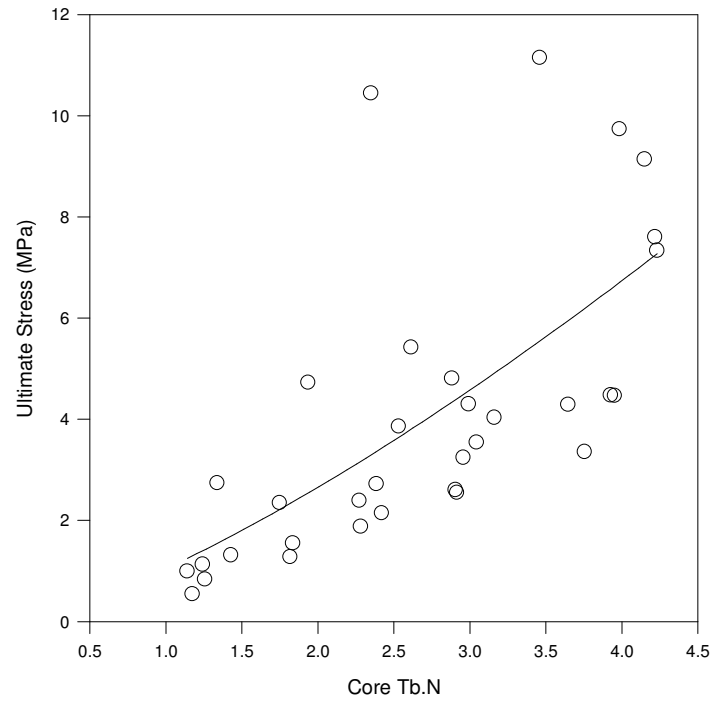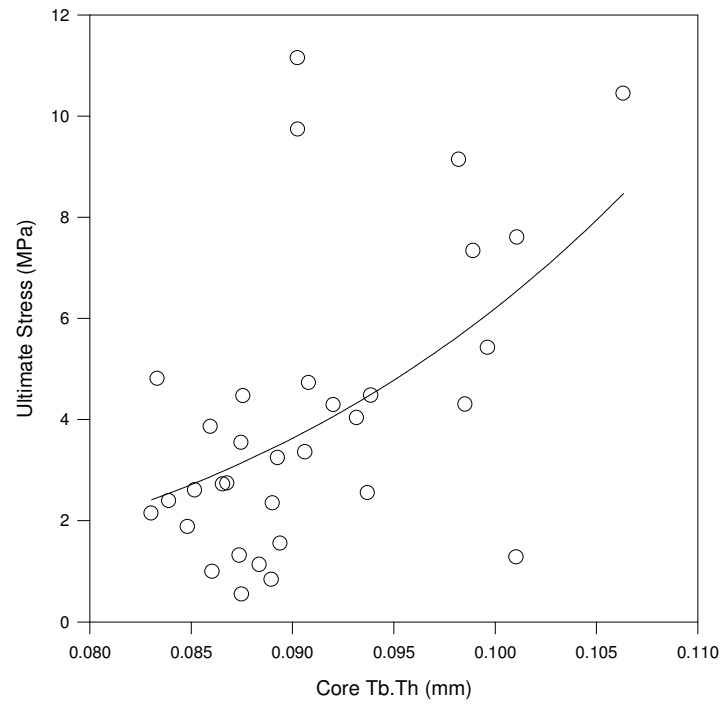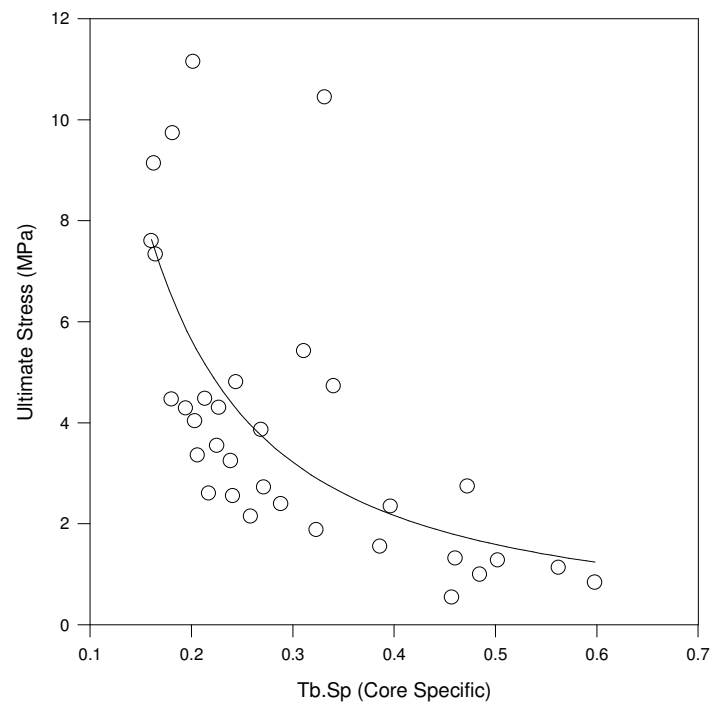# POWER LAW REGRESSIONS
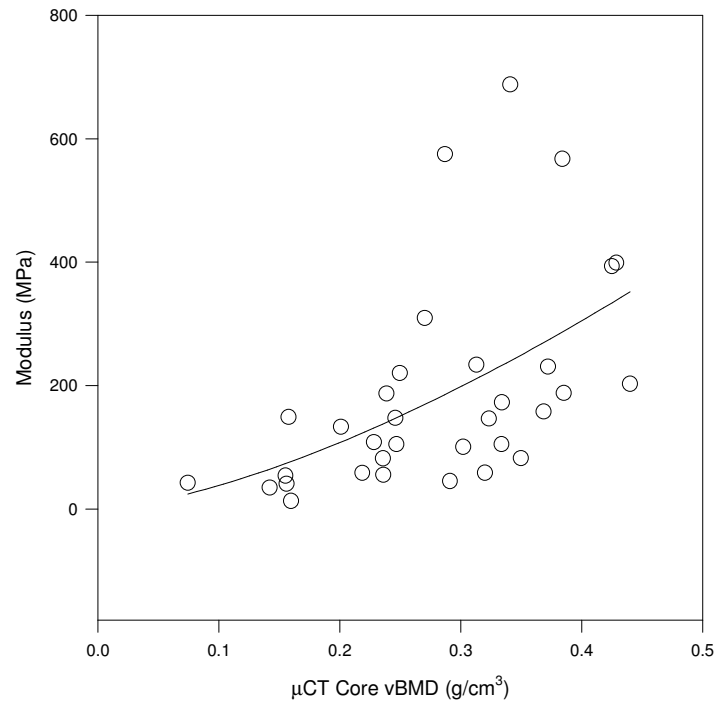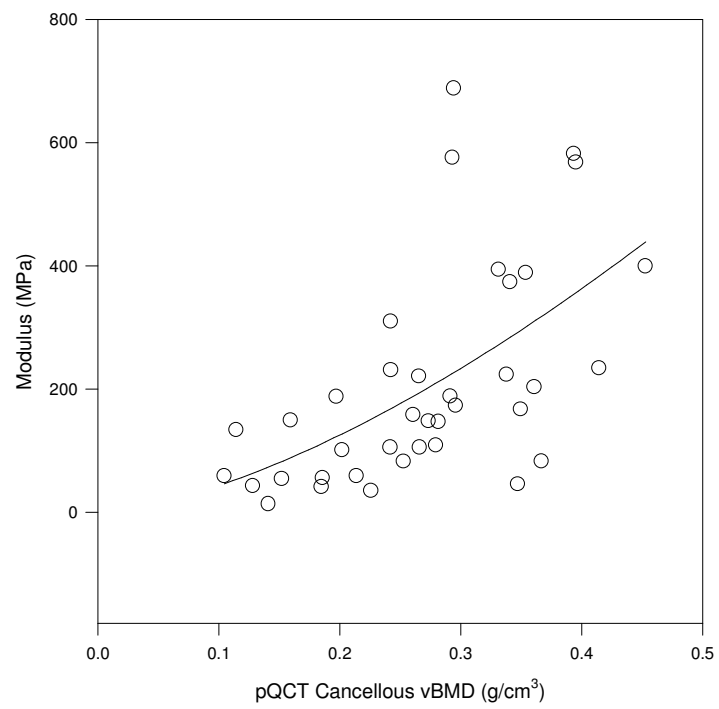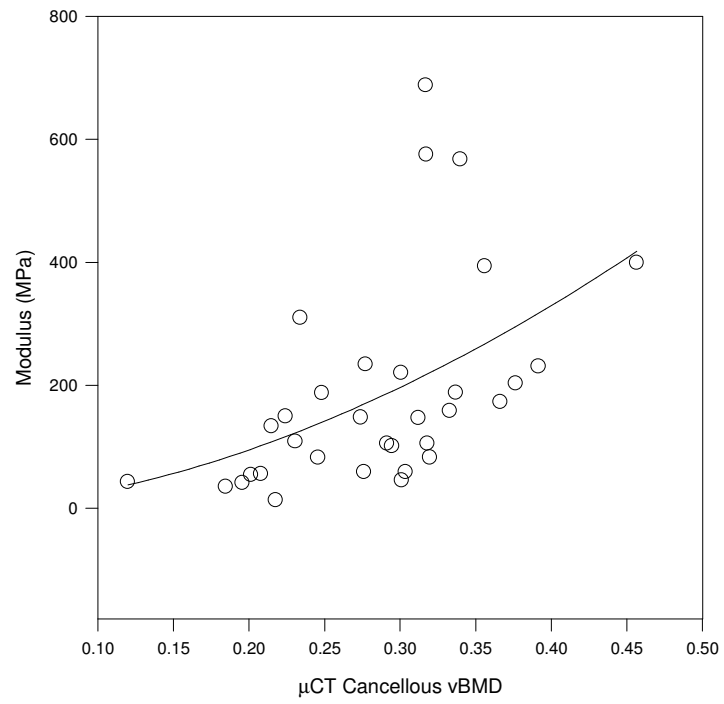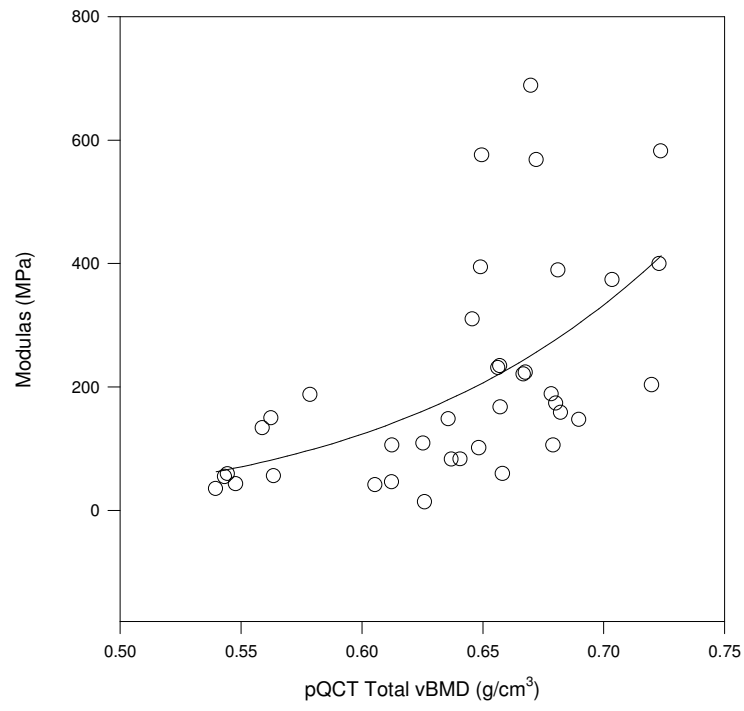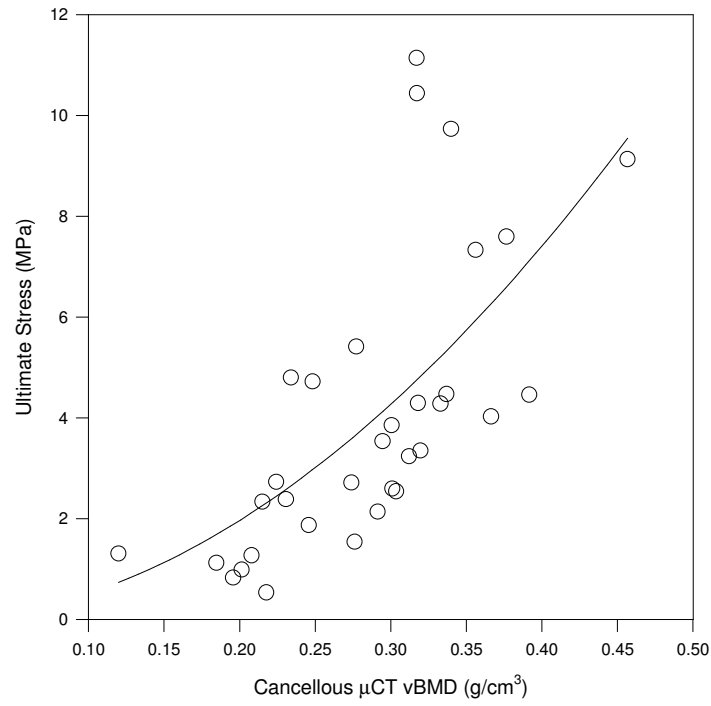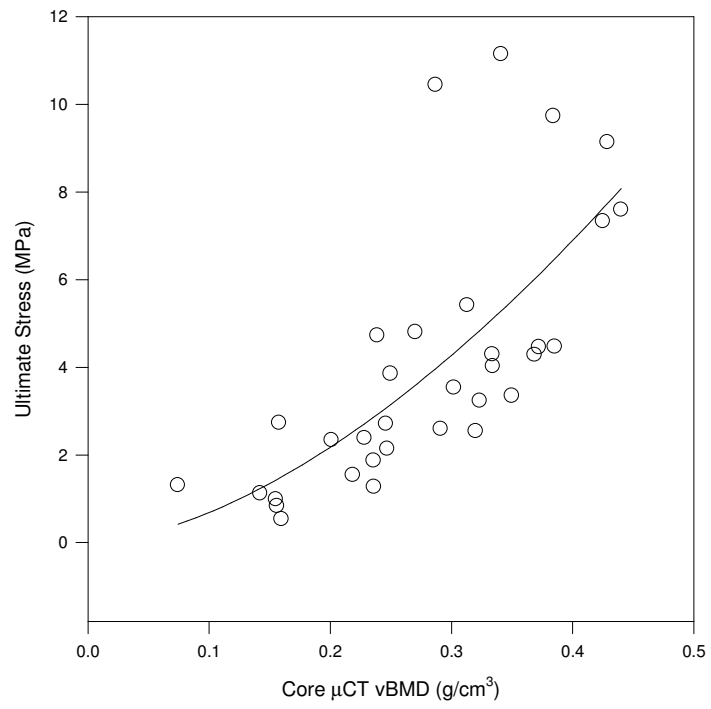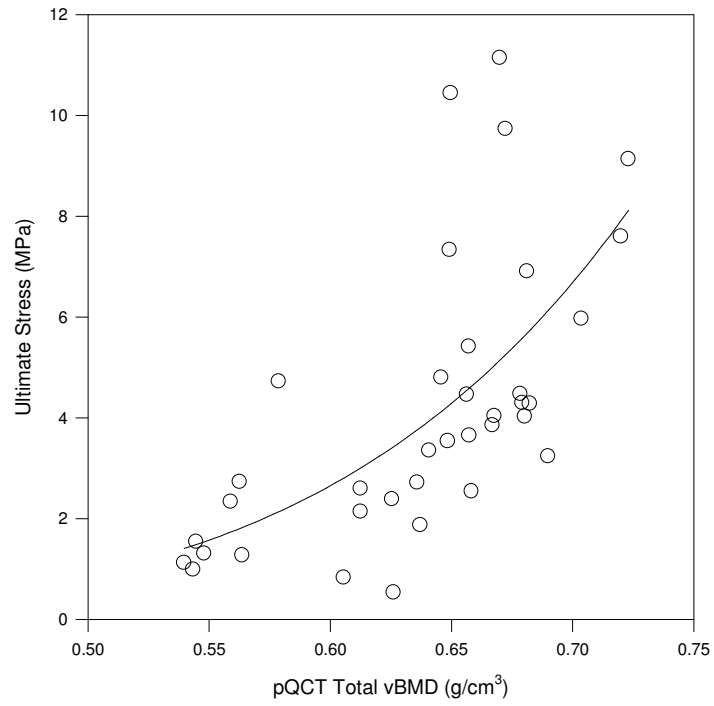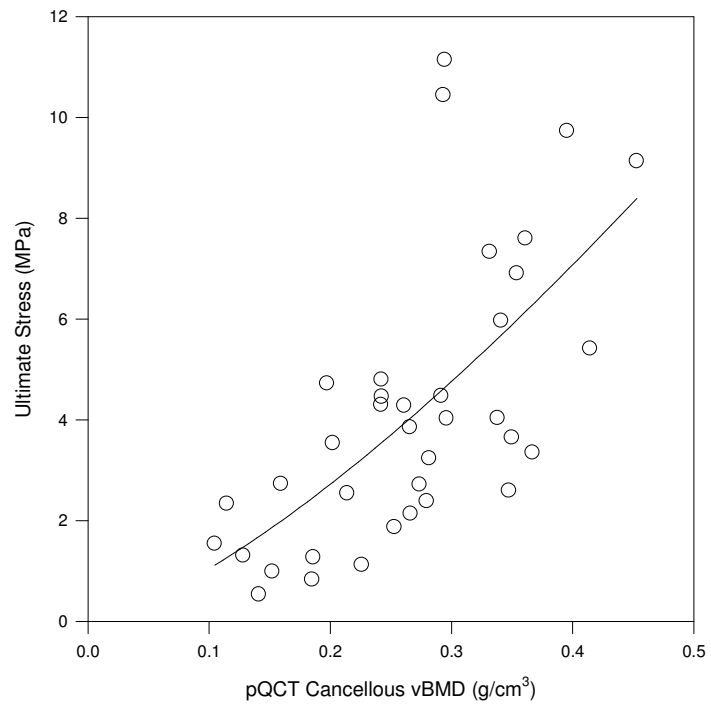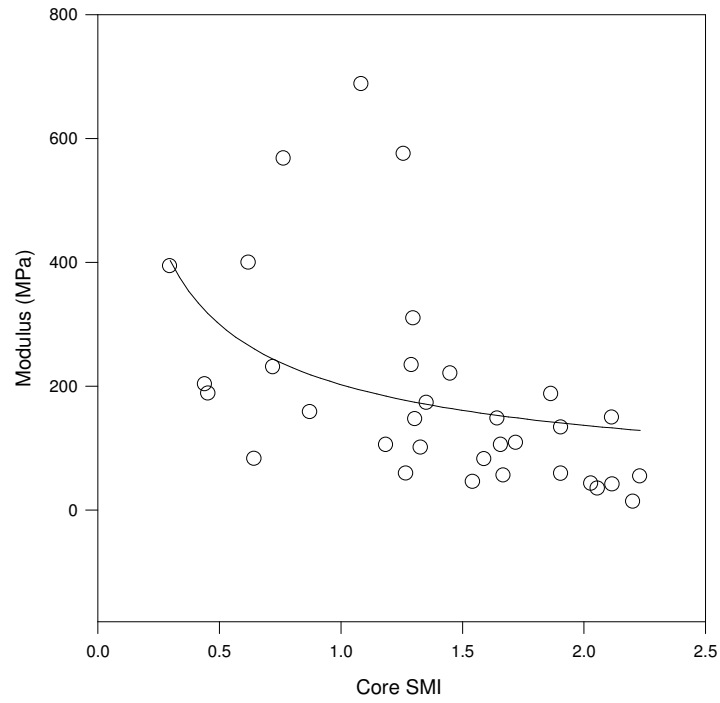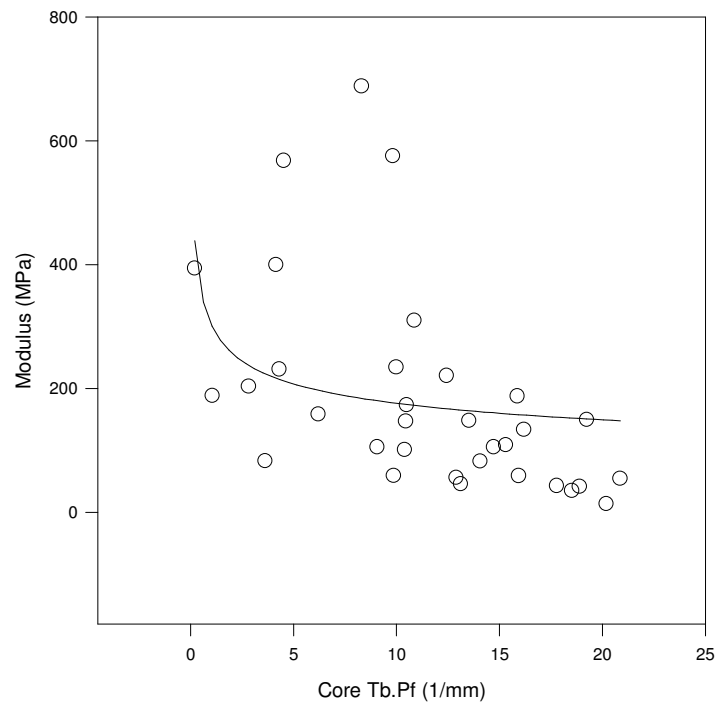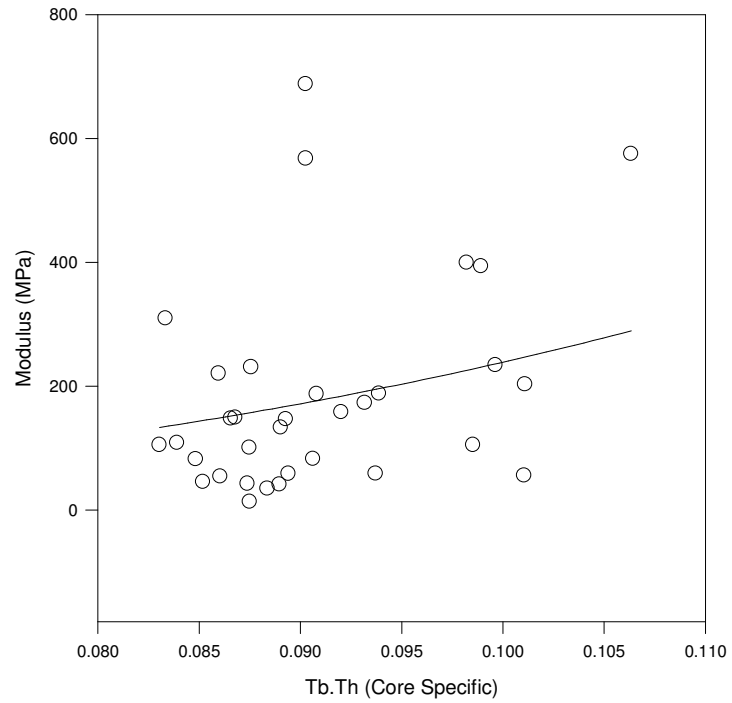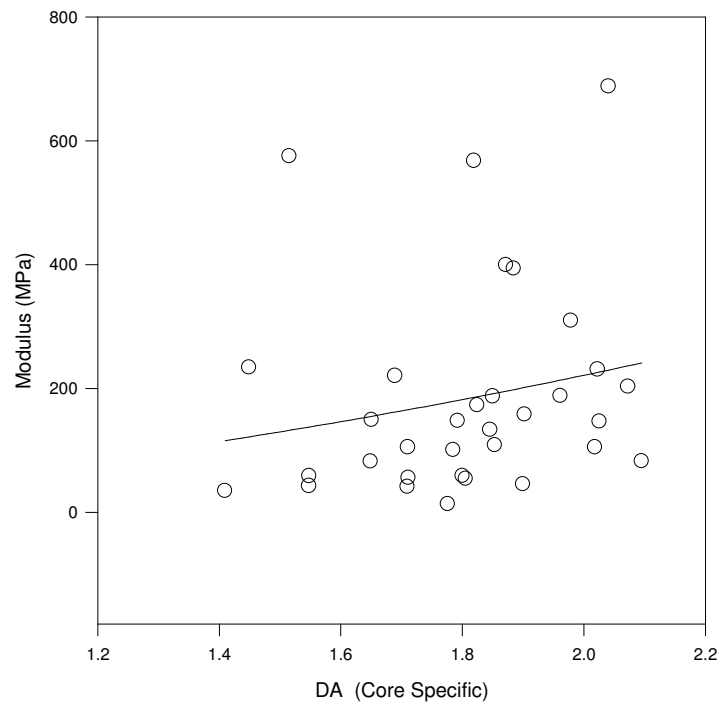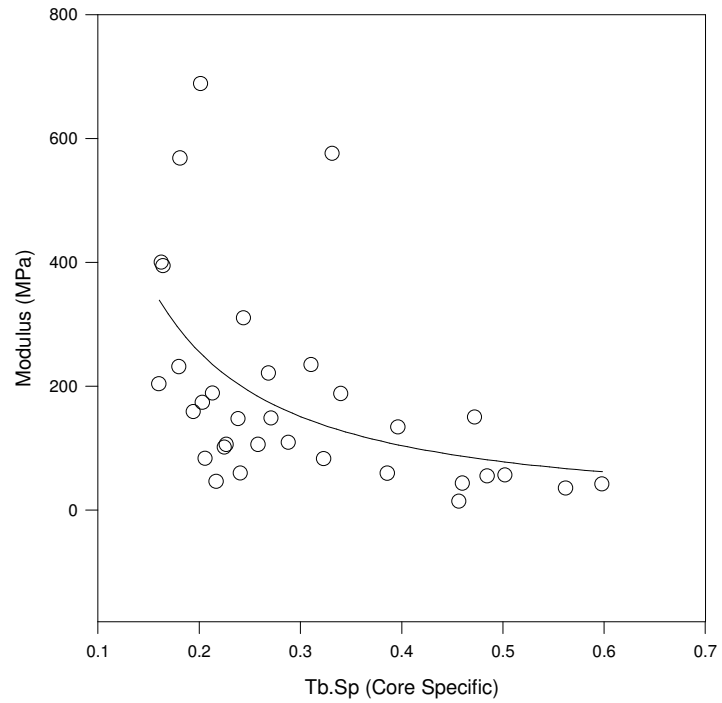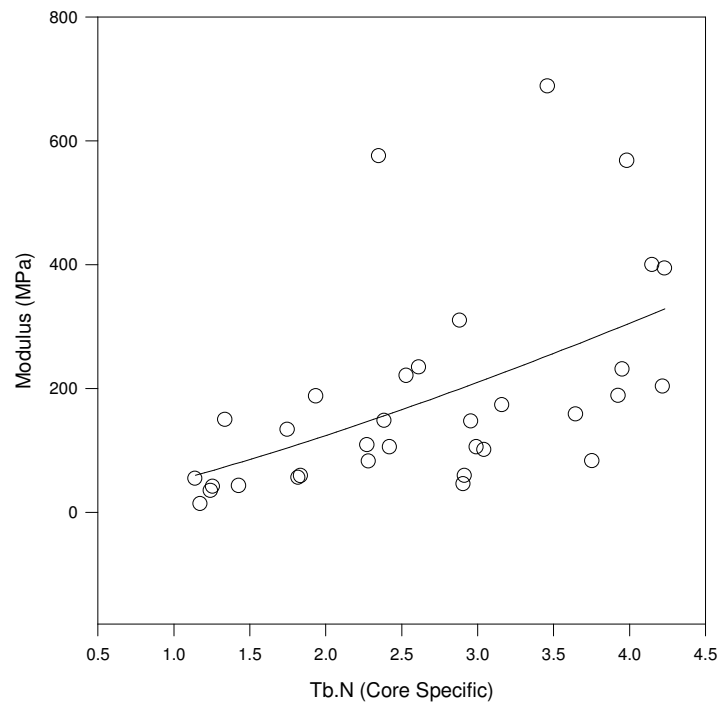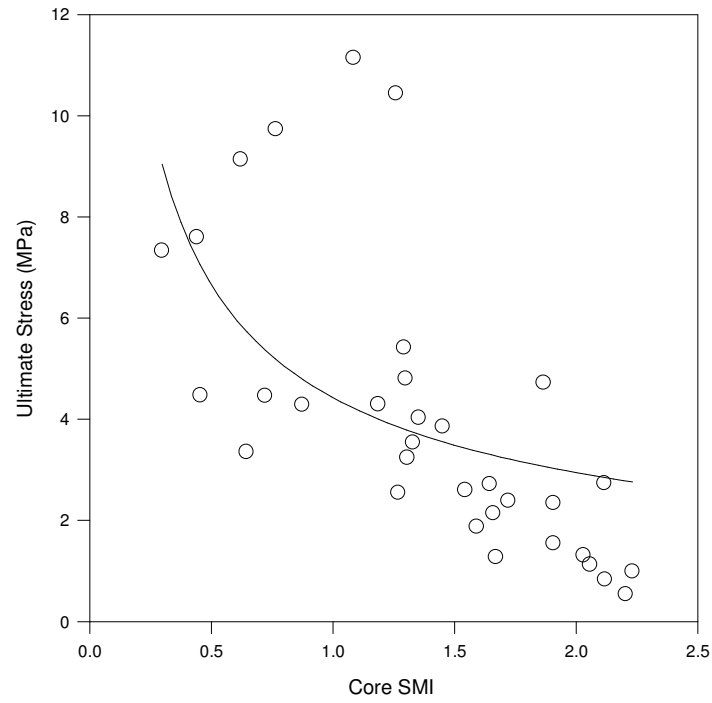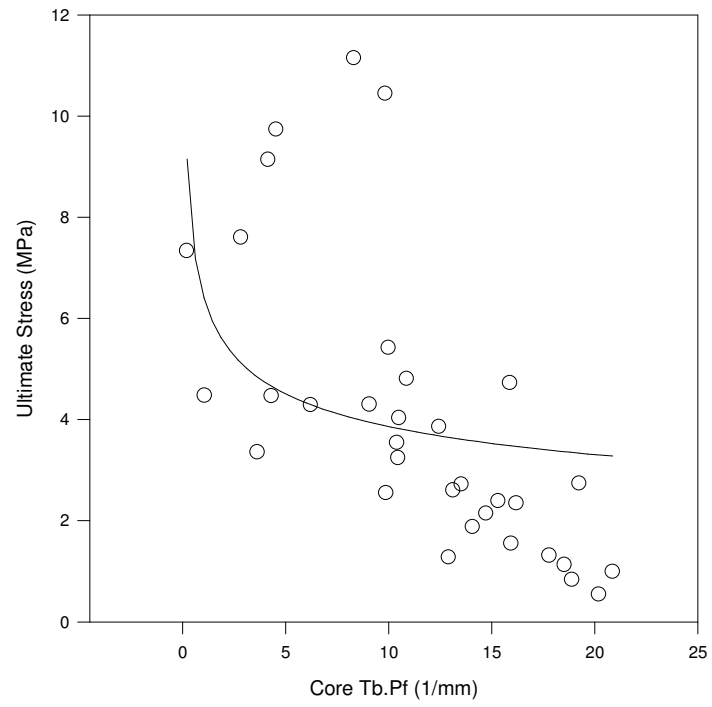
VITA

Name:	Matthew Walton Lucas
Address:	3123 TAMU, College Station, TX 77843, C/O: Dr. Harry Hogan, Department of Mechanical Engineering
Email Address:	matthew.w.lucas@gmail.com
Education:	B.S., Engineering Mechanics, Lipscomb University, 2007
	M.S., Mechanical Engineering, Texas A&M University, 2009